VNIVERSITAT DE VALÈNCIA

Biopolymer-Based Hybrid Hydrogels for Biomedical Applications: From Macroscopic to Nanosized Systems

Doctoral Thesis

presented by

Asmaa Mohamed Ibrahim Elzayat

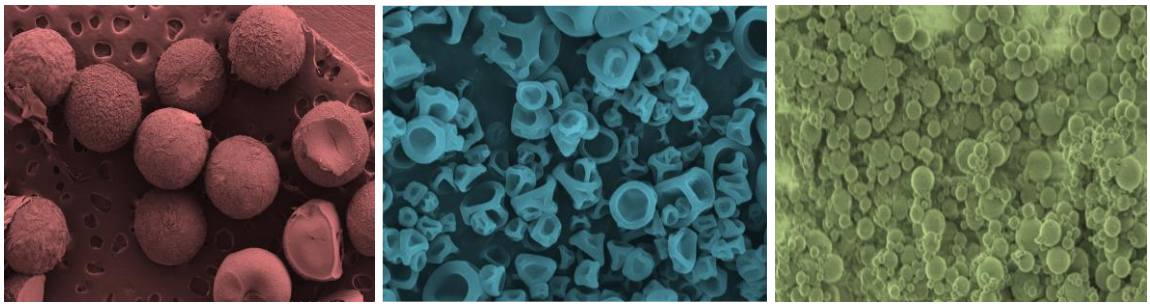

Thesis Advisor: Rafael Muñoz-Espí

Doctoral Program in Chemistry
(Line of Research: Materials Science)

November, 2021

ICMUV
INSTITUT DE CIÈNCIA DELS MATERIALS de la Universitat de València

Institute of Materials Science (ICMUV) · University of Valencia
C/ Catedràtic José Beltrán 2 · 46980 Paterna, València, Spain

Rafael Muñoz-Espí, Associate Professor at the Department of Physical Chemistry and the Institute of Materials Science of the University of Valencia

***Rafael Muñoz-Espí**, professor titular d'universitat del Departament de Química Física i de l'Institut de Ciència dels Materials de la Universitat de València*

I CERTIFY

CERTIFIQUE

That the present Doctoral Thesis, entitled

Que la present tesi doctoral, titulada

"Biopolymer-Based Hybrid Hydrogels for Biomedical Applications: From Macroscopic to Nanosized Systems",

and submitted by

i presentada per

***Asmaa Mohamed Ibrahim Elzayat**,*

student of the Doctoral Program in Chemistry of the University of València, was carried out under my supervision at the Institute of Materials Science (ICMUV).

estudiant del Programa de Doctorat en Química de la Universitat de València, va ser realitzada sota la meua direcció a l'Institut de Ciència dels Materials (ICMUV).

Hereby, I authorize the submission of this doctoral thesis.

Amb el present escrit autoritze el dipòsit d'aquesta tesi doctoral.

October 29, 2021

29 d'octubre de 2021

Rafael Muñoz-Espí

Thesis Advisor / Director de la tesi

VNIVERSITAT DE VALÈNCIA

This thesis is the result of a collaborative work between the Institute of Materials Science at the University of Valencia, Spain, and the Physics Department at the Faculty of Science of Mansoura University, Egypt,

conducted by

Asmaa Mohamed Ibrahim Elzayat

under the guidance of

Prof. Dr. Rafael Muñoz-Espí (University of Valencia)

and

Prof. Dr. Ahmed Hamza Oraby (Mansoura University)

Abstract

Biopolymer-based carrier particles are biocompatible and offer the ability to incorporate hydrophilic and hydrophobic active agents. The incorporation of a drug into a polymeric matrix can enhance its protection against degradation in harsh physiological media. In addition, it can control the release to the specific site of action, with increased therapeutic bioavailability and minimized side effects or toxicity.

This thesis presents the preparation of different polysaccharide hybrid systems for encapsulating hydrophilic substances, which are subsequently released. Carriers ranging from macroscopic to nanometric size are produced by different methods: ionotropic gelation, spray drying, and nanoemulsion techniques. Chitosan and alginate are used as matrix polymers and silica is applied as a structuring additive.

In the first part of the work, an organic–inorganic macroscopic gel is prepared by a simple process involving ionotropic gelation, and the efficiency of the method for entrapping hydrophilic molecules (erioglaucine disodium salt and ephedrine hydrochloride) is investigated. The release of the encapsulated substances is controlled by tailoring the hybrid network structure.

The second approach involves the preparation of microcapsules by using ionotropic gelation followed by spray drying. In this process, which is fast and continuous, a liquid feed is transformed into dry particles. The release behavior of hydrophilic drugs is studied and compared with the results obtained in the first part for macroscopic particles. In addition, the biopolymer microparticles are loaded with Pd(II) ions and, after reduction to Pd(0), applied as catalysts for a model reaction, namely the reduction of 4-nitrophenol by sodium borohydride.

The third approach consists in the preparation of an organic–inorganic nanogel by two different inverse nanoemulsion methods. The first method is a “one-nanoemulsion” process in which chitosan nanoparticles are produced by allowing the diffusion of a cross-linking agent to a nanoemulsion containing a solution of chitosan in the dispersed phase. In the second method, a polysaccharide nanoemulsion is mixed with a second

cross-linking nanoemulsion. A nanogel is formed after fusion of the droplets of the two nanoemulsions.

In the systems prepared by the three approaches, silica nanostructures are homogeneously incorporated within the polymer matrix. The release behavior depends on the preparation method, the size of the structures, and the presence or not of silica.

Overall, it can be concluded that silica plays a very important role in both increasing the structural stability of the hydrogel carriers and retarding the release in different media.

Resumen

Las partículas portadoras basadas en biopolímeros son biocompatibles y ofrecen la capacidad de incorporar agentes activos hidrófilos e hidrófobos. La incorporación de un fármaco en una matriz polimérica puede mejorar su protección contra la degradación en medios fisiológicos severos. Además, puede controlar la liberación al sitio de acción específico, con una biodisponibilidad terapéutica aumentada y efectos secundarios o toxicidad minimizados.

Esta tesis presenta la preparación de diferentes sistemas híbridos de polisacáridos para encapsular sustancias hidrófilas, que posteriormente son liberadas. Se preparan portadores que varían de tamaño macroscópico a nanométrico mediante diferentes métodos: gelificación ionotrópica, secado por pulverización y técnicas de nanoemulsión. El quitosano y el alginato se utilizan como polímeros de matriz y la sílice se aplica como aditivo estructurante.

En la primera parte del trabajo se prepara un gel macroscópico orgánico-inorgánico mediante un proceso simple que implica una gelificación ionotrópica y se investiga la eficiencia del método para incorporar moléculas hidrófilas (sal disódica de erioglaucina y clorhidrato de efedrina). La liberación de las sustancias encapsuladas se controla adaptando la estructura de la red híbrida.

El segundo enfoque implica la preparación de microcápsulas usando gelificación ionotrópica seguida de secado por pulverización. En este proceso, que es rápido y continuo, el líquido inicial se transforma en partículas secas. Se estudia el comportamiento de liberación de fármacos hidrófilos y se compara con los resultados obtenidos en la primera parte para partículas macroscópicas. Además, las micropartículas biopoliméricas se cargan con iones Pd(II) y, después de la reducción a Pd(0), se aplican como catalizadores para una reacción modelo, la reducción de 4-nitrofenol mediante borohidruro de sodio.

El tercer enfoque consiste en la preparación de un nanogel orgánico-inorgánico mediante dos métodos diferentes de nanoemulsión inversa. El primer método, en el que interviene una sola nanoemulsión, es un proceso en el que se obtienen nanopartículas de quitosano cuando se produce la difusión de un agente entrecruzante a una nanoemulsión

que contiene una disolución de quitosano en la fase dispersa. En el segundo método, se mezcla una nanoemulsión de polisacárido con una segunda nanoemulsión de un agente reticulante. Se forma un nanogel después de la fusión de las gotitas de las dos nanoemulsiones.

En los sistemas preparados por los tres enfoques, las nanoestructuras de sílice se incorporan de manera homogénea dentro de la matriz del polímero. El comportamiento de la liberación depende del método de preparación, del tamaño de las estructuras y de la presencia o no de sílice.

Con carácter general, se puede concluir que la sílice tiene un papel muy importante tanto en el aumento de la estabilidad estructural de los portadores de hidrogel como en el retraso de la liberación en diferentes medios.

Resum

Les partícules portadores basades en biopolímers són biocompatibles i ofereixen la capacitat d'incorporar agents actius hidròfils i hidròfobs. La incorporació d'un fàrmac en una matriu polimèrica pot millorar-ne la protecció contra la degradació en mitjans fisiològics severs. A més, pot controlar-ne l'alliberament al lloc d'acció específic, amb una biodisponibilitat terapèutica augmentada i efectes secundaris o toxicitat minimitzats.

Aquesta tesi presenta la preparació de diferents sistemes híbrids de polisacàrids per a encapsular substàncies hidròfiles, que posteriorment són alliberades. Es preparen portadors que varien de mida macroscòpica a nanomètrica mitjançant diferents mètodes: gelificació ionotròpica, assecat per polvorització i tècniques de nanoemulsió. El quitosà i l'alginat s'utilitzen com a polímers de matriu i la sílice s'aplica com a additiu estructurant.

En la primera part del treball es prepara un gel macroscòpic orgànico-inorgànic mitjançant un procés simple que implica una gelificació ionotròpica i s'investiga l'eficiència del mètode per a incorporar molècules hidròfiles (sal disòdica d'erioglaucina i clorhidrat d'efedrina). L'alliberament de les substàncies encapsulades es controla adaptant l'estructura de la xarxa híbrida.

El segon enfocament implica la preparació de microcàpsules usant gelificació ionotròpica seguida d'assecat per polvorització. En aquest procés, que és ràpid i continu, el líquid inicial es transforma en partícules seques. S'estudia el comportament d'alliberament de fàrmacs hidròfils i es compara amb els resultats obtinguts en la primera part per a partícules macroscòpiques. D'altra banda, les micropartícules biopolimèriques es carreguen amb ions Pd(II) i, després de la reducció a Pd(0), s'apliquen com a catalitzadors per a una reacció model, la reducció de 4-nitrofenol mitjançant borhidrur de sodi.

El tercer enfocament consisteix en la preparació d'un nanogel orgànico-inorgànic mitjançant dos mètodes diferents de nanoemulsió inversa. El primer mètode, en el qual intervé una sola nanoemulsió, és un procés en què s'obtenen nanopartícules de quitosà quan es produeix la difusió d'un agent entrecreuant a una nanoemulsió que conté una dissolució de quitosà en la fase dispersa. En el segon mètode, es mescla una nanoemulsió

de polisacàrid amb una segona nanoemulsió d'un agent entrecreuant. Es forma un nanogel després de la fusió de les gotetes de les dues nanoemulsions.

En els sistemes preparats pels tres enfocaments, les nanoestructures de sílice s'incorporen de manera homogènia dins de la matriu del polímer. El comportament de l'alliberament depèn del mètode de preparació, de la mida de les estructures i de la presència o no de sílice.

Amb caràcter general, es pot concloure que la sílice té un paper molt important tant en l'augment de l'estabilitat estructural dels portadors d'hidrogel com en el retard de l'alliberament en diferents medis.

.

الملخص

تم استخدام البوليمرات الحيوية كناقلات للدواء. وفي هذا السياق، يمكن أن يؤدي دمج الدواء في مصفوفة بوليمرية الى تعزيز حمايته ضد التدهور في البيئات الفسيولوجية المختلفه ويمكن أن يطيل النشاط البيولوجي عن طريق التحكم في تحريره الى المكان المستهدف للمعالجه، مع زيادة التوافر البيولوجي العلاجي وتقليل الآثار الجانبية أو السميه

وانطلاقا من هذا المبدأ فالهدف من هذا البحث هو تخليق هيدروجيل حيوى هجين قائم على البوليمراتالحيويه (البولى سكاريد) للتحكم في سلوك تحرر وانطلاق المواد الحيويه في الاوساط المختلفه، علي الصعيد المجهري إلى النانوني. باستخدام مادتى الكيتوزان والألجينات كمواد دراسيه فى هذا العمل، وايضا تعد السيليكا واحدة من أكثر فئات الجسيمات النانوية التي تمت دراستها فيما يتعلق بالمواد المهجنة القائمة على البوليمر. في دراسة منظمة ، ينقسم هذا البحث الى ثلاثه اجزاء رئيسيه :

أولا: هو تخليق ماكروجيل عضوي وغير عضوي (كبسولات كبيرة) بواسطة التكوّن الهلامي المؤين للتأين وكفاءته في حبس الجزيئات المحبة للماء (ملح ثنائي الصوديوم إيريوجلوسين وهيدروكلوريد الإيفيدرين) داخل مصفوفة البوليمر ومن ثم دراسه تحرر هذه الجزيئات في الاوساط المختلفه كدراسه خارج الجسم البيولجى

ثانيًا، باستخدام تقنيه الاسبراى دراينج والتى توضح كفاءتها في الحصول على كبسولات ميكرومتريه الحجم لاستخدامها فى تغليف المواد المحبة للماء داخل تجويفها وكذلك دراسه تحرر الماده المحمله بداخلها كمقارنه دراسيه للطرق المختلفه لتكوين الهيدروجل الحيوي باحجام مختلفه من الماكرو للميكرو ومن ثم الى النانو. بالاضافه الى ذلك يتم تحميل الجسيمات الدقيقه من البوليمر الحيوى بايونات Pd (II) وبعد الاختزال الى Pd (0) يتم تطبيقها كمحفزات لتفاعل نموذجى ويشمل اختزال تفاعل 4 نتيتروفينول بواسطه بورهيدريد الصوديم.

ثالثا: فكانت تشتمل على تخليق جسيمات نانوية عضوية وغير عضوية عن طريق عملية النانو ايملشن والتى تتضمن تفتيت جزيئات البوليمرات الحيويه (البولى سكاريد) باستخدام تقنيه الالتراسوند الى جزيئات صغيره ذات حجم نانوى تحوى بداخلها الماده المراد تغليفها داخل المصفوفه البوليمريه والطريقه الاخرى تتضمن دمج القطرات البوليمريه كل على حده لكل من البوليمر والعامل المساعد بعد استخدام تقنيه الالتراسوند ليتم الترابط بينهم من خلال خاصيه التداخل السطحى والاندماج بينهم.

وباستخدام الطرق الثلاثة ، يتم دمج الهياكل النانوية للسيليكا بشكل متجانس في مصفوفة البوليمر. يعتمد سلوك الإطلاق على طريقة التحضير ، وحجم الهياكل ، ووجود السيليكا أم لا.

بشكل عام ، يمكن استنتاج أن السيليكا تلعب دورًا مهمًا للغاية في زيادة الاستقرار الهيكلي لحاملات الهيدروجيل وتأخير الإطلاق في الوسائط المختلفة

Acknowledgments

First of all, I express my deepest gratefulness and my heartily profound thanks and appreciation to my thesis supervisor, Prof. Rafael Muñoz-Espí, for his constant teaching and his confidence in me during my research period. He guided me with patience and concern through my dissertation, and never accepted less than my best efforts. Thank you for being there for me all the way. It was and will be always a privilege. Many thanks, Rafa!

I thank very especially the Egyptian Ministry of Higher Education and the Egyptian Missions Department for the doctoral fellowship and the financial support to get qualified with more experience by traveling abroad, to finalize my research and to obtain the doctoral degree from the University of Valencia.

Many thanks as well to Prof. Katharina Landfester for being an exemplary leader and for allowing me to be part of her group at the Max Planck Institute for Polymer Research, in Mainz, during my six-month research period granted by the German Academic Exchange Service (DAAD).

I would like to show my gratitude and respect to Prof. Francisco Pérez for his help and contribution to this thesis, very especially to the kinetic studies.

My appreciation and many thanks to my Egyptian supervisor, Prof. Ahmed Oraby, from Mansoura University, for his continuous guidance since the beginning of my scientific and research career. Many thanks, Dr. Oraby.

I would also like to thank the Advanced Materials Research Group at Mansoura University, which I come from, and the head of the group, Prof. Elmetwally Abdelrazek, for his highly appreciated support and guidance at the early stage of my academic research.

I thank Prof. Clara Gómez for her invaluable support and her scientific and non-scientific advice during all my stay in Valencia

I am very grateful to all my colleagues and friends from the CM3-Lab, especially my friend Inés Adam, who has shared with me the office and has helped in everything from the first moment since I arrived to the ICMUV. I also thank my closest friend José Serrano and his girlfriend Lola: for me they are considered as members of my family. Thanks, as well to my friend Juan Fran Ferrer: he was always there when I needed his help.

Thanks to my instructor and friend Emad Tolba, from the National Research Centre in Dokki, Giza, for his beneficial guidance. He was always there when I looked for help.

Thanks to Marie Albus for her contribution to the catalytic work during her Erasmus internship in our group. Thanks, Marie!

I thank very especially Dr. David Vie for his help and advice with the characterization by DLS, TGA, DSC and other characterization techniques. Many thanks as well to Dr. Pilar Gómez for her effort and help with the characterization by SEM; she always did her best to make me satisfied with the results. Thanks a lot, my dear Pilar!

I owe a deepest thanks to the Dean of the Faculty of Science of Mansoura University, Prof. Osama El-Ayaan and to all the staff of the Physics Department, very especially the Head, Prof. Adel Sadiq, for helping me to pursue my PhD in Spain.

Many thanks to my "scientific father", Prof. Ahmed Amen Hamza, former Head of the Physics Department and former President of the Mansoura University, for his constant support and all the advice that he has always given me during my university career.

Last but not least, there are no words to express my gratitude to my husband and my family, especially my affectionate father for supporting me not only during my studies but also throughout all my life. Special thanks to my children, Abdelrahman and Rayan: you have always been a source of hope and happiness for me under different circumstances and pressure.

Table of Contents

Chapter 1

Motivation and Scope of the Thesis

Controlling the release of pharmaceutical compounds to the specific site of action, with increased therapeutic bioavailability and minimized side effects or toxicity, has attracted much attention in recent years.[1-2] The incorporation of a drug into a polymeric matrix can enhance its protection against degradation in harsh physiological media and it can prolong the biological activity by controlling the release. In this context, the research on hybrids and composites is being greatly developed. The attractiveness of polymer–inorganic hybrid materials relies on the synergic combination of the features of polymers (e.g., biocompatibility, chemical stability, and easy processability).[3-4]

Hydrogels are cross-linked three-dimensional hydrophilic polymers, which swell without dissolving when brought into contact with water or other biological fluids. Hydrogels possess numerous properties that make them ideal candidates for use as biomaterials, finding significant use in the fields of drug delivery, tissue engineering, implants, and more. The preparation of hybrid hydrogel materials has been approached by different methods from macro- to nanoscale, but the control of their structure remains still a challenge.[5]

The development of new encapsulation techniques had led to an increasing use of biopolymers (especially polysaccharides) in pharmaceutical applications. This work presents the preparation of polysaccharide–inorganic hybrid hydrogels, from macro- to nanoscale, by different techniques involving ionotropic gelation, either alone at macroscopic level or in combination with spray drying or the miniemulsion technique. The structures are specifically designed for the encapsulation and entrapment of hydrophilic substances, so that their release behavior can be controlled in different media.

The technique of ionotropic gelation with polyelectrolyte complexation provides an eco-friendly pharmaceutical product that minimizes the use of toxic organic solvents or cross-linking agents. Carried out at the macroscale, the process is simple and forms rapidly hydrogels by extrusion of an aqueous solution in the form of droplets into the cross-linking agent receptor. The mechanism of hydrogel formation involves electrostatic interactions between opposite charges, resulting in an ionotropic gelation.[6-8]

The combination of ionotropic gelation with spray drying allows the formation of micro-sized hydrogels. It is a fast and continuous process based on the transformation of a liquid feed into dry particles in three steps: the atomization, the mixing of fine droplets with a gas stream, and the separation and collection of dried microparticles, which can be used for different applications.

On the nanoscale, the preparation of hybrid polymer–inorganic nanoparticles takes place by the nanoemulsion technique through two different protocols: a "one-nanoemulsion" process, in which the cross-linking occurs during the ionotropic gelation, and a "two-nanoemulsion" process, in which the ionically cross-linking mechanism is allowed to take place during the mixing and fusion process of two separated nanoemulsions with a polycationic biopolymer and a polyanionic cross-linker in the disperse phase. In both cases, hydrophilic compounds are entrapped in situ within a polymer matrix.

The thesis is organized as follows. After the motivation (***Chapter 1***), a general introduction chapter (***Chapter 2***) explains the theoretical background and the use of different methods for the synthesis of polymer–inorganic hybrid nanoparticles and capsules from macro- to nanoscopic size for biological applications, particularly drug delivery. Afterward, ***Chapter 3*** describes the different techniques and methodology used in this thesis for the preparation and characterization of the hybrid polysaccharide-based materials. The following chapters are organized in the same way: an introductory part is followed by the discussion of the results and the main conclusions; the experimental details are given at the end of the chapter.

Chapter 4 is dedicated to the establishment of the synthetic strategies for the preparation of an organic–inorganic macrogel (macrocapsules) by ionotropic gelation and its efficiency for entrapping hydrophilic molecules (erioglaucine disodium salt and ephedrine hydrochloride, used as model systems). The chapter offers an insight on the influence of silica nanoparticles, produced in situ by a sol–gel process, on the

morphology and release behavior with respect to pure polymer materials. The following chapter is a complementary part of the macroscopic study. ***Chapter 5*** presents a strategy for the application of the macrocapsules in the formation of a 3D network scaffold for entrapping two different hydrophilic substances.

Chapter 6 discusses the preparation of polysaccharide microcapsules by using the spray drying technique. These microparticles are used for encapsulating model hydrophilic molecules, studying thereby their release behavior. In addition, the prepared particles are used as a catalytic support for palladium catalysts, which are tested for the reduction reaction of *p*-nitrophenol, used as a model catalytic reaction. The results are compared with those obtained with the macroparticles prepared by ionotropic gelation in Chapter 4.

Chapter 7 reports the preparation of biopolymer nanogels by the miniemulsion technique, using the two methods indicated above. Also in this case, the release behavior of hydrophilic drugs is investigated.

Finally, ***Chapter 8*** summarizes the main results obtained in our research. It is clearly proven that the presence of silica nanostructures embedded within the polymer matrix retards and enhanced the release behavior of different hydrophilic substances in different media.

Chapter 2

Theoretical Background

This chapter provides the general theoretical background of the thesis and reviews the relevant concepts of drug delivery by using biopolymer hydrogel carriers, including preparation, drug encapsulation, and controlled release in different media. Different methods for the preparation of biopolymeric carriers are discussed, making special emphasis on hydrogel formations for a wide size range, from macro- to nanoscale.

2.1 Drug Delivery Systems

Drug delivery systems are the approaches of administering different pharmaceutical substances to achieve a therapeutic effect in humans or animals. Drug delivery systems control the rate at which a drug is released and the location in the body where it is targeted.[9-10] The goal is to obtain systems with optimized drug loading and release properties, long shelf-life, and low toxicity.[9] Different natural and synthetic polymers have been used to formulate drug delivery systems. These systems are developed based on interdisciplinary methods that integrate the fields of pharmaceutics, chemistry, polymer and colloid science, and molecular biology. This multidisciplinarity aims at regulating basic pharmacokinetics, pharmacodynamics, and non-specific toxicity to enhance the biorecognition and therapeutic efficiency.[11-14]

Polysaccharides, such as pectin, agarose, agar, cellulose, dextran, alginate, or chitosan, have been evaluated in a number of preparation strategies.[15] They include the formation of hydrogels, microparticles, nanoparticles, nanogel, micelles, and dendrimers by physical or chemical cross-linking methods for being used in drug delivery, because of their biocompatibility, biodegradability, safety, and cost-effectivity.[16]

Hydrophilic components are dispersed in a hydrophilic polymeric excipient, which upon contact with fluids swells and has the ability to form gels or colloids of high viscosity. During a specific period of time, drugs can be delivered locally or systemically at a predetermined rate through these systems. The kinetic release of the drug from these matrices is mainly influenced by different factors, such as swelling rate, rate of dissolution, diffusion of the drug through the swollen material, and erosion of the matrix.[17] In addition, polymer concentration and polymer properties (e.g., porosity of the matrix or size of the pores) have also been demonstrated to have an effect on the drug release rate.[18] The advantage of the polymeric delivery forms are protecting the drug and reducing the fluctuations of the drug plasma level through a controlled release manner. The difference between the traditional and the controlled release behavior is schematically described in Figure 2.1.[19] Depending on the nature of the polymer employed and on its interaction with the biological media, the system will exhibit a particular release behavior by diffusion through the initial pores of the matrix and the pores that are formed when the drug is dissolved.[20-21]

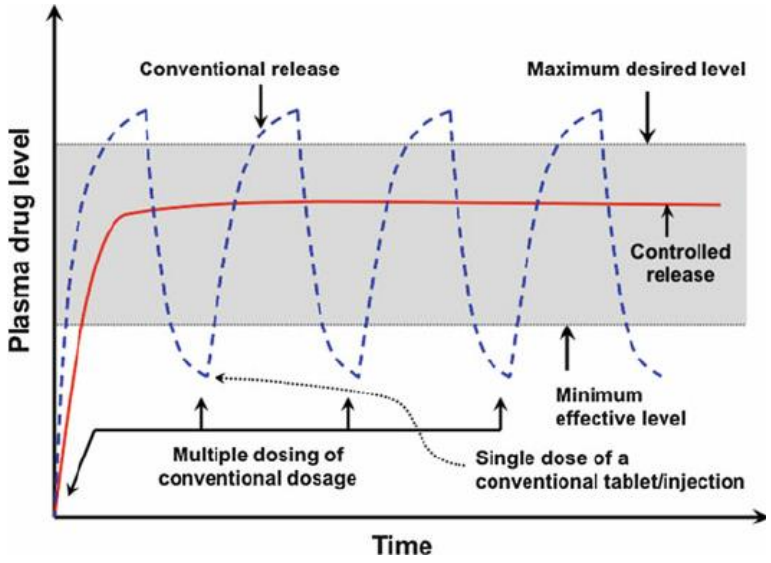

Figure 2.1. Drug levels in the plasma released from a traditional release system, a combination of multiple oral capsules or injection dosing (blue dashed curve), and controlled release system (red continuous curve). [Reproduced with permission from Lee et al.[22]]

2.1.1 Chitin and Chitosan

Chitin is a naturally occurring biopolymer, which is extracted from crustacean shells, including crabs, shrimps, and lobsters. Chitin is recognized as a renewable bio-resource

found in nature.[23] In the molecular structure of chitin, 2-deoxy-2-(acetylamino) glucose is present as the primary structural unit.

Chitosan is produced by the alkaline *N*-deacetylation of chitin.[24] Chemically, the chitosan molecule comprises randomly distributed β (1→4)-linked D-glucosamine and *N*-acetyl-D-glucosamine (Figure 2.2). Chitosan refers to a family of copolymers with different fractions of acetylated units. It is considered to be soluble at acidic pH (less than 6.5), in most of the organic acid solutions, including acetic acid, formic acid, and tartaric acid.[25-26] However, a study of the solubility of chitosan in acidic media by Gaborieau et al.[27] demonstrated that clear "solutions" of chitosan do not ensure complete solubility. These authors proved that acetic acid does not completely dissolve chitosan, while HCl does, but at the expense of reducing the deacetylation. With that respect, many of the chitosan "solutions" found in literature may be in reality "suspensions", even if they are clear. The presence of free amino groups and *N*-acetyl groups in the molecular structure of chitosan determine its aqueous solubility. The presence of those free amino groups exploited chitosan cross-linking ability to produce hydrogels.[28]

On the account of its intrinsic properties, chitosan is used as a biopolymeric excipient in the formulations of various pharmaceutical dosage forms, including matrix tablets, buccal films, microparticles, nanoparticles, pellets, gels, and implants.

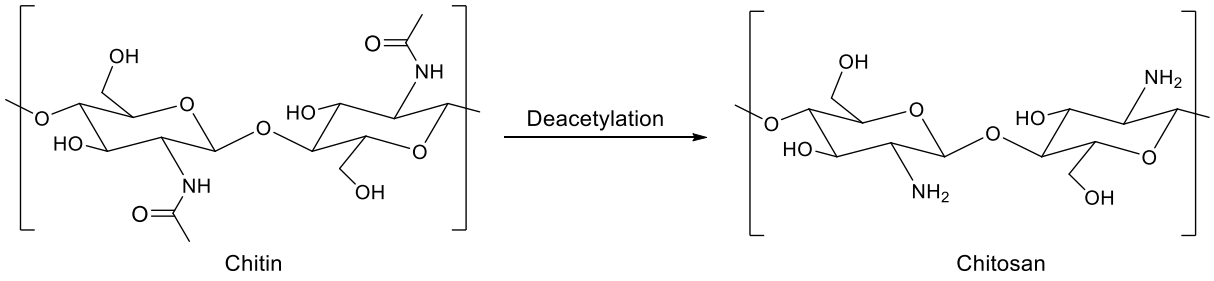

Figure 2.2. Chemical structure of chitosan (right) is obtained by deacetylation of chitin (left).

The nitrogen present on chitosan backbone varies depending on its degree of deacetylation.[29] The nitrogen presents mostly in the form of primary aliphatic amino groups. For this reason, chitosan can be considered as a reactive polymer.[30] Chemical and physical properties can be summarized as follows:

- It is a cationic polyamine, which has a high positive charge density at lower pH values.
- It forms hydrogels with polyanions, it attracts to negatively charged surfaces.
- It forms highly viscous solutions.
- It has reactive amino/hydroxyl groups, readily undergoing chemical modifications and being able to chelate transition metals.

On the other hand, chitosan is safe and nontoxic to normal body constituents and it possesses many desirable biological properties, including hemostatic, bacteriostatic, fungistatic, and anti-cancerogenic properties.[31-32] Chitosan has a wide range of applications, as presented in Figure 2.3, mainly involving biomedicine and environmental protection.

- ***Chitosan in Controlled Drug Release Formulation and Biological Applications***. Chitosan is an ideal candidate for developing hydrogels, which can be used in controlled drug release formulations. However, it also has some limitations, such as its hydrophobicity and a high pH dependence on its physical properties. Therefore, it is not easy to control drug release with chitosan itself because of the various pH values of the internal organs of the human body. This may negatively reflect on the human body because of drug over-release.[33-34] The most commonly used strategy to overcome these limitations is the incorporation of chitosan in an interpenetrating polymeric network hydrogel.
- ***Chitosan as Antibacterial Agent***. Chitosan was found to inhibit the growth of the bacteria families *Fusarium*, *Alternaria*, and *Helminthosporium*. This antibacterial activity may be attributed to the binding of the cationic protonated amino groups of chitosan with the anionic groups of the microorganisms, leading to growth inhibition.[35]
- ***Chitosan as Fat Trapper***. Chitosan fibers are positively charged; they have the ability to bind chemically with the negatively charged lipids, fats, and bile acids.[36] This binding takes place before the digestion of fats and bile acids in the stomach by entrapping them and consequently preventing their absorption by the digestive tract. In addition to that, the combinations of chitosan fibers and fats form a mass, which cannot be readily absorbed and thus can be easily eliminated by the body.

- ***Chitosan in Metal Capture and Treatment of Waste Water.*** Several studies indicated that chitosan has an intrinsic selectivity for some heavy metal ions and it can be therefore exploited in the treatment of wastewater. For instance, some studies have shown that chitosan can be used for the removal of mercury from solutions.[37-38] The results indicate that the efficiency of adsorption of Hg^{2+} by chitosan depends mainly on the quantity of chitosan, the period of treatment, the initial concentration of Hg^{2+}, and the particle size. Chitosan derivatives have also been prepared and investigated for adsorbing different metal ions.[39] These derivatives can be obtained by grafting new functional groups onto the chitosan backbone. These groups increase sorption sites, which can increase the selectivity for the target metal.

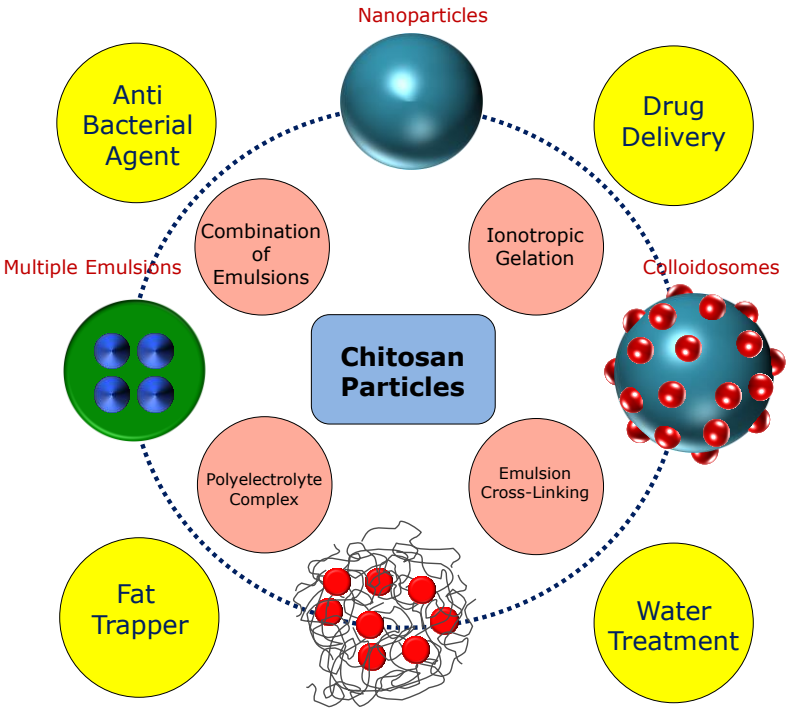

Figure 2.3 General representation of applications of chitosan prepared by using different techniques.

2.1.2 Alginate

Alginate is an anionic polysaccharide occurring in the brown algae cell walls. It is a biopolymer commonly used for pharmaceutical excipients in various kinds of pharmaceutical dosage forms, such as tablets, capsules, gels, beads, microparticles, and nanoparticles.[40-41] Different formulations of alginate-based materials, such as cross-

linked, grafted, oxidized, and thiolated alginates, have been synthesized and used to create improved and smart biopolymeric systems for drug delivery.[42-44]

Both organic and inorganic materials have been combined with alginate matrices to modify the drug-releasing profile over a longer period. The combination can rapidly produce a viscous hydrocolloid by interacting with water.[45]

The geometries of the G-block regions, M-block regions, and alternating regions are substantially dissimilar because of the specific shapes of these monomers and their linkage modes in the alginate molecular structure. An advantage of alginate is its liquid–gel behavior in aqueous solutions.[45-48] Physical cross-linking of alginate is accomplished primarily through the exchange of monovalent sodium ions present in the sodium alginate with divalent and trivalent metal cations (e.g., Zn^{2+}, Ca^{2+}, Ba^{2+}, Cu^{2+}, Cd^{2+}, Pb^{2+}, Al^{3+}, and Fe^{3+}), allowing these guluronic groups to form characteristic “egg-box” modeling structures the reaction proceeds almost immediately, changing from a low viscosity solution to a gel structure.[49] Divalent and trivalent metal cations induce the inter-polysaccharide binding at the cross-linking sites, which are known as junction zones to form cross-linked alginate of insoluble nature.[47, 49]

2.2 Polymeric Hydrogels

Hydrogels are water-swollen three-dimensional networks based on hydrophilic polymer chains, which are held together by chemical or physical cross-linking (Figure 2.4). In a hydrogel, polymer chains maintain well-defined structures with interstitial spaces that are capable of harboring aqueous fluids, such as the physiological ones. Thus, molecules of different drugs can be incorporated into the hydrogel and diffuse from the interstitial spaces to the biological medium, allowing their use as a reservoir for controlled release applications.[50] Therefore, over the years, hydrogels have become key players in the biomedical field in general and pharmaceutical research and development in particular.

On the basis of the responsive nature, gels are generally distinguished by two different types: stimuli-responsive and non-responsive. Stimuli-responsive gels, sometimes named as “smart gels”, have the ability to exhibit unusual changes in their swelling behavior, network structure, or mechanical properties as a response to different external stimuli, such as pH, light, temperature, ionic stretch, or electric field. In general, this swelling occurs in a reversible manner and the structure returns to the original state

upon the removal of the stimulus.[51] For that reason, these gels can be used as sustained-release drug delivery systems to control the release of their load in response to those external changes. Non-responsive hydrogels are simply swollen in water up to thermodynamic equilibrium. The high hydrophilicity of hydrogels is mainly caused by the presence of a number of hydrophilic moieties, such as amino, carboxyl, amide, and hydroxyl groups, distributed along the backbone of the polymeric strands.[52-53] The choice of the material for the synthesis of the hydrogel depends on the application and ranges from fully synthetic polymers, such as poly(ethylene glycol) (PEG) and poly(vinyl alcohol) (PVA), to natural ones, such as polysaccharides (e.g., hyaluronic acid, alginate, chitosan) and proteins (e.g., gelatin).[54-55]

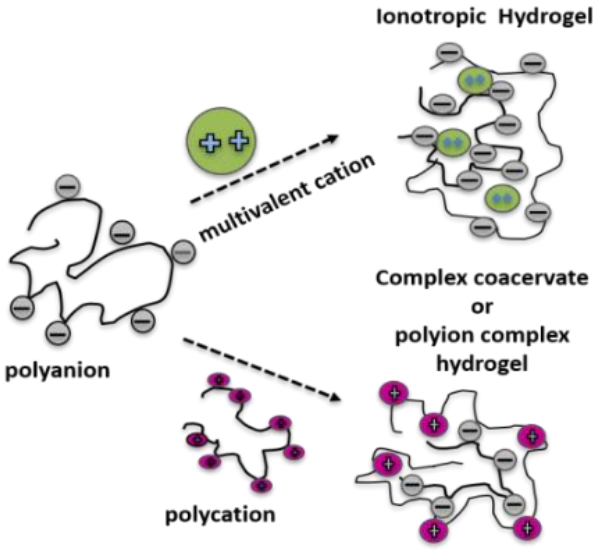

Figure 2.4. Schematic representation of different hydrogel-forming mechanisms: ionotropic cross-linking and complex coacervate formation. [Based on Hoffman et al.[51]]

The equilibrium swelling of the hydrogels usually happens when there is a balance between the osmotic driving forces, which encourages the entrance of water or biological fluids into the hydrophilic polymer, and the cohesive forces exerted by the polymer strands. The magnitude of these forces mainly depends on the cross-linking density and tends to resist the hydrogel expansion. In general, the more hydrophilic the polymer forming the hydrogel is, the higher is the total water absorbed by the hydrogel. In contrast, the higher the cross-linking extent of a particular hydrogel is, the lower is the extent of the gel hydration. The hydrogels in their dried form are usually referred to as xerogels. When some drying techniques, such as freeze-drying or drying using solvent

extraction, are applied, the resulting hydrogels are extremely porous and called aerogels.[56-57]

The appearance of synthetic hydrogels dates back more than forty years ago, in 1955−1960, when Wichterle et al.[58] synthesized and investigated a hydrogel based on poly(2-hydroxy ethyl methacrylate) (PHEMA) for application in contact lenses. Since then, the research and application in the area of hydrogels have dramatically expanded, and the uses have extended to cover various applications, including drug delivery, wound dressing, and tissue engineering.[51, 59]

2.3 Formation of Hydrogels

Depending on the desired structure and application, hydrogels can be formed through different mechanisms of interaction between the polymer strands or between the polymer and the cross-linking agent. These methods, involving either chemical or physical cross-linking, are described below.

2.3.1 Chemical Cross-Linking

The chemical cross-linking of hydrophilic polymers is one of the fundamental methods of hydrogel preparation.[60] This method is based on the addition of a bifunctional cross-linking agent to a dilute solution of the hydrophilic polymer, which should have a suitable functionality to react with the cross-linking agent. The gelation reaction is typically performed in solution, but may also be carried out through a suspension reaction if the desired hydrogel is required to be in the form of beads, spheres, and microparticles. This method is suitable for preparation of hydrogels based on either naturally occurring or synthetic hydrophilic polymers.

2.3.2 Physical Cross-Linking

In addition to chemical cross-linking, the use of physical interactions is a common and easy route for hydrogel formation. Physical cross-linking is present in polymeric hydrogels synthesized by hydrogen bonding, a hydrophobic association, or ionic interactions.[61] Hydrogels can be cross-linked under mild conditions, at room temperature and at physiological pH. Physical cross-linking may not be permanent in nature, but it is sufficient to form hydrogels insoluble in aqueous media. In this thesis, polysaccharides,

such as chitosan and alginate, are used for the preparation of physically cross-linked hybrid hydrogels by ionic interactions.

i. Hydrogen Bonding

Hydrogen bonding between macromolecular chains can also participate in the hydrogel formation. A hydrogen bond is formed through the association of an electron deficient hydrogen atom and a functional group with high electron density.[62] The hydrogel is affected by a variety of factors, such as the polymer concentration, the molar ratio of each polymer, the temperature, the type of solvent and the polymer structure (degree of associations between the polymer functionalities).

ii. Hydrophobic Association

Hydrogels can also be formed through hydrophobic interactions. Polymer systems, such as graft copolymers, block copolymers, and polymer blends, usually form structures separated by hydrophobic microdomains.[63] These hydrophobic domains act as associated cross-linking sites in the whole polymeric structure (Figure 2.5). In general, the mechanical properties of these hydrophobically combined polymers are poor due to the poor interfacial adhesion

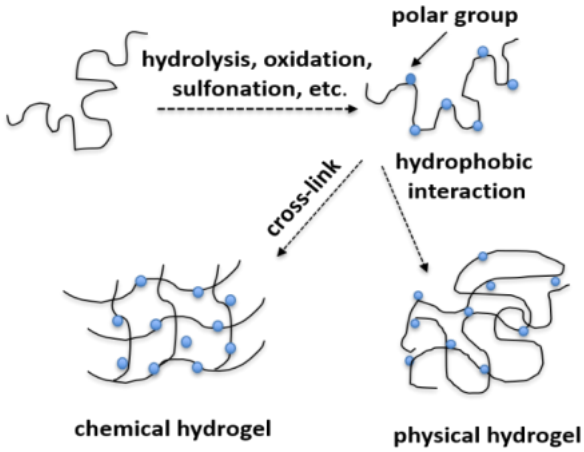

Figure 2.5. Schematic of methods for formation of hydrogels by chemical modification of hydrophobic polymers. [Based on Hoffman et al.[51]]

iii. Polyelectrolyte Complexation (Ionic Interaction)

In polyelectrolyte complexation, the links are formed between pairs of oppositely charged sites along the polymer backbones results in the formation of a complex based on electrostatic interaction. The hydrogels formed by this method are insoluble in water

and the formed electrolytic links vary in their stabilities depending on the pH of the system. This avoids the use of chemical cross-linking agents, thereby reducing the possible toxicity and other undesirable effects of the reagents. Combinations of two oppositely charged biocompatible polymer results in the formation of polyelectrolyte complexes. These complex systems can be used as carriers for active substances.[64] An example of this method is the hydrogel resulting from the polyelectrolyte complexation of the carboxylate groups of sodium alginate with the amino group distributed along the chitosan backbones.[65]

2.4 Different Strategies for the Synthesis of Polymeric Hydrogel Carriers

Several methods have been developed to produce polymeric hydrogel carriers. They may efficiently modify the release or improve the stability and performance of drug substances. The different production methods may result in particles with different properties, including size and charge, which can affect their targeting ability, as well as their capacity for drug encapsulation. The techniques used in this thesis are briefly commented below: ionotropic gelation, spray drying, and the nanoemulsion technique.

2.4.1 Ionotropic Gelation/Polyelectrolyte Complexation

Ionotropic gelation is a method by which hydrogel beads can be generated. It involves the interaction of an ionic polymer with opposite charge ions to initiate the cross-linking. Unlike simple monomeric ions, the interaction of a polyanion with cations (or a polyanion with a polycation) cannot be completely explained by the electro-neutrality principle. The three-dimensional structure and the presence of other groups influence the ability of cations (or anions) to conjugate with anionic (or cationic) functionalities. The advantage of this method is the formation of hydrogel beads by using aqueous solvents, which minimizes the use of toxic organic solvents.[66-71]

In this thesis, chitosan and alginate have been successfully employed to form highly cross-linked hydrogel structures able to encapsulate hydrophilic substances.

2.4.2 Spray Drying

Spray drying is a fast and reproducible method used to prepare dry microparticles. First, an aqueous solution of the polysaccharide is prepared. Then, an atomization of the solution is conducted in an atomizer, which leads to the production of small droplets. Afterward, these small droplets are mixed with a drying gas to evaporate the liquid phase, leading to the formation of polymeric microparticles.[72-73]

In this thesis, we use the spray drying technique for forming a micron-sized gel, which can be applied as a carrier for hydrophilic loads.

2.4.3 Nanoemulsion Technique

Nanoemulsions are very versatile for encapsulating components in the disperse phase. Direct systems (i.e., oil-in-water nanoemulsions) are convenient for encapsulating hydrophobic components, while inverse systems (i.e., water-in-oil nanoemulsions) allow the easy encapsulation of hydrophilic cargos. Here, this method is used to prepare nanohydrogels starting from a nanoemulsion that contains the biopolymer dissolved in the disperse phase. The use of nanoemulsion for the preparation of biomedical nanocarriers is explained with certain detail in the next section, including not only the strategy used in this thesis, but also other nanoemulsion methods found in literature.

2.5 Nanoemulsions for the Preparation of Biomedical Nanocarriers*

Nanoemulsions are kinetically stabilized emulsions with droplet sizes in the nanometer scale. These nanodroplets are able to confine spaces in which reactions of polymerization or precipitation can take place, leading to the formation of particles and capsules that can act as nanocarriers for biomedical applications.

The use of nanoparticles and nanocapsules as carriers of active substances for diagnosis (e.g., bioimaging or biosensing), therapeutics (e.g., drug delivery), or theragnostic (i.e., therapeutic and diagnosis) has evolved a lot in the last two decades and has become a very active and productive research field.[74-76] In preparative chemistry,

* This section is based on the publication: Elzayat, A.; Adam-Cervera, I.; Álvarez-Bermúdez, O.; Muñoz-Espí, R. Nanoemulsions for synthesis of biomedical nanocarriers. *Colloids and Surfaces B: Biointerfaces* **2021**, *203*, 111764.

nanoemulsions have been used as a strategy to synthesize nanoparticles and nanocapsules for a wide range of applications.[77]

The synthetic strategies used in the preparation of biomedical nanocarriers can be divided into those involving polymerization in nanoemulsions (so-called miniemulsion polymerization) and those in which the polymer has been pre-formed and the particle formation takes place without polymerization. The latter case includes the so-called nanoemulsion–solvent evaporation technique and spontaneous emulsification processes ("ouzo effect"). In some approaches, a pre-formed polymer is cross-linked during the particle formation, so that these situations are a somehow at the borderline between both cases; a common example for this is the cross-linking of polysaccharides. Finally, another possibility to form inorganic or hybrid nanocarriers is given by sol–gel processes taking place in nanoemulsions. At the end of this section, we will briefly refer to hybrid cases, in which two polymers are integrated into one material by combination of techniques or in which inorganic components are incorporated in a polymer matrix. The different possibilities described are schematically summarized in Figure 2.6.

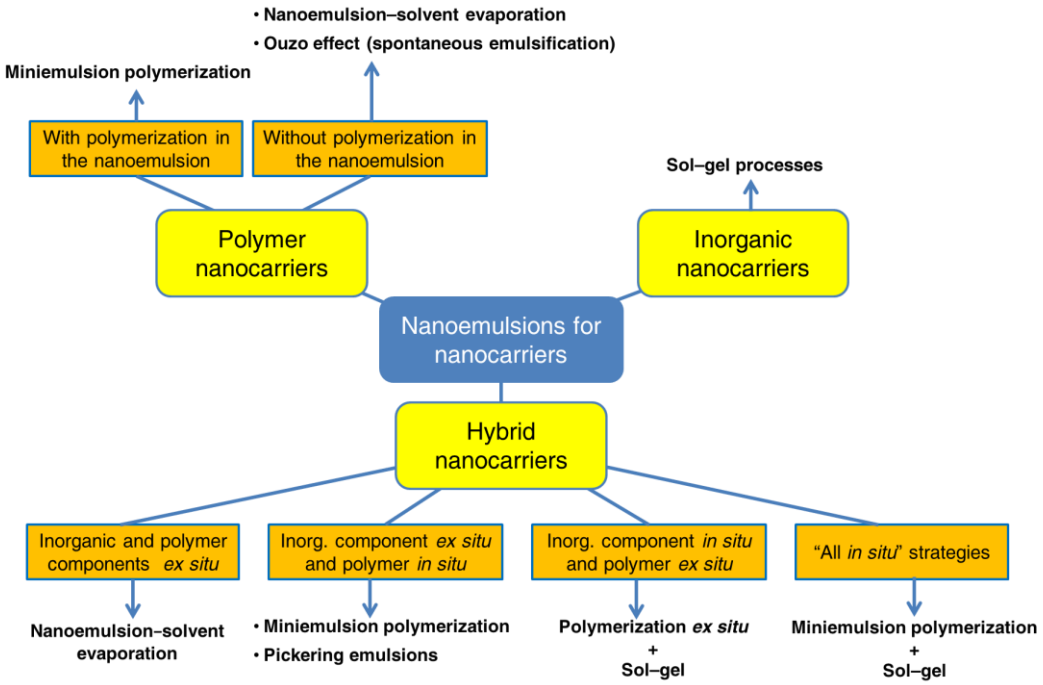

Figure 2.6. General scheme of the synthetic strategies for preparation of nanocarriers from nanoemulsions.

2.5.1 Polymer Nanocarriers Prepared by Miniemulsion Polymerization

The preparation of nanocarriers in nanoemulsions involving polymerization is essentially linked to the miniemulsion polymerization technique, periodically reviewed by Landfester and her team.[78-81] Considering that microemulsions are not supposed to be included within nanoemulsions (nanoemulsions are metastable while microemulsions are thermodynamically stable by definition), microemulsion polymerization has not been included here. The use of microemulsion polymerization in biomedicine is reviewed in literature.[82-83]

Although the term "nanoemulsion polymerization" as such is almost non-existent in literature, there are a few relevant exceptions. In a quite recent publication, Paulis and her group.[84] reported that miniemulsions of lauryl methacrylate polymerized near the phase inversion temperature, following a mechanism of polymerization that differs from conventional miniemulsion polymerization and that they decided to coin as "nanoemulsion polymerization". Other authors, differently, seem to speak about nanoemulsion polymerization without a clear differentiation to miniemulsion.[85] Leaving intentionally aside these rather rare cases, the examples included in the following refer to what traditionally has been termed as miniemulsion polymerization.

- **Direct Systems (Oil-in-Water Nanoemulsions)**

Free-radical polymerization in direct nanoemulsions is probably the most common option to incorporate hydrophobic active substances into polymer nanoparticles. Landfester and her team[86] used 5,6-benzo-2-methylene-1,3-dioxepane to obtain degradable polymeric nanoparticles by a statistical free-radical copolymerization with methyl methacrylate (MMA) and styrene in direct miniemulsion. The obtained particles were tested as drug carriers for paclitaxel bound to human albumin. De Araujo and coworkers[87] synthesized poly(methyl methacrylate) (PMMA) nanoparticles with lecithin as a biocompatible and biodegradable surfactant. They tested the cytotoxicity of the prepared nanoparticles in a leukemia human cell line (THP1) and a human lung adenocarcinoma cell line (A549).

The functionalization with acryloyl groups to obtain polymerizable compounds allows the easy preparation of a great variety of polymers by miniemulsion polymerization, including also amino-acid-based nanoparticles.[88-89] Yamala et al.[90] used

nanocapsules with a shell of poly(*N*-acryloyl-L-phenylalanine methyl ester) to encapsulate sodium nitroprusside.

Hydrogels and nanogels are convenient systems for drug release applications. Chapman and his team[91] prepared a poly(PEGME-MA-*b*-DMAEMA-*b*-*t*BuMA) (PEGMEMA: polyethylene glycol methyl ether methacrylate, DMAEMA: *N*,*N*-dimethyl aminoethyl methacrylate, *t*BuMA: tert-butyl methacrylate) triblock copolymer by RAFT polymerization, which was subsequently dissolved in *t*BuMA, ethylene glycol dimethacrylate, and dodecane. This mixture, containing also the azoinitiator azobisisobutyronitrile (AIBN) as a thermal initiator of the polymerization, served as the disperse phase of an O/W nanoemulsion. The prepared nanogels were fluorescently labeled and loaded with hydrophilic charged peptides. The release behavior was studied by Förster resonance energy transfer (FRET). Also through free-radical polymerization, Malzahn et al.[92] prepared dextran–methacrylate/polyacrylamide nanogels, which were loaded with a zinc salt and used as a bactericide.

In the examples given so far, the polymerization takes place within the nanodroplets. However, in a less common situation, the polymerization can also take place in the continuous phase, yielding a hydrogel. Doyle and coworkers.[93] presented an interesting system based on an “oil-in-pregel” nanoemulsion comprised of low molecular weight silicon oil droplets stabilized in a continuous aqueous phase containing poly (ethylene glycol) diacrylate (PEGDA) and the photoinitiator Darocur1173. After cross-linking of the emulsion by free-radical photopolymerization, a hydrogel is formed. A lipophilic carbocyanine dye (PKH26) was included in the oil core, so that it becomes encapsulated in the matrix and can be liberated upon degradation.

- **Inverse Systems (Water-in-Oil Nanoemulsions)**

The incorporation of hydrophilic substances in the disperse phase of a nanoemulsion requires systems in which the continuous phase is a polar solvent. Often, this solvent may not be biocompatible and even toxic, but it is typically evaporated prior to use of the nanocarriers, which can be resuspended in water or in the desired polar medium. The stabilization of inverse systems is typically more challenging than direct systems, and surfactants with a low value of the hydrophilic–lipophilic balance (HLB) are required. Polyacrylamide hydrogel nanoparticles of about 100 nm in diameter were prepared by free-radical miniemulsion polymerization with Span 80 as a surfactant.[94] The particles

were dried by injection in supercritical CO_2. According to the authors, this supercritical CO_2 drying process allows an efficient extraction of possible residues of the synthesis, such as surfactant and solvents residues, which is of special interest for the pure products needed for many biomedical applications. In another work, Musyanovych and coworkers[95] synthesized a hydrogel based on chitosan nanoparticles by free-radical graft copolymerization. A peroxide-containing chitosan derivative was reacted with 1-vinyl-2-pyrrolidone in the inverse miniemulsion droplets. The decomposition of the peroxide groups in the chitosan generates radicals that start the copolymerization. *N,N*-methylenebisacrylamide is used as a cross-linker. The model dyes sulforhodamine101 (anionic) and rhodamine 123 (cationic) were loaded in the particles and the release kinetics from the hydrogel matrix was studied.

Teymour and his group.[96] reported a synthetic process for poly(ethylene glycol) diacrylate (PEGDA) hydrogel nanoparticles through inverse miniemulsion polymerization. They studied the encapsulation of different phosphate salts, such as sodium hexametaphosphate and potassium phosphate monobasic. In another work about this type of nanoparticles, the same group studied how the variation of the synthetic parameters affects the physical characteristics of the nanoparticles, such as particle size and swelling ratio.[97] In a different work, Peres et al.[98] synthesized physically and chemically cross-linked poly(L-AGA) and poly(L-AGA-*co*-BIS) (L-AGA: N-acryloyl-L-glutamic acid; BIS: *N,N'*-methylenebis (acrylamide)) nanogels by free-radical polymerization in inverse miniemulsion. The authors studied the encapsulation and release of doxorubicin in the particles, as well as the in vitro citotoxicity in HeLa and L929 cells. Controlled radical polymerization techniques, namely atom transfer radical polymerization (ATRP) and reversible addition/fragmentation chain transfer polymerization (RAFT), have also been used in inverse mininemulsion polymerization to form biomedical nanocarriers. The application of ATRP in inverse miniemulsion for drug delivery was reviewed in a feature article by Oh et al.[99]

2.5.2 Polymer Nanocarriers Prepared by Strategies not Involving In Situ Polymerization

The previous subsection has focused on cases in which the polymer formation takes place in situ during the nanocarrier preparation or, at least, in which a polymerization reaction takes place starting from existing polymers (e.g., cross-linking reactions). In the

following, in contrast, we will discuss examples in which the emulsion process leads to the formation of the nanocarrier starting from an existing polymer, previously prepared ex situ. This situation involves a nanoprecipitation of the polymer either after evaporation of a solvent present in the disperse phase (i.e., nanoemulsion–solvent evaporation) or after spontaneous emulsification driven by solubility issues of the components (i.e., so-called ouzo effect).

The emulsion–solvent evaporation process involves the dissolution of a previously formed polymer in a suitable solvent. This polymer solution is dispersed in a continuous phase of a second solvent, immiscible in the first one. After evaporation of the solvent in which the polymer is dissolved, the polymer precipitates in the droplet, forming nanoparticles. If the solvent contains a cargo dissolved, it will be trapped in the formed particles. This method was reviewed with some detail a few years ago by Staff et al.[100] The emulsion–solvent evaporation technique has been often used in pharmaceutical applications for microsized particles,[101] but in recent years it has also been used in nanoemulsions. When nanoemulsions are used, the technique is obviously termed as "nanoemulsion–solvent evaporation". This technique has been used for a wide range of polymeric drug carriers, including polyphosphate,[102] poly(L-lactide),[103-105] or polycaprolactone.[106] Crespy's group has contributed quite importantly to the development of the method in the last years.[106-108]

2.5.3 Inorganic Nanocarriers Prepared by Sol–Gel Process in Nanoemulsion

Silica (SiO_2) is by far the most common inorganic material used for biomedical nanocarriers. Porous silica involving preparation in nanoemulsions is often presented as a very convenient system for drug encapsulation and release.[109-110] The synthesis of silica takes place through a sol–gel process. The alkoxide groups of a silane precursor are immediately hydrolyzed to silanol groups in contact with water, which can occur either under acidic or under basic catalysis. A silica network is produced through condensation of silanol groups, also under acidic or basic catalysis. Sol–gel processes are always controlled by the kinetics of the hydrolysis and the condensation steps. The preparation of silica systems is possible in both direct and inverse systems. In direct systems, alkoxysilane precursors such as the most traditional tetraethoxysilane (TEOS) or bis [3-(triethoxysilyl)propyl]tetrasulfide (TESPT) are dissolved in an organic phase (e.g., hexadecane), which is emulsified in an aqueous phase.[111] Behzadi et al.[112] prepared silica

nanocapsules by hydrolysis of functional alkoxysilanes and subsequent condensation in miniemulsion droplets. Tetrasulfide groups were used as shell-forming materials to achieve redox-responsive shells. Controlled release of cargos from mesoporous silica nanocapsules shows high potential for applications in self-healing materials and drug release. By using a similar methodology, Wu and his group[113] reported the preparation of hollow silica nanospheres with large through-holes by one-step method via a lysozyme-assisted miniemulsion technique. In a more recent work, Jiang et al.[114] demonstrated that different hydrophobic liquids can be encapsulated in the core of silica nanocapsules prepared in inverse nanoemulsions. If solvents with low boiling point are encapsulated, an oil– water exchange can be carried out, as a result of the permeability of silica, which allows the penetration of water after evaporation of the organic solvent. Drugs, such as dextromethorphan can be dissolved in the organic dispersed phase, composed of hexadecane and TEOS. Alternatively, iron oxide nanoparticles can also be dispersed in this phase to a chive multicomponent material. In a further work, the same research group has also studied the uptake of such capsules in T-cell.[115] In inverse systems, the silica precursor is added through the continuous phase, so that it hydrolyzes when it enters in contact with water at the water–oil interface, as schematically represented in Figure 2.7. By using an inverse nanoemulsion, with cyclohexane as a continuous phase and polyglycerol polyrincoleate (PGPR) as a surfactant, Hood et al.[116] synthesized silica nanocapsules with various degrees of surface hydrophobicity, resulting from the concurrent hydrolysis of TEOS and other organosilanes containing a variety of hydrophobic ligands (e.g., cyclohexyl and octadecyl). It was observed that, in general, hydrophobic ligands with longer chain lengths resulted in a greater hydrophobic character on the outer surface of the nanocapsules. The hydrophobicity of the nanocapsules was related to their ability to repulse a basic aqueous medium, thus delaying the degradation of the silica network. In a recent study, Jo et al.[117] prepared silica capsules loaded with glucose oxidase, which are able to produce H_2O_2 to be used in oxidative cancer therapy. The authors dissolve (3-aminopropyl)trimethoxysilane (APTMS) en the aqueous phase and add TEOS from the disperse phase, comprised of toluene and the surfactant PGPR. As a result, silica capsules are formed. By employing similar sol–gel processes in inverse nanoemulsions, hydrous zirconia and hafnia ($MO(OH)_2 \cdot nH_2O$, M = Zr, Hf) can also be prepared by interfacial precipitation in water-

in-oil nanoemulsions, which can also be used to encapsulate hydrophilic substances, such as albumin–fluorescein isothiocyanate conjugate.[118]

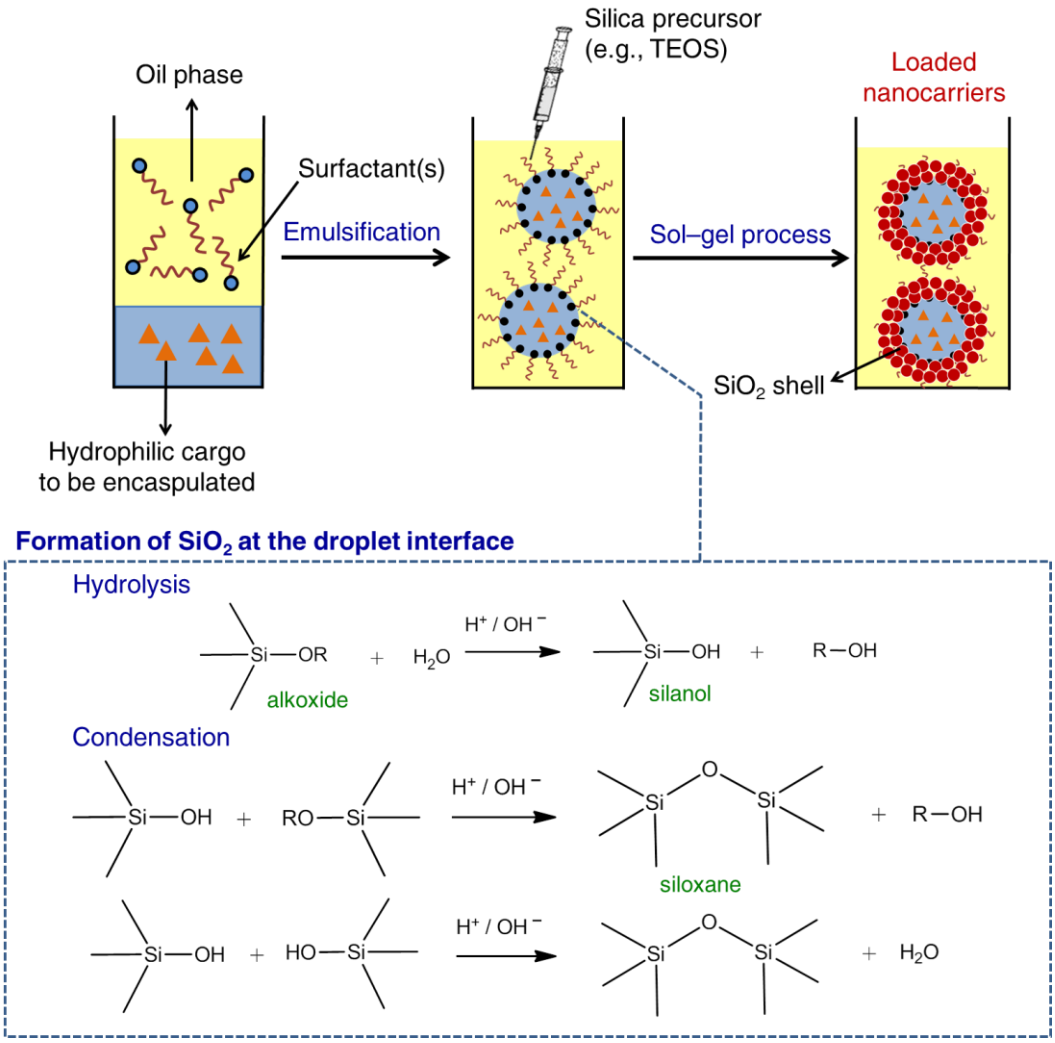

Figure 2.7. Scheme of the formation of silica nanocarriers in inverse nanoemulsions. The reactions present the hydrolysis and condensation of a general alkoxide with rest R.

2.5.4 Polymer/Inorganic Hybrid Nanocarriers by Nanoemulsions

The combination of techniques allows for the preparation of composite systems with more than one polymer component and for the encapsulation of different drugs in the same system. Typically, the preparation of polymer/inorganic hybrid nanocarriers simplifies also the combination of at least two processes: one related to the formation of a polymer matrix and one related to the formation or incorporation of the inorganic component. Most of the situations can be classified in one of the following groups:[119]

(i) Cases in which the formation of both polymer and inorganic components takes place ex situ, and the final carrier is formed by any process leading to their integration.

(ii) Cases in which the inorganic component is formed ex situ and incorporated afterward into a polymer matrix formed in situ in its presence.

(iii) Cases in which the polymer has been formed ex situ and the inorganic component is formed in situ.

(iv) Cases with simultaneous formation in situ of both polymer and inorganic component.

The strategy used in this thesis (Chapter 7) follows the cases of type (iii). Chitosan is dissolved in the disperse phase of an inverse nanoemulsion and the formation of silica nanostructure takes place in situ by a sol–gel process.

Chapter 3

Methodology

3.1 Methods of Preparation of Polysaccharide Hydrogel Carriers

Certain properties of the polysaccharides, such as biodegradability, biocompatibility, and nontoxicity, make them ideal candidates for the preparation of hydrogels for controlled drug release. In this thesis, we used three main different techniques for the preparation of the polysaccharide/silica hybrid hydrogels, from macroscopic to nanosized systems.

3.1.1 Ionotropic Gelation/Polyelectrolyte Complexation

The ionotropic process is simple and mild, and the entire preparation process can be conducted in aqueous media without using any organic solvent. Polysaccharide beads and nanoparticles, made of ionically cross-linked hydrogels, have been widely used in pharmaceutical applications. The schematic representation of gelation process of our work is shown in Figure 3.1. In ionic cross-linking, the entities reacting with polysaccharides are ions or ionic molecules with a well-defined molecular weight. In contrast, in polyelectrolyte complexation, the entities reacting are polymers with a broad molecular weight distribution.[120] In this thesis, a cationic solution of chitosan (aqueous solution in diluted acetic acid) is combined with an anionic solution of sodium triphosphate (STP). The cationic solution of chitosan is added dropwise into the cross-linker STP solution. The formation of chitosan beads is mainly based on the complexation between positively charged amine group of chitosan and negatively charged anions led to the formation of a network through ionic bridges between

polymeric chains by electrostatic force.[121] In addition to the positively charged ammonium groups of chitosan, other groups along the chitosan chains, such as hydroxyl groups can also react with the ionic cross-linker.[122]

Cross-linked macrogel beads form under continuous stirring after precipitation. Physiochemical properties of the resulting particles, such as particle size and surface charge, could be modulated by varying the concentration of chitosan and cross-linking agent and the pH value of the solution.[123] Alginate possesses carboxylate groups (COO^-) that are able to interact with Ca^{2+} ions in the same manner by the gelation process.

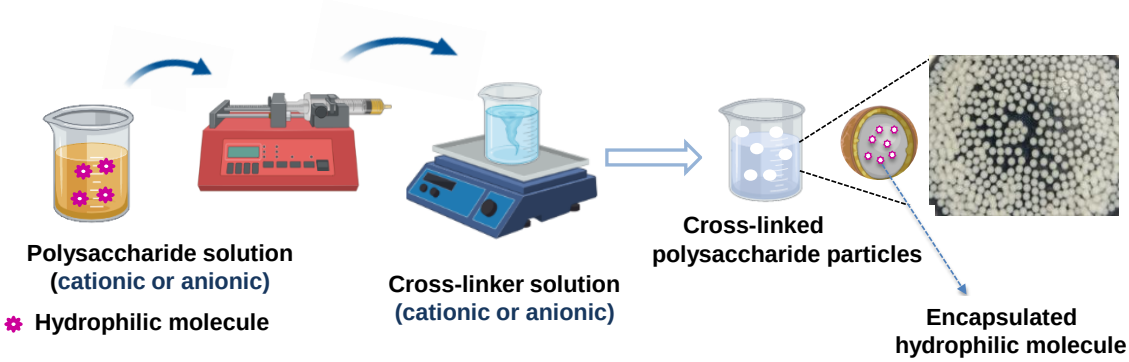

Figure 3.1. Schematic representation of the method of ionic gelation/polyelectrolyte complexation.

The loss of hydrophilic drug during the formation of beads is a limitation of this method. In addition, the matrix formed is usually very permeable, and the drug release is fast and cannot be easily controlled. In this thesis, the incorporation of silica, recognized as safe by the US Food and Drug Administration (FDA), can help to overcome these limitations. Silica has emerged as a component for promising drug vehicles because it is nearly nontoxic, biocompatible, and easy to be surface-modified.[124] Following the same preparation steps as expressed in Figure 3.1, tetraethyl orthosilicate (TEOS) was added in situ to the polysaccharide solution to allow the formation of silica nanoparticles in suspension by a sol−gel process, yielding the formation of a hybrid polymer structure with potential use in the delivery of therapeutic agents. Organic–inorganic hybrid structures are able to protect the encapsulated payloads from the surrounding environment and allow their release in a controlled manner.[108, 113, 125]

3.1.2 Spray Drying

Spray drying is a simple, fast, and reproducible technique that can be used for producing micrometric particles with controlled size. In this work, a nanospray dryer is used to prepare polysaccharides (chitosan and alginate) microcarriers encapsulating hydrophilic substances. A mixture solution of the drug and the excipient was atomized into small droplets and blown into a chamber filled with hot air. The preparation of drug-loaded polysaccharide microcarriers by spray-drying technique is shown in Figure 3.2.

Drug-loaded powders, granules or agglomerates were obtained upon drying of the droplets. First, chitosan was directly dissolved in an aqueous acidic solution (acetic acid 2 wt%) and alginate was dissolved in distilled water. Hydrophilic molecules (model drug systems) were dissolved in the polysaccharide solution.[72] After that, the cross-linking agent was added to the mixture solution of polysaccharide and drug. We used sodium triphosphate (STP) and calcium chloride ($CaCl_2$) as cross-linking agents for chitosan and alginate, respectively. This solution was then atomized into a chamber with a stream of hot air. Small droplets were formed upon atomization and formation of flowing particles with evaporation of solvent. The particle size of the final products could be modulated by varying the preparation parameters, such as atomization pressure, spray flow rate, nozzle size, inlet air temperature, and extent of cross-linking.[73, 126]

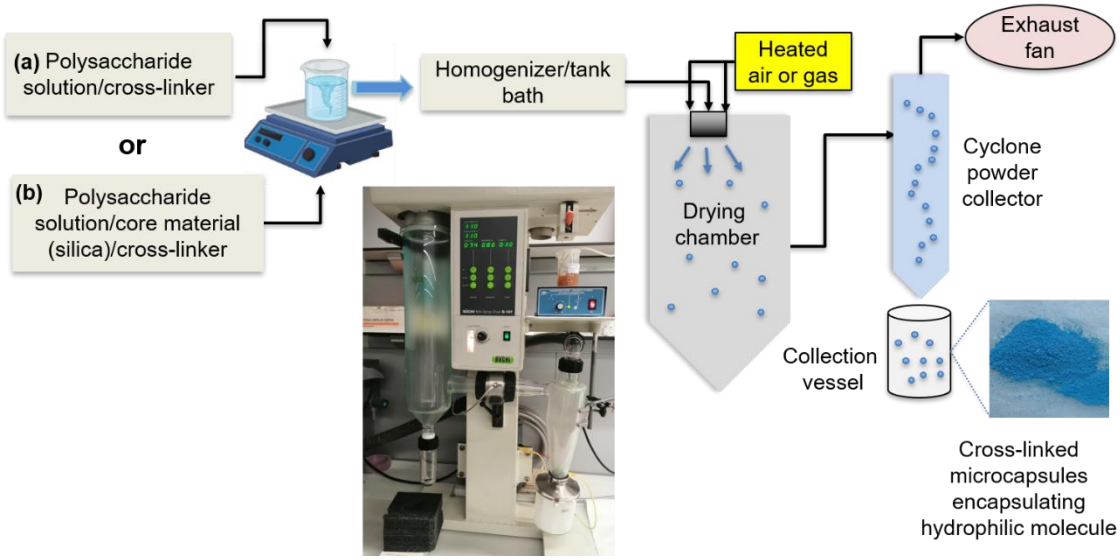

Figure 3.2. Preparation of polysaccharide particle systems by spray drying.

3.1.3 Nanoemulsion Method

Emulsions with droplet sizes in the nanometer scale are referred to as nanoemulsions. Nanoemulsions have been used as a strategy to synthesize nanoparticles and nanocapsules for a wide range of applications.[77] The use of nanoparticles and nanocapsules as carriers of active substances for diagnosis (e.g., bioimaging or biosensing), therapeutics (e.g., drug delivery), or theragnostic (i.e., therapeutic and diagnosis) has evolved a lot in the last two decades and has become a very active and productive research field.[74-76]

Nanoemulsions are very versatile systems for encapsulating components dissolved in the disperse phase. In this work, two different nanoemulsion processes were used for the synthesis of chitosan and chitosan/silica hybrid nanoparticles or nanocapsules through a gelation method.

3.1.3.1 Nanoemulsion Cross-Linking Method

The first route for the preparation of chitosan nanoparticles was based on a water-in-oil (W/O) nanoemulsion, which was prepared by adding an aqueous chitosan solution in an oil phase (cyclohexane). A suitable surfactant (i.e., Span 80) was used to stabilize aqueous droplets. The mixture was ultrasonicated using a ½" sonication tip (Branson W450 digital Sonifier). Then, the cross-linking agent sodium triphosphate was added to allow the ionic interactions between the negative charges of the cross-linker and positively charged amino groups of chitosan.[127-128] The schematic representation of this method is shown in Figure 3.3.

Most of the cross-linkers used to perform covalent cross-linking may induce toxicity if found in free traces before administration. Our method to overcome this problem and to avoid a purification and verification step before administration is to prepare hydrogels by reversible ionic cross-linking.

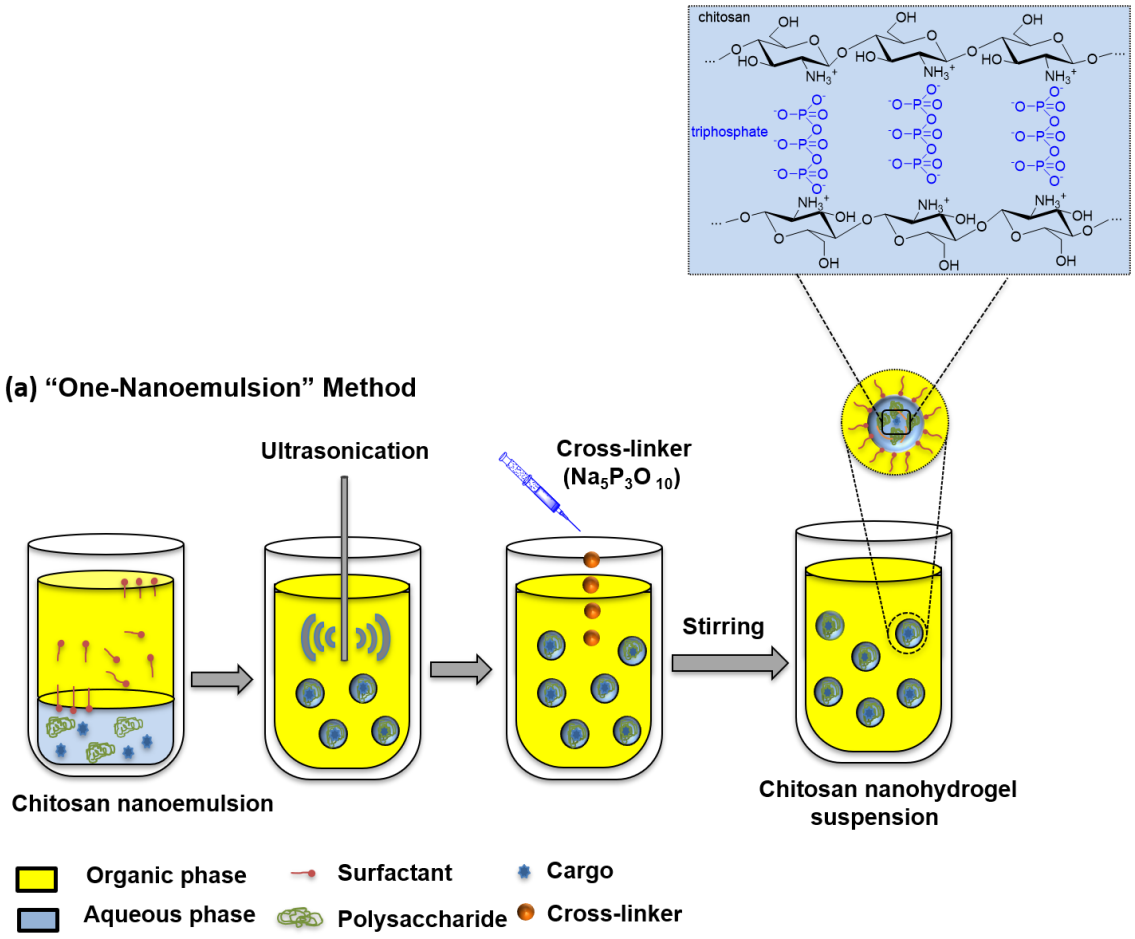

Figure 3.3. Schematic representation of the formation of cross-linked chitosan and hybrid chitosan/silica nanohydrogels by the nanoemulsion cross-linking method for encapsulating active hydrophilic molecules.

3.1.3.2 Nanoemulsion Droplet-Fusion Method

In this method, a first nanoemulsion (W/O) was prepared by adding an aqueous solution of chitosan along with drug to the organic phase (cyclohexane) containing the surfactant (Span 80). The mixture was then ultrasonicated. A second nanoemulsion (W/O) was prepared by adding sodium triphosphate (STP) to an oil phase (cyclohexane) containing Span 80 and then ultrasonicating under the same conditions. Finally, the two nanoemulsions were mixed together. The coalescence of the droplets of both nanoemulsions led to a localized gelation; as a result of that, chitosan nanoparticles were formed by precipitation.[129] The schematic representation of this method is shown in Figure 3.4.

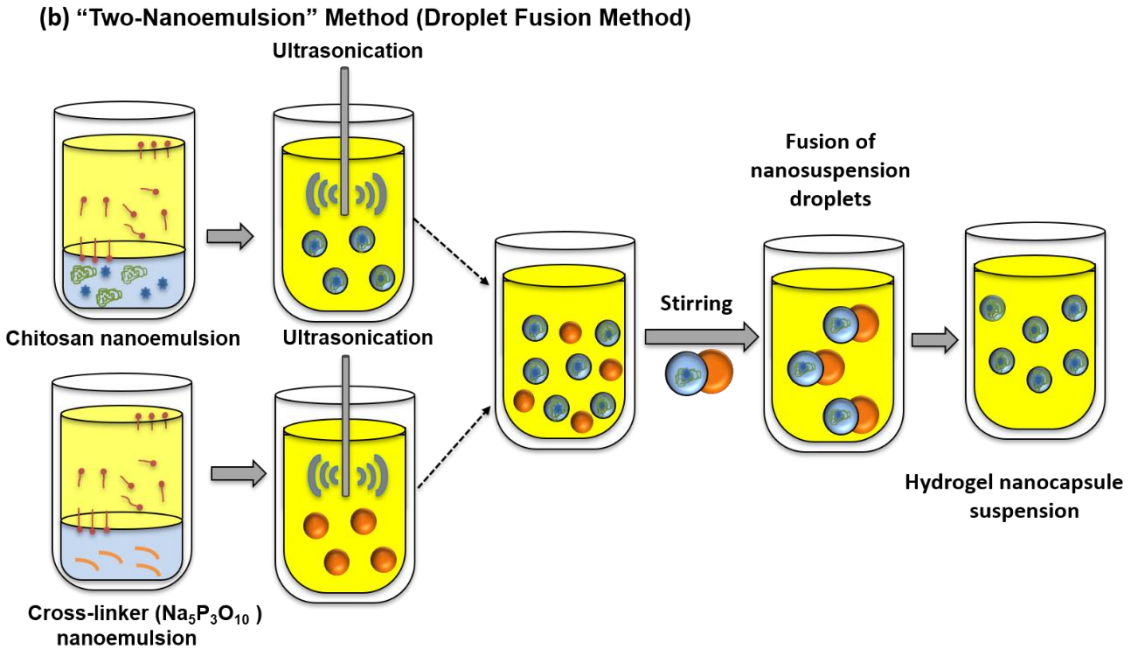

Figure 3.4. Schematic representation of the formation of cross-linked chitosan by the two-nanoemulsion method (fusion droplet-method).

3.2 Characterization Techniques

3.2.1 Scanning Electron Microscopy (SEM)

Scanning electron microscopy (SEM) is based on the detection of secondary electrons emitted from the surface of a sample as a result of the interaction of the material with an electron beam. The beam is generated by thermal emission at acceleration voltages of 0.1–30 kV, and the secondary electrons are observed via a detector sideways located above the sample. SEM is used to determine morphology and size of the particles, the scanning measurements were performed using a Hitachi S4800 scanning electron microscope. Diluted dispersions of chitosan nanoparticles were placed on silicon wafers and dried at ambient conditions. To minimize electrostatic charging, samples of Chapters 4, 5, and 6 were sputter-coated with platinum. For the nanoparticles of Chapter 7, the images were registered in deceleration mode, with an acceleration voltage of 2.0 kV and a final voltage of 0.5 kV.

3.2.2 Thermogravimetric Analysis (TGA)

Thermogravimetric analysis (TGA) offers an evaluation of the thermal degradation experienced by materials within a certain range of temperature. The technique allows us

to detect fusion and evaporation processes and to determine the amount of organic matter present in a sample via the decomposition of C–C bonds. The measurements on this thesis were carried out in a TGA-50 thermobalance (TA Instruments) by heating the samples from room temperature to 1000 °C with a heating rate of 10 ºC min^{-1} under air atmosphere.

3.2.3 Dynamic Light Scattering (DLS)

The technique of dynamic light scattering (DLS) uses the Brownian motion of the particles present in a dispersion to establish a correlation with the particle size and size distribution. The solvent molecules and the surrounding nanoparticles in a colloidal dispersion promote the continuous and random Brownian motion of individual particles. Measurements of size of chitosan nanoparticles were performed by DLS in a Zetasizer ZEN 3600 NanoZS instrument (Malvern Instruments) equipped with a 4 mW He–Ne Laser (λ = 632.8 nm). Scattering photons were collected in back-scattering mode at an angle of 173°. The reported sizes are the intensity-based z-average diameters of three measurements (> 8 runs each).

3.2.4 Transmission Electron Microscopy (TEM)

Transmission electron microscopy (TEM) is a direct imaging technique based on the detection of the electrons transmitted from the interaction between the sample and an electron beam generated by thermal emission in a thermoionic cathode at acceleration voltages of 50–200 kV. The size distribution and morphology of the nanoparticles was checked in a JEOL TEM1010 microscope. A drop of the diluted samples was on a copper grid then left for drying and kept for analysis. Images were taken at an accelerating voltage of 80 kV.

3.2.5 Ultraviolet-Visible (UV-vis) Spectroscopy

Ultraviolet-visible (UV-vis) spectroscopy is an absorption (or reflectance) spectroscopic technique, which determines the amount of light with a certain wavelength in the electromagnetic spectra from the ultraviolet to visible region that is absorbed (or reflected) by a sample. UV-vis spectroscopy has been used in our thesis to study the release of the model hydrophilic substances (the dye Brilliant Blue FCF and ephedrine hydrochloride) encapsulated within the polysaccharide matrix. Concentrations were

determined spectrophotometrically by measuring the maximum absorbance at 629 nm for erioglaucine sodium salt and at 256 nm for ephedrine hydrochloride (SECOMAM UVI Light UV-visible spectrophotometer).

3.2.6 Nanoemulsion Stability Assessment

Nano-emulsion stability was assessed by light backscattering by means of a Turbiscan Lab Expert apparatus at constant temperature (25 ºC) and λ = 880 nm. For this purpose, 15 g of the nanoemulsion were filled in a glass cell tightly closed to avoid solvent evaporation. Backscattering and transmission data were acquired at 180º and 45º, respectively, from the incident beam, for 24 h in intervals of 1 h.

3.3 Release Kinetics and Data Analysis

The release profiles of the substances encapsulated in this thesis were evaluated spectrophotometrically. In the following, we describe the parameters used for comparing the release of different systems and the different models used for fitting the data.

For all systems, the cumulative release (Q, as used in the following equations) was represented as a function of time (t). Model-independent comparison of release profiles was performed thorough the difference (f_1) and similarity (f_2) factors,[130] calculated according to the equations

$$f_1 = \frac{\sum_{j=1}^{n} \left| Q_j - Q_{\mathrm{ref},j} \right|}{\sum_{j=1}^{n} Q_j} \times 100 \tag{3.1}$$

$$f_2 = 50 \log_{10} \left\{ \left[1 + \frac{1}{n} \sum_{j=1}^{n} \left(Q_j - Q_{\mathrm{ref},j} \right)^2 \right]^{-1/2} \times 100 \right\} \tag{3.2}$$

where n is the number of time measurements and $Q_{\mathrm{ref},j}$ stands for the delivery curve with regard comparison is made. Observation of f_1 values below 10, together with f_2 values comprised between 50 and 100, are indicative that the compared profiles are similar. The values of f_1 and f_2 were exclusively taken as model-independent mathematical parameters for comparison of data sets, with no further standardized procedures.

Five kinetic models, described in the following, were tested. The empirical zero-order model in Eq. (3.3) is used when the substance is released into the medium at a constant rate,

$$\hat{Q}(t) = k_0 t \tag{3.3}$$

The Higuchi model,[131] given by Eq. (3.4), describes the release from insoluble/non-erodable matrices, assuming that the diffusion process follows Fick's law. The cumulative release depends on both the square root of time and the Higuchi coefficient K_H, which is related to the diffusive coefficient of the compound:

$$\hat{Q}(t) = K_H t^{1/2} \tag{3.4}$$

Korsmeyer and Peppas[132-133] developed a two parameter kinetic model to rationalize the drug release from polymeric matrices:

$$\hat{Q}(t) = K_{KP} t^n \tag{3.5}$$

The cumulative drug release depends on the rate constant K_{KP} and the exponent n, the value of which is related to the type of release process. Particularly, for matrices with cylindrical shape, the exponent is interpreted as follows: $n = 1$, case II transport; $n = 0.5$, Fickian diffusion; $0.5 < n < 1$, non-Fickian diffusion.[134]

Alfrey et al.[135-136] proposed the empirical model in Eq. (3.6) that maintains the time functionality of the model developed by Narasimhan and Peppas.[137] The last model accounts for drug release from polymeric matrices controlled by both solute diffusion and/or polymer dissolution.

$$\hat{Q}(t) = k_0 t + k_1 t^{1/2} \tag{3.6}$$

Finally, the release profiles were evaluated according to the Hill equation,

$$\hat{Q}(t) = \frac{Q_{max} t^n}{t_{\frac{1}{2}} + t^n} \tag{3.7}$$

where Q_{max} is the maximum percentage of released load at time infinity, $t_{1/2}$ is the time required for 50% of the load to be released, and n is a sigmoidicity exponent. Fixing the value of n to 1 implies a simple sigmoidal model analogous to a Michaelis–Menten-type kinetics. Since the Hill equation (and its simplified Michaelis–Menten form) is formally

analogous to the Langmuir model in heterogeneous catalysis, it is typically used to analyze quantitative drug–receptor relationships.[138] Nevertheless, it can also be used as a convenient empiric relationship to fit release data as a function of time.[139]

Experimental cumulative releases were analyzed according to the different models by minimizing the weighted sum of squares of residuals,

$$\phi(p) = \sum_{t}^{n} w_t \left(Q_t - \hat{Q}_t\right)^2, w_t = 1/s_{Qt}^2 \tag{3.8}$$

where standard deviations of cumulative release (s_{Qt}) were calculated from 4 replicates of the release curves, and the model parameters (p) worked out by minimizing the least-squares function $\phi(p)$ by means of the scaled Levenberg–Marquadt method.[140] The goodness of fittings was stablished through the r^2-adjusted statistical (it was used because the models have different number of parameters), and the lack of fit (LOF) defined in Eq. (3.9), which indicates the percentage of the answer that is not explained by the model:

$$\text{LOF} = \sum_{t}^{n} \frac{\left(Q_t - \hat{Q}_t\right)^2}{Q_t^2} \times 100 \tag{3.9}$$

Chapter 4

Increased Stability of Polysaccharide/Silica Hybrid Submillicarriers for Retarded Release of Hydrophilic Substances*

In this chapter, a loaded organic/inorganic macrogel was prepared by ionotropic gelation, and its efficiency for entrapping hydrophilic molecules was investigated. Chitosan and alginate were used as the main polymer component, and silica was used as a structuring additive to reach a high encapsulation efficiency. Various formulations were selected to study how active hydrophilic molecules (erioglaucine disodium salt (also known as Brilliant Blue FCF) and the drug ephedrine hydrochloride as model hydrophilic loads are entrapped and how the subsequent release can be controlled by tailoring the network structure of the sol–gel matrix, in addition to improve the stability of the drug (e.g., against the hydrolytic and enzymatic degradation of the gastrointestinal tract).

4.1 Introduction

Controlling the release of pharmaceutical compounds to the specific site of action, with increased therapeutic bioavailability and minimized side effects or toxicity, has attracted much attention in recent years. Oral drug delivery is one of the most convenient and preferred routes of drug administration due to both ease of production and flexibility in the design of dosage form, but the barrier of the gastrointestinal tract remains the main obstacle.[1-2]

* This chapter is based on the publication: Elzayat, A.; Tolba, E.; Pérez-Pla, F.F.; Oraby, A.; Muñoz-Espí, R. Increased Stability of Polysaccharide/Silica Hybrid Sub-Millicarriers for Retarded Release of Hydrophilic Substances. *Macromolecular Chemistry and Physics* **2021**, *222*, 2100027.

The incorporation of the drug into a polymeric matrix can enhance its protection against degradation in harsh physiological media and it can prolong the biological activity by controlling the release.[3-4] Recently, a wide range of biopolymers have been used as drug carriers that effectively protect the load from the highly acidic environment of the stomach and enhance the absorption of hydrophilic substances to the specific target.[141]

Natural polymers are good candidates for drug carriers due to their excellent biocompatibility and biodegradability.[142-144] Chitosan is a natural linear polyaminosaccharide obtained by alkaline deacetylation of chitin, which is the second most abundant polysaccharide, next to cellulose.[145] Because of its biocompatibility, nontoxicity, and antibacterial properties, it is a very attractive biomaterial to be used as a drug carrier.[146-148] Sodium alginate is another readily available polysaccharide of nontoxic and biocompatible nature.[30, 149-150]

Chitosan and sodium alginate can both form hydrogel beads when cross-linked with a suitable polyvalent cationic or an anionic cross-linking agent and, hence, they are potentially able to encapsulate a large number of therapeutic molecules in their structure.[151] Depending on the polarity of the polymer matrix, the release of the encapsulated drugs can follow different mechanisms. Water-soluble drugs are mainly released through diffusion, while poorly water-soluble drugs are released by polymer degradation.[152]

The development of new encapsulation techniques had led to an increasing use of these biopolymers in pharmaceutical applications. The technique of ionotropic gelation with polyelectrolyte complexation provides an eco-friendly pharmaceutical product that minimizes the use of toxic organic solvents or cross-linking agents. The process is simple and forms rapidly hydrogels by extrusion of an aqueous solution in the form of droplets into the cross-linking agent receptor. The mechanism of hydrogel formation involves electrostatic interactions between opposite charges, resulting in an ionotropic gelation reaction.[153-156] The loss of hydrophilic drug during the bead formation is a main limitation of this method. In addition, the matrix formed is usually very permeable and causes a fast uncontrolled drug release.

The incorporation of silica, recognized as safe by the US Food and Drug Administration (FDA), can help to overcome these limitations.[124] Silica has emerged as a component for promising drug vehicles because it is nearly nontoxic, biocompatible, and

easy to be surface-modified.[113] Silica nanoparticles in suspension can be formed by sol−gel process in the presence of polysaccharides, yielding the formation of a hybrid polymer structure with potential use in the delivery of therapeutic agents.[106,108-109,125,157-160] Organic/inorganic hybrid structures are able to protect the encapsulated payloads from the surrounding environment and allow their release in a controlled manner.[112,118, 161-162]

4.2 Synthesis and Characterization of Hybrid Submillispheres

Chitosan and alginate cross-linked submillispheres were synthesized by ionotropic gelation through an electrostatic interaction between polyelectrolyte and an oppositely charged cross-linking agent. Chitosan is a cationic polyelectrolyte, with amino groups ($–NH_3^+$) that can interact with the anions of the cross-linker ($P_3O_{10}^{5–}$) Figure 4.1a. Alginate, in contrast, possesses carboxylate groups (COO−) that are able to interact with Ca^{2+} ions Figure 4.1b. To prepare chitosan/silica and alginate/silica hybrid particles, the ionotropic gelation was combined with a sol–gel process leading to the formation of silica, as schematically depicted in Figure 4.1c. Tetraethyl orthosilicate (TEOS) was added to a polysaccharide solution, yielding silica nanostructures upon contact with water.[108] The alkoxide groups of TEOS hydrolyzed to silanol groups in water, which occurs either in acidic (the chitosan case) or under basic media (as it was the case of the alginate systems). A network of nanostructured silica was produced by polycondensation of silanol groups, also under acidic or basic conditions. Subsequently, biopolymer submillispheres were precipitated in a solution of the cross-linker agent during extrusion with a syringe. The forming silica was trapped in the biopolymer matrix, leading to hybrid polymer/silica structures.

The same strategy was carried out during the encapsulation of hydrophilic molecules (i.e., erioglaucine disodium salt and ephedrine hydrochloride) within the polymer/silica network structure.

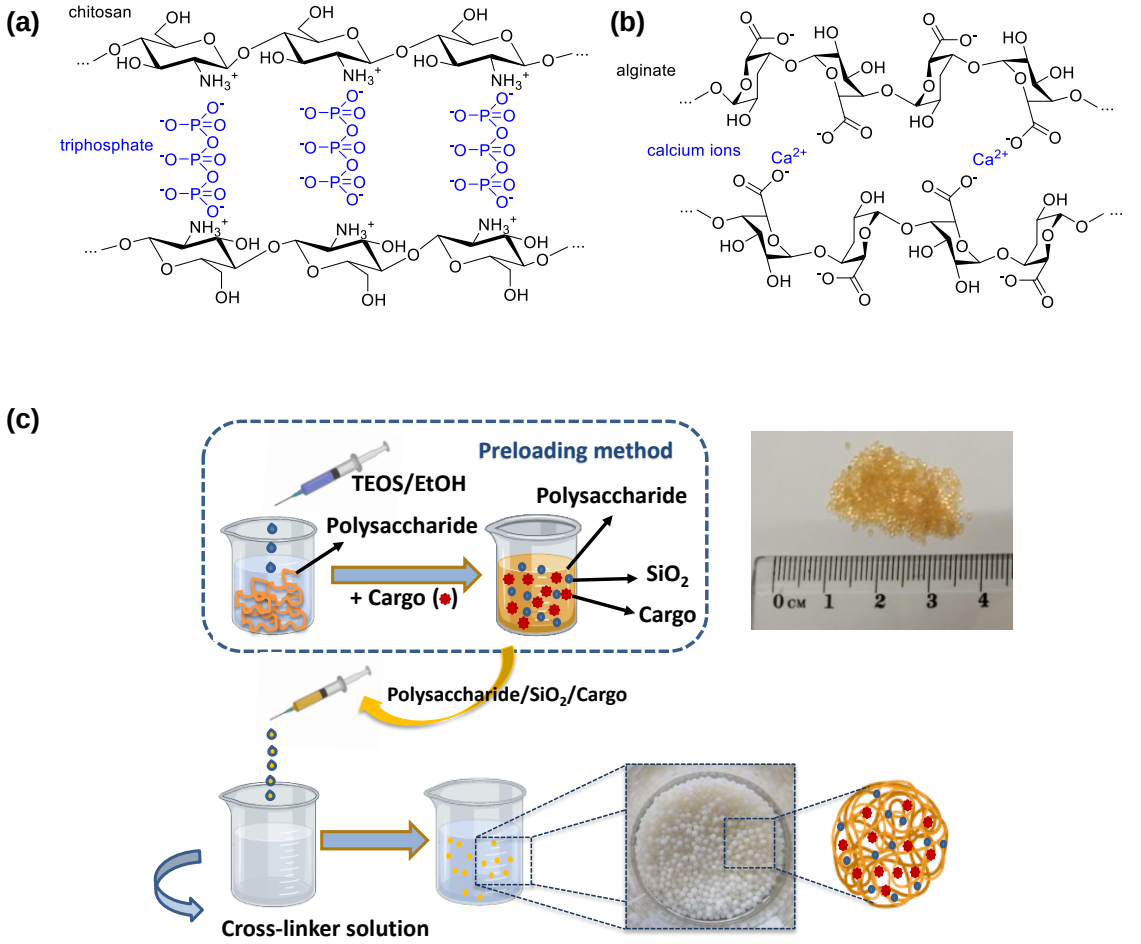

Figure 4.1 (a) Physical cross-linking of chitosan with triphosphate ions. (b) Physical cross-linking of alginate with calcium ions. (c) Schematic representation of the formation of cross-linked polysaccharide/silica hybrid submillispheres encapsulating active hydrophilic linked polysaccharide/silica hybrid submillispheres encapsulating active hydrophilic molecules. The spheres change from white to a more yellowish color (upper photograph) after the drying process

4.2.1 Compositions of the Hybrid Submillispheres

The different compositions of the polysaccharide submillicarriers prepared in this work are summarized in Table 4.1 Chitosan samples were cross-linked with sodium triphosphate (STP) and were prepared either without loading (for subsequent post-loading, samples **S1** to **S3**) or loaded in-situ with erioglaucine (samples **S4** to **S6**) or ephedrine hydrochloride (samples **S10** and **S11**). Alginate samples, labeled as **S7** to **S9**, were cross-linked with calcium chloride ($CaCl_2$) and post-loaded with erioglaucine. The hybrid polysaccharide/silica systems were prepared with two different polymer-to-TEOS weight ratios; namely 3:1 and 3:4.

Table 4.1 Compositions of chitosan and alginate/silica submillicarriers

Sample	System	Cross-linker	Polymer: cross-linker: TEOS weight ratio	Initial load (in situ) [a]
S1	Chitosan	STP	3:12:0	—
S2	Chitosan/silica	STP	3:12:1	—
S3	Chitosan/silica	STP	3:12:4	—
S4	Chitosan	STP	3:12:0	Erioglaucine
S5	Chitosan/silica	STP	3:12:1	Erioglaucine
S6	Chitosan/silica	STP	3:12:4	Erioglaucine
S7	Alginate	$CaCl_2$	3:24:0	—
S8	Alginate/silica	$CaCl_2$	3:24:1	—
S9	Alginate/silica	$CaCl_2$	3:24:4	—
S10	Chitosan	STP	3:12:0	Ephedrine
S11	Chitosan/silica	STP	3:12:4	Ephedrine

[a] Samples without initial load were subsequently post-loaded with erioglaucine

The swelling behavior with time of the prepared submillicarriers, which relates to the ionic character of the polymer network, was evaluated in neutral and in highly acidic media ([HCl] = 0.2 M, pH ≈ 0.7). Figure 4.2a presents the swelling behavior in water (in percentage with respect to the initial mass) at different times for chitosan samples **(S1** to **S3)**, together with optical photographs of the swollen particles.

The swelling percentage under highly acidic conditions is about an order of magnitude higher than in pure water (pH ≈ 7), which is related to the fully protonation of the amino groups in chitosan and the strong ionic interactions with the phosphate groups. Under neutral conditions, the hybrid submillispheres containing silica in the structure decrease the swelling ability about a factor of 2 with respect to the pure chitosan particles, and they remain stable even after 48 h. Under acidic conditions, chitosan spheres are almost fully degraded after 10 h.

In contrast, the incorporation of silica in the structure increases the structural stability, as seen in the photographs Figure 4.2b. At the highest silica content (sample **S3**, polymer-to-TEOS ratio of 3:4), the spheres swell very remarkably with time (more than 1,500% after 24 h), but they retain their structure. This important result indicates that the presence of silica retards or even avoids the dissolution of the chitosan polymer network, which will have implications in the release profile of any encapsulated molecule, as discussed in the last part of this work. The swelling behavior and weight loss at even higher acid concentration ([HCl] = 0.4 M, pH ≈ 0.4) of chitosan particles was also studied (Figure 4.3, Table 4.2).

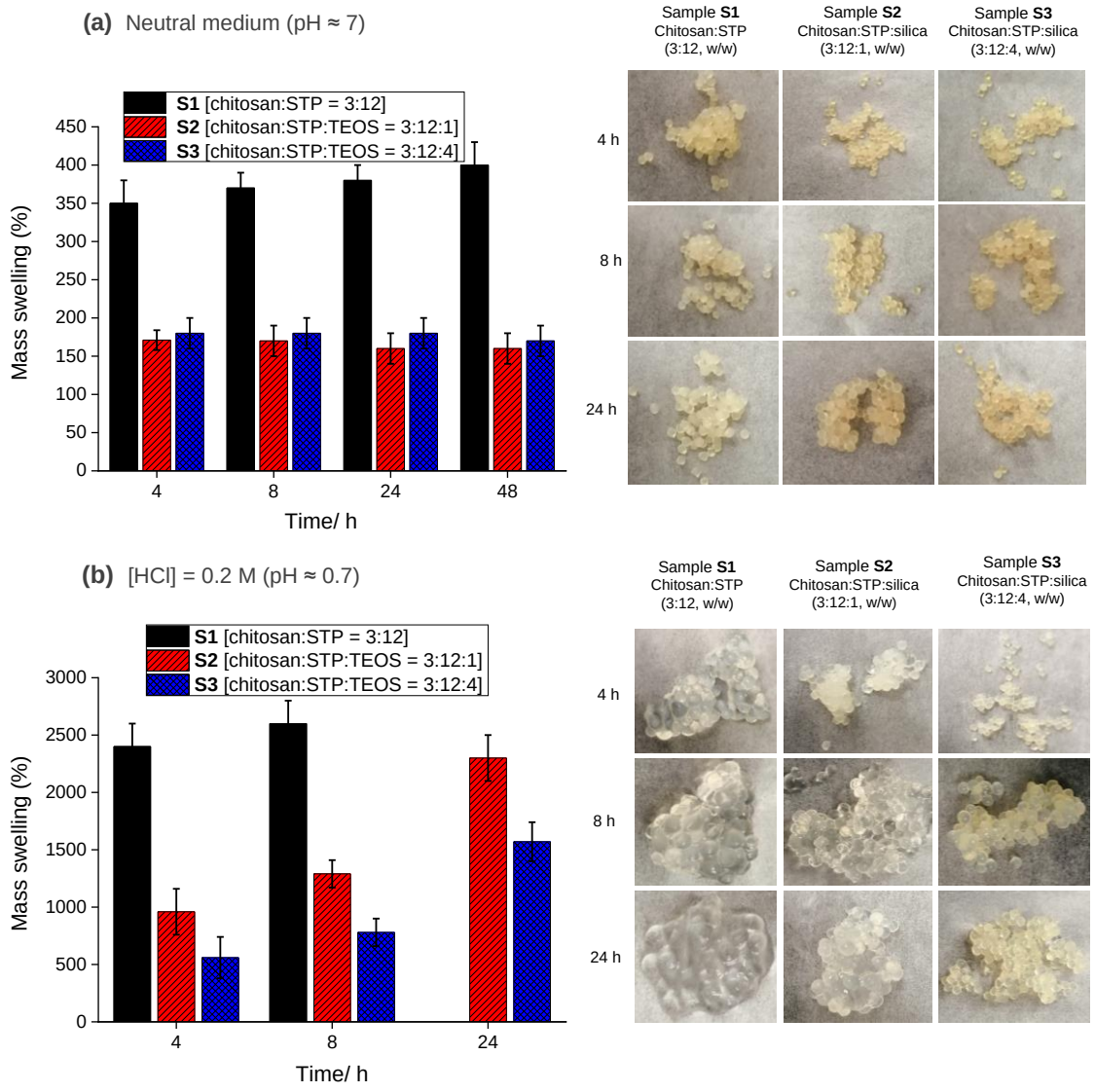

Figure 4.2 Swelling percentage and macroscopic photographs of cross-linked chitosan and chitosan/silica submillispheres with different polymer:cross-linker:TEOS weight ratio (3:12:0, 3:12:1, and 3:12:4, respectively) in two different immersion media: (a) neutral (pH ≈ 7) and (b) acidic ([HCl] = 0.2 M, pH ≈ 0.7) at different times.

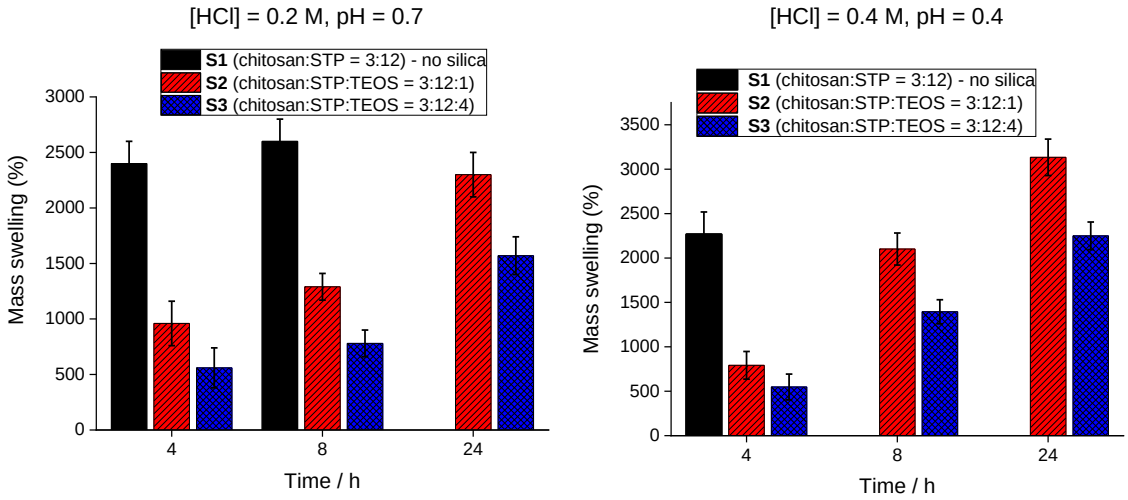

Figure 4.3. Swelling behavior after different times of chitosan and chitosan/silica cross-linked submillispheres in highly acidic media at ([HCl] = 0.2 M and [HCl] = 0.4 M).

Table 4.2. Swelling behavior after different times of chitosan and chitosan/silica cross-linked submillispheres in highly acidic media at ([HCl] = 0.4 M, and [HCl] = 0.2 M).

Time (h)	Mass swelling (%)					
	S1 (chitosan:STP = 3:12)		**S2** (chitosan:STP:TEOS = 3:12:1)		**S3** (chitosan:STP:TEOS = 3:12:4)	
	[HCl] = 0.4 M	[HCl] = 0.2 M	[HCl] = 0.4 M	[HCl] = 0.2 M	[HCl] = 0.4 M	[HCl] = 0.2 M
4	2260 ± 250	2400 ± 200	790 ± 160	960 ± 200	550 ± 150	560 ± 180
8	Hydrogel	2600 ± 200	2100 ± 200	1290 ± 120	1390 ± 140	780 ± 120
24	Hydrogel	Hydrogel	3100 ± 250	2300 ± 200	2250 ± 160	1570 ± 170

Analogously to the chitosan systems, the swelling behavior and the stability of alginate submillispheres (S7–S9) was also investigated Figure 4.4 Alginate spheres are more stable than the chitosan ones in acidic medium, even in the absence of silica, which is related with the different chemistry of alginate and the strong interaction between Ca^{2+} ions and the carboxylic groups of alginate.

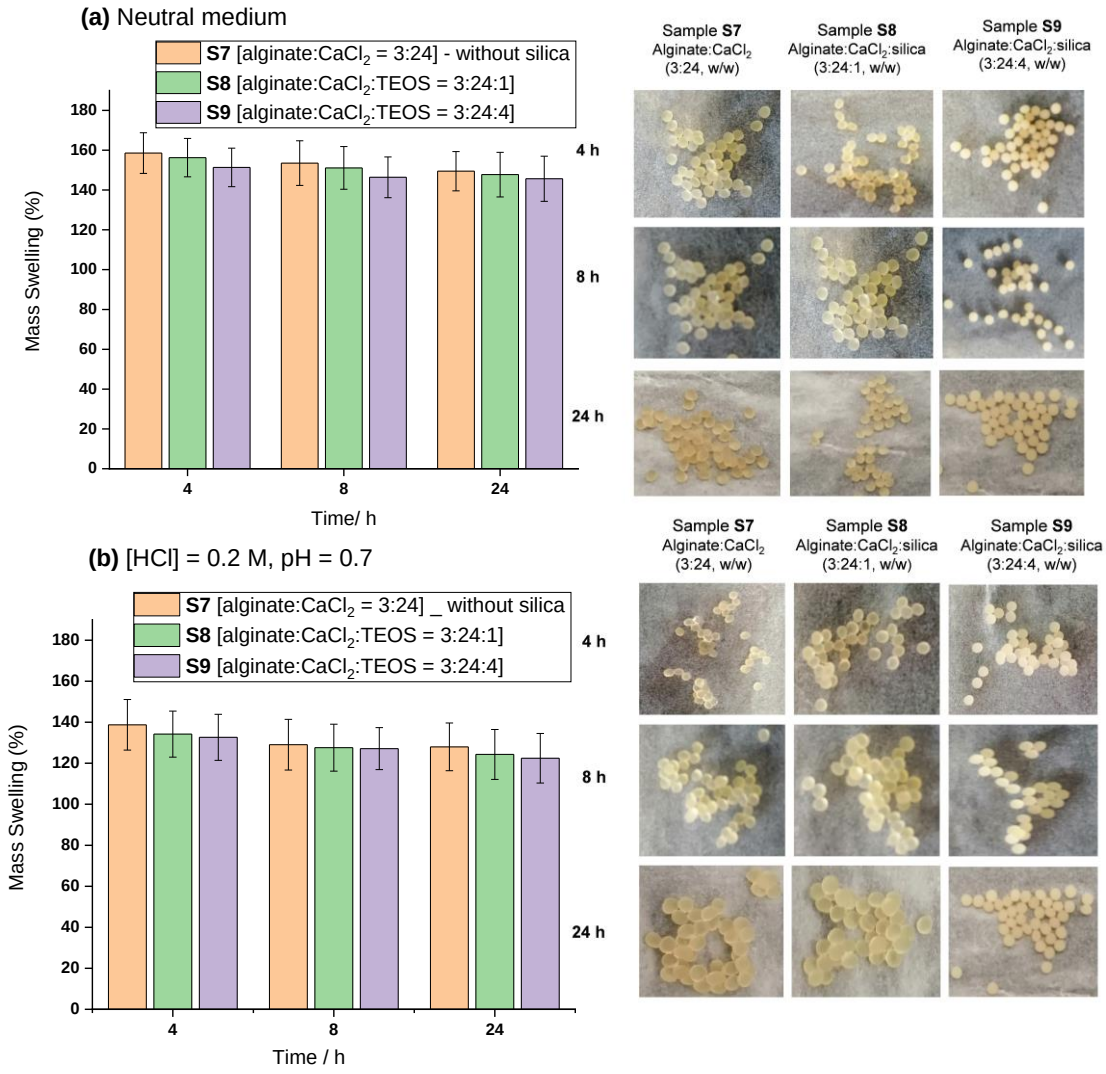

Figure 4.4. Swelling percentage and macroscopic photographs of cross-linked alginate and alginate/silica submillispheres with different polymer:cross-linker:TEOS weight ratio (3:12:0, 3:12:1, and 3:12:4, respectively) in two different immersion media: (a) neutral (pH ≈ 7) and (b) acidic ([HCl] = 0.2 M) at different times.

4.2.2 Morphology of the Hybrid Sub-Millispheres

The morphology of the prepared polymer spheres was compared to the hybrid polymer/silica ones by means of scanning electron microscopy (SEM). The corresponding electron micrographs are shown in Figure 4.5**.** Chitosan submillicarriers (sample **S1**) present a regular and spherical structure with a smooth surface, while chitosan/silica spheres (sample **S3,** polymer-to-TEOS ratio of 3:4) show a certain

roughness, attributed to the presence of silica nanostructures embedded within the chitosan matrix during the formation process. The average size of the particles is 800 ± 50 μm, as statistically measured from SEM micrographs. The formation of silica in alginate submillispheres takes place by a sol–gel process at basic conditions, different from the acidic conditions of chitosan. These different conditions are justified by the different chemistry of the two polysaccharides. Amino groups of chitosan are protonated under acidic conditions, while the carboxylic groups of alginate are deprotonated in basic medium. It is noticeable that alginate particles have an oval shape rather than the spherical one of chitosan particles.

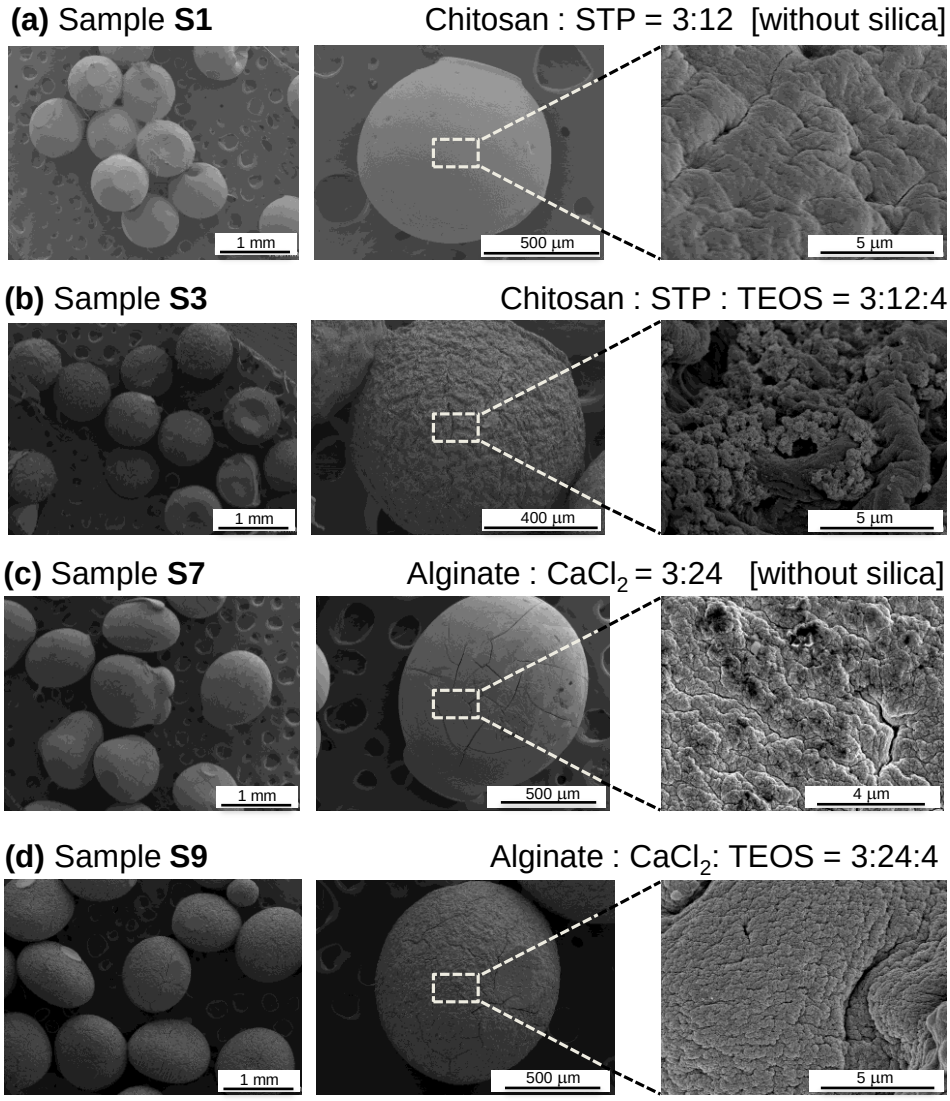

Figure 4.5. Scanning electron microscopy (SEM) images of (a, b) cross-linked chitosan and hybrid chitosan/silica submillispheres, and (c, d) cross-linked alginate and hybrid alginate/silica submillispheres.

4.2.3 Thermogravimetric Analysis of the Hybrid Sub-Millispheres

A thermal analysis (TGA) of the polysaccharide submillispheres was carried out to determine the silica content in the hybrid structures. Figure 4.6 presents the TGA traces of both chitosan and alginate samples. The pristine non-cross-linked polymers (in bulk, without forming spheres) are also shown as a reference.

In chitosan samples, a first decomposition step corresponding to the evaporation of absorbed water is observed at temperatures below 100 ºC, followed by the thermal degradation of the polymer between 200 and 300 ºC. Under the air atmosphere of the measurements, the polymer present in sample **S1** (without silica) degrades completely to water and CO_2, and the final residue corresponds to sodium triphosphate, so that the percentage of polymer is about 60%. Silica-containing samples (samples **S2** and **S3**) show a lower mass loss, in correlation with the formation of silica by hydrolysis of TEOS and subsequent polycondensation. Taking into account that all samples have been prepared with the same initial amounts of chitosan and cross-linker, the amounts of silica are about 4.5% and 9.8%, and the amounts of chitosan are 55.8% and 50.7% for samples **S2** and **S3**, respectively.

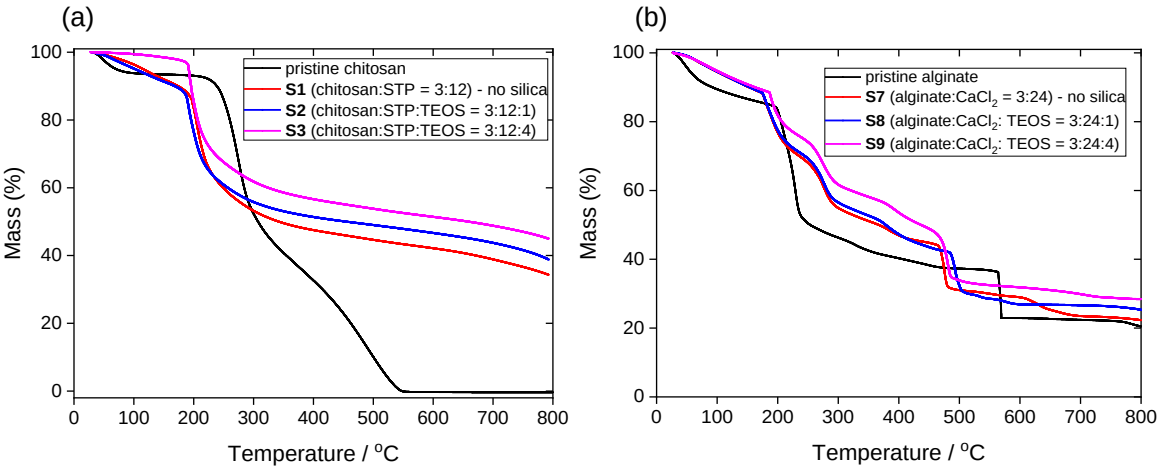

Figure 4.6. TGA traces of (a) chitosan and (b) alginate submillicarriers with different polymer:cross-linker:TEOS weight ratios. Pristine non-cross-linked polymers are also shown for comparison (black lines).

In pristine sodium alginate, an initial and progressive dehydration process at low temperatures (<200 ºC) is followed by two distinct decomposition steps at 200–250 ºC and 550 ºC), with a final solid residue of about 20%, corresponding to the formation of Na_2O. In addition to the dehydration process below 200 ºC, alginate and alginate/silica spheres show several degradation steps between 200 and 500 ºC. The final residue of

samples **S8** and **S9** is higher than for the sample without (sample **S7**), confirming again the formation of silica (about 3% and 5% for samples **S8** and **S9**).

4.3 Encapsulation and Release of Hydrophilic Substances

The submillispheres were loaded with a model hydrophilic substance, namely erioglaucine disodium salt (often referred to as Brilliant Blue FCF), either by an in-situ process involving the dissolution of the drug in the chitosan solution or by a passive loading (i.e., post-loading after formation of the particles). As an example of a real hydrophilic drug, we also carried out a representative release experiment with ephedrine hydrochloride, loaded in situ in chitosan submillispheres.

4.3.1 Release of Erioglaucine Disodium Salt

In the in-situ process, a definite amount of the drug model with respect to the polymer weight is mixed with a chitosan solution that contains nanostructured silica formed during the sol–gel process. The addition of this mixture to the cross-linker solution leads to the desired loaded spheres. The entrapment efficiency for systems with silica increases very significantly with respect to the systems without, almost by a factor of 2 for sample **S6**, which reaches a value close to 40% (Figure 4.7). The release kinetics for those loaded spheres, shown in Figure 4.8, was investigated in neutral (phosphate buffer at pH = 7.4) and acidic media (pH ≈ 0.7) at different times.

In the neutral buffer, the release of the erioglaucine salt is fast and reaches a plateau close to 95% in less than 10 hours. The incorporation of silica in the submillispheres retards the release rate and the system prepared with the highest TEOS ratio (sample **S6**) requires more than double of the time (> 20 h) to reach a constant maximum, about 5% lower than without silica. The effect of silica in the release is much more evident in a highly acidic medium, as observed in Figure 4.8b. Under these conditions, the maximum release is lower than in neutral medium, which could be explained by the strong interaction between the protonated amino groups of chitosan, $–NH_3^+$, and the $–SO_3^–$ groups of erioglaucine (which, even if protonated, would have an electronegative character). As discussed above, chitosan spheres show less stability in acidic conditions, so that for the pristine chitosan sample no plateau is achieved even after more than 25 h.

In contrast, samples with silica, clearly more stable under the same conditions, reach a maximum constant release in about 10 hours, with a cumulated dye release of about 40%. This lower value with respect to the neutral conditions is explained by both the strong complexation of the dye to the chitosan and the adsorption on silica. The experimental curves are empirically fitted to a Hill equation, an empiric model chosen according to the arguments stated in the section of methodology for fitting data to different models.

In the post-loading experiments (so-called passive loading), the prepared submillispheres were inserted in a solution containing a known concentration of the dye. The loading takes place by swelling, diffusion, and adsorption. The maximum loading efficiency was similar to that obtained with the in-situ loading and the entrapment of the erioglaucine was also in this case double as high for the silica-containing samples than for the sample without silica (Figure 4.7). As shown in Figure 4.9, the difference between the silica-containing systems and the ones without silica is very remarkable in this case even under neutral conditions. The mechanism of interaction of erioglaucine with the polymer matrix is different for chitosan and for alginate, because the former contains amino groups, while the latter contains carboxylic groups. This difference is also reflected in the release profiles: as a general trend, the chitosan systems have a higher and faster release than the alginate ones. When comparing acidic and neutral medium, the differences in the chitosan systems are more pronounced than in the case of alginate, in correlation with the observations during the swelling experiments.

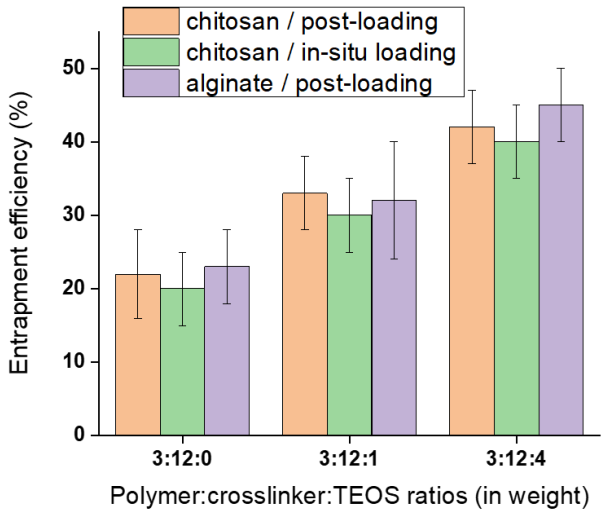

Figure 4.7. Entrapment efficiency (%) for erioglaucine sodium salt loaded in polysaccharide/silica hybrid submillicarriers prepared with different polymer:cross-linker:TEOS weight ratios. In the case of chitosan samples, in-situ loading during particle preparation is compared with the post-loading.

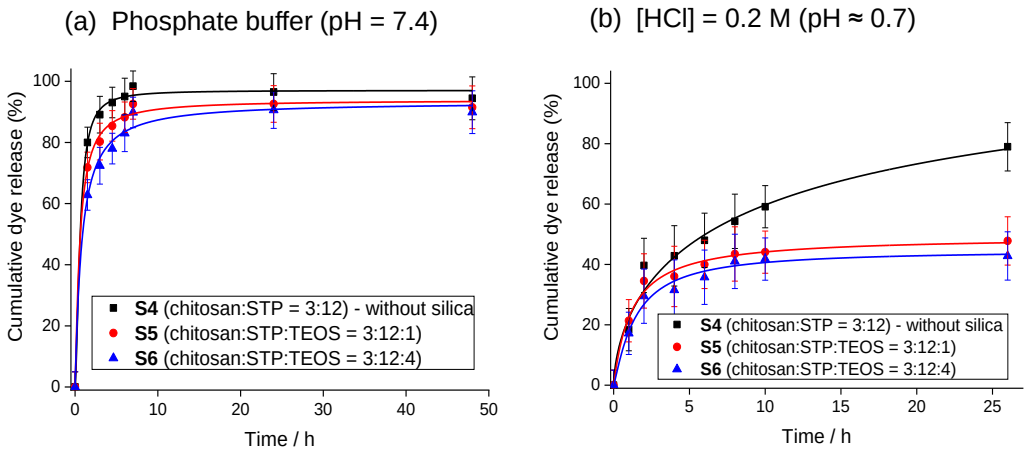

Figure 4.8 Cumulative release of erioglaucine, loaded in-situ process (preloading) in chitosan and chitosan/silica hybrid submillispheres: (a) in phosphate buffer (pH = 7.4) and in (b) highly acidic medium ([HCl] = 0.2 M, pH ≈ 0.7). The solid lines represent the theoretical fitting according to a Hill equation

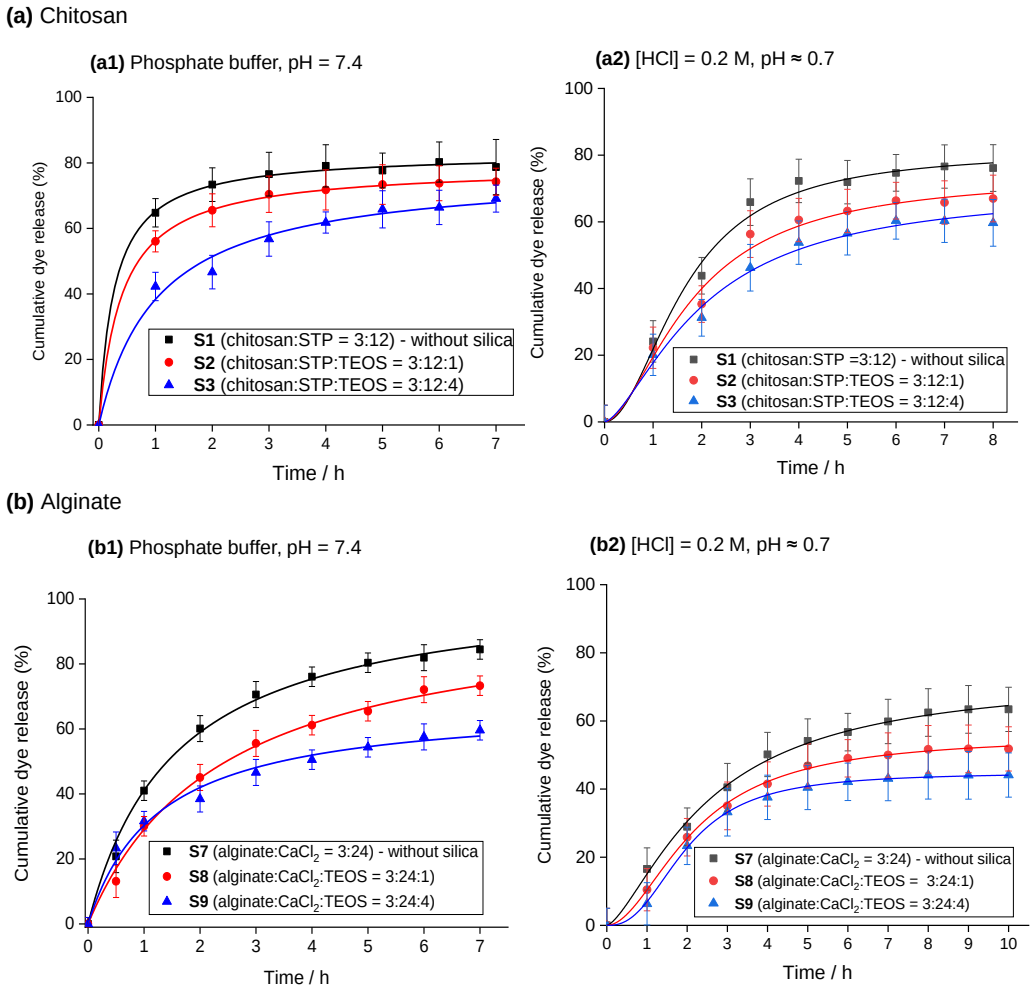

Figure 4.9. Cumulative release in phosphate buffer (pH = 7.4) and highly acidic medium ([HCl] = 0.2 M, pH ≈ 0.7) of (a) chitosan and (b) alginate submillispheres post-loaded with erioglaucine disodium salt. The solid lines represent the theoretical fitting according to a Hill equation.

4.3.2 Release of Ephedrine Hydrochloride

Ephedrine hydrochloride, model for a real hydrophilic drug, was loaded in situ in chitosan carriers. The corresponding results are shown in Figure 4.10. In comparison with erioglaucine, this hydrophilic drug is a much smaller molecule and can be very easily adsorbed. As in the rest of the cases, the entrapment is very efficient in silica-containing particles (Table 4.3) and the release under neutral conditions is not only significantly retarded, but it reaches cumulated values below 20%.

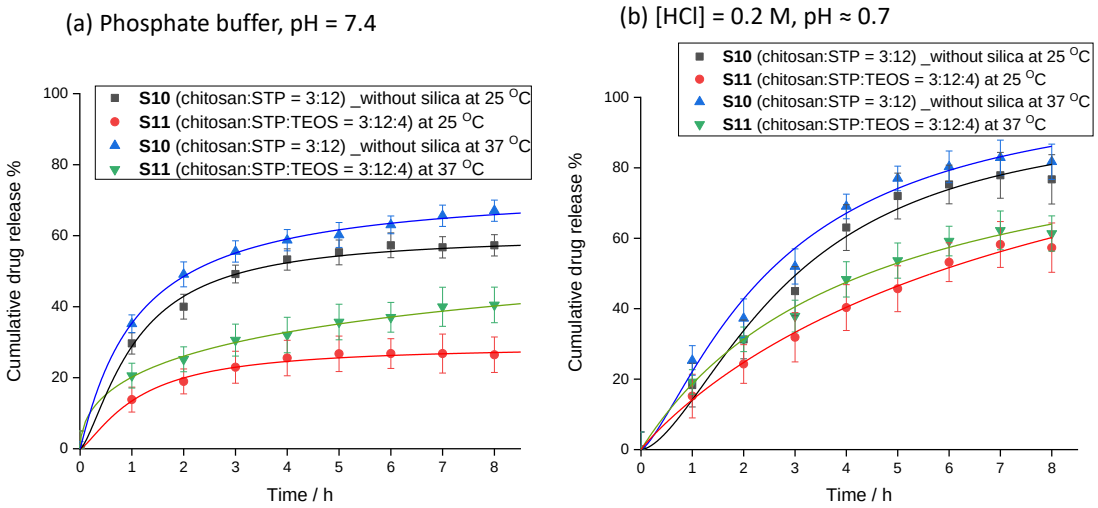

Figure 4.10. Cumulative release at 25 and 37 ºC of ephedrine hydrochloride loaded in situ during preparation of cross-linked chitosan and chitosan/silica submillispheres (phosphate buffer, pH=7.4, [HCl] = 0.2 M, pH ≈ 0.7). The lines represent the theoretical fitting according to a Hill equation.

Table 4.3. Entrapment efficiency (%) for ephedrine hydrochloride loaded in situ during particle preparation in polysaccharide/silica hybrid submillicarriers

Sample	Composition (weight ratios)	Entrapment efficiency (%)
S10	chitosan:STP (no silica) = 3:12	25 ± 10
S11	chitosan:STP:TEOS = 3:12:4	40 ± 10

In this case, the release was measured at 25 and 37 ºC, since the latter temperature is the commonly used for testing biologically relevant drugs. As expected, the release is slightly faster and higher at the uppermost temperature. The higher release at 37 ºC can be easily explained by an Arrhenius-type kinetics, and the higher values point towards an entropy-driven process. In acidic conditions, the release of the drug reaches higher values than in the neutral medium. This behavior, different from the observed for

erioglaucine, is coherent with the degradation of the polymer in acidic media, which facilitates the release. The strong interactions between the cargo and the matrix under acidic conditions taking place in the case of erioglaucine do not occur with ephedrine.

The morphology of the particles loaded with ephedrine was analyzed by scanning electron microscopy (SEM). The corresponding electron micrographs, shown in Figure 4.11 indicate that the sample with silica presents a very distinct and homogeneously distributed roughness in the surface, resulting from the nanostructures formed during the sol–gel process and responsible for the high entrapment of the drug.

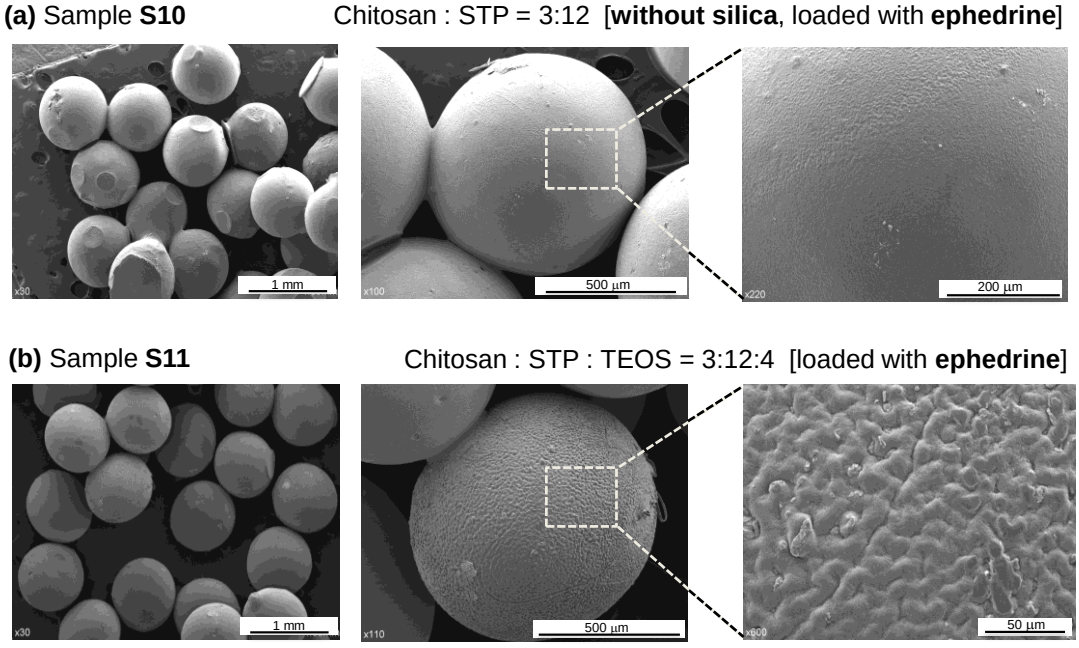

Figure 4.11 Scanning electron microscopy (SEM) images of (a) chitosan and (b) chitosan/silica cross-linked sub-millispheres loaded ephedrine hydrochloride.

4.3.3 Evaluation of Different Kinetic Models

Regardless of the theoretical or empiric model used for the fitting, the difference between experimental release profiles can be directly evaluated with the difference factor (f_1) and the similarity factor (f_2), explained in Chapter 3, Section 3.3. We have mathematically compared with these parameters the experimental sets of each of the graphs contained in the work (i.e., the systems with silica with the one without, and the two systems with silica with each other, when appropriate). The calculated values of f_1 and f_2 for the different profiles, presented in Table 4.4, are consistent with the observable differences of the release curves.

Table 4.4. Difference factors (f_1) and similarity factors (f_2) for the different release profiles shown along the paper (the figure number corresponds to the number in Chapter 4).

Figure	Loading method (cargo)	pH	Samples			f_1			f_2		
			i	*J*	*K*	*Ij*	*Ik*	*Jk*	*Ij*	*Ik*	*Jk*
4.8 a	In situ (erioglaucine)	7.4	**S4**	**S5**	**S6**	6.3	14.1	7.3	62.7	46.7	60.1
4.8 b	In situ (erioglaucine)	0.7	**S4**	**S5**	**S6**	23.4	42.4	11.6	43.4	39.1	70.1
4.9 a1	Post-loaded (erioglaucine)	7.4	**S1**	**S2**	**S3**	8.5	22.9	15.7	60.0	38.3	47.8
4.9 a2	Post-loaded (erioglaucine)	0.7	**S1**	**S2**	**S3**	13.6	23.2	11.1	53.4	41.9	60.5
4.9 b1	Post-loaded (erioglaucine)	7.4	**S7**	**S8**	**S9**	43.7	21.3	19.3	34.7	50.3	46.0
4.9 b2	Post-loaded (erioglaucine)	0.7	**S7**	**S8**	**S9**	16.6	27.8	13.4	54.8	42.3	62.0
4.10 a	In situ (ephedrine), 25 °C	7.4	**S10**	**S11**	–	52.9	–	–	29.4	–	–
	In situ (ephedrine), 37 °C	7.4	**S10**	**S11**	–	41.9	–	–	31.7	–	–
4.10 b	In situ (ephedrine), 25 °C	0.7	**S10**	**S11**	–	29.0	–	–	38.1	–	–
	In situ (ephedrine), 37 °C	0.7	**S10**	**S11**	–	26.2	–	–	38.7	–	–

For a more accurate evaluation of the release process in our systems, experimental data were analyzed using the five different models described in Chapter 3, Section 3.3 (Eq. 3.1–3.7): zero-order, Higuchi, Alfrey, Korsmeyer–Peppas, and Hill models. As a representative example, Figure 4.12 contains the fittings to the different models corresponding to Figure 4.8a. The rest of the fittings are presented at the end of this thesis in the Appendix (**A1** to **A7**).

The choice of the best model was made by comparing the values of the lack-of-fit (LOF, Eq.3.9), calculated from the least-squares fitting to the various models (the values for the different curves of the work and the different models are given in Table 4.5). As a general conclusion, the Hill model (LOF ≈ 3% and LOF ≈ 5% with n = 1), explains better the drug release kinetics than the other tested models.

The Korsmeyer–Peppas and Alfrey models exhibit similar LOF values (slightly higher than 7%), whereas the Higuchi model (LOF ≈ 19%) is far from explaining most of the experiments. It is worth noting that the zero-order model does not fit the experimental data in most cases, as curvature of release profiles occurs from the very beginning. Nevertheless, such zero-order kinetics could be admitted for some experiments carried out in acidic media (see Figures **A3**, **A5**, and **A7**, Appendix) and the corresponding LOF values in Table 4.6.

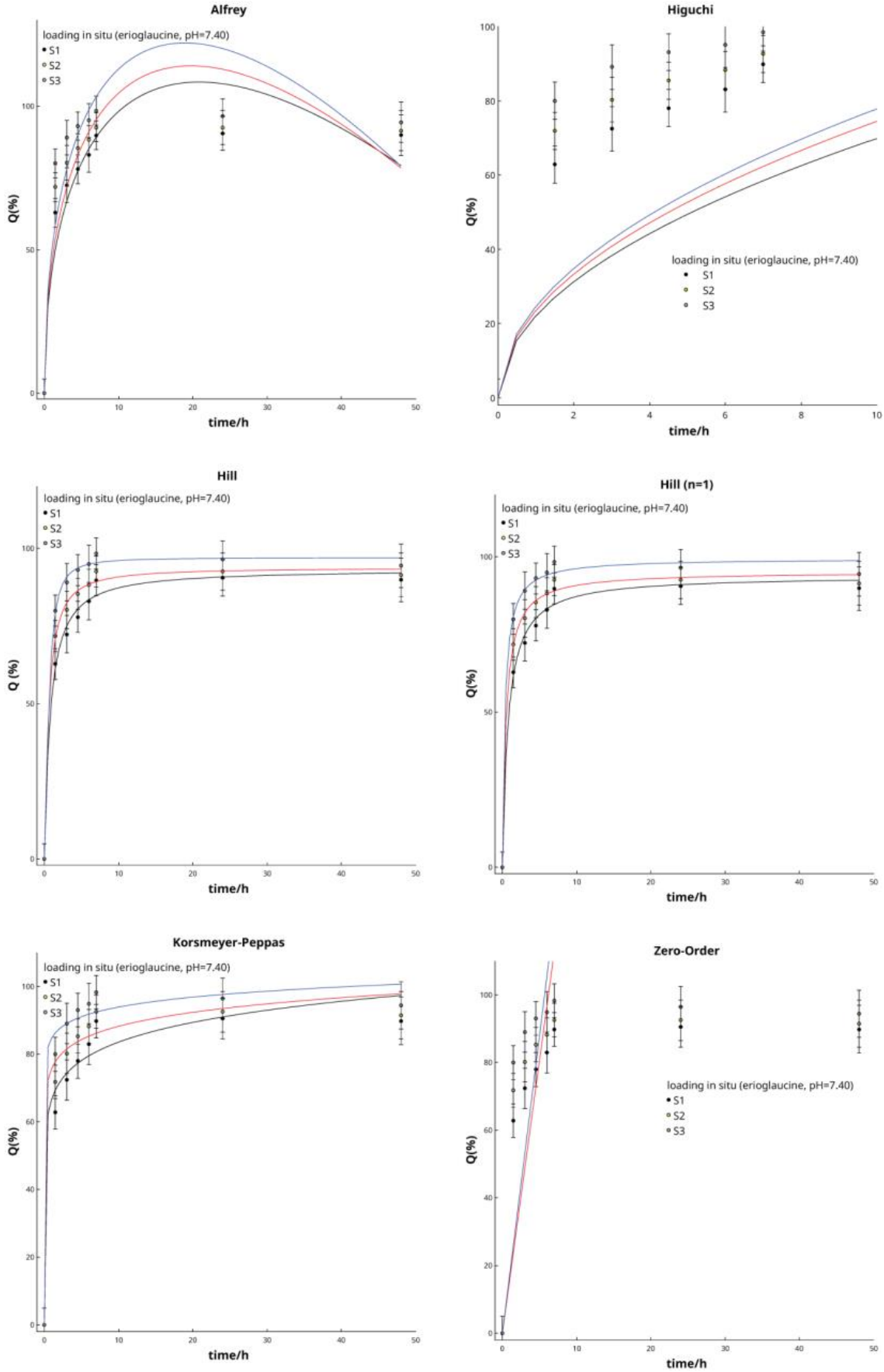

Figure 4.12. Fittings to the different models corresponding to Figure 4.8a.

Table 4.5. Fitting parameters for the release profiles of this chapter according to the different studied models (cf. Figures A1–A7) in the Appendix section.

		Hill					Hill (n=1)			Higuchi		Kosmayer-Peppas			Alfrey				Zero-order	
Figure No.	Carrier	Q_{max}	*s*	$t_{1/2}$	*s*	*n*	*s*	Q_{max}	*s*	$t_{1/2}$	*s*	K_H	*s*	K_{KP}	*s*	*n*	*s*	k_1	*s*	k_2	*s*	k_0	*s*
Fig. 4.12	S4	93.26	3.9	0.78	0.1	1.06	0.3	93.97	2.1	0.77	0.1	22.09	4.0	66.84	3.9	0.10	0.0	47.51	2.9	-5.21	0.6	17.61	3.0
	S5	93.84	2.2	0.51	0.1	1.19	0.3	95.24	1.4	0.49	0.1	23.54	4.5	75.86	3.3	0.07	0.0	51.33	3.7	-5.77	0.7	16.15	2.5
	S6	97.03	1.6	0.43	0.1	1.66	0.5	99.49	1.5	0.34	0.1	24.61	5.1	84.86	3.4	0.04	0.0	56.13	4.6	-6.45	0.9	17.61	3.0
Fig. A1 Appendix	S4	44.83	2.8	1.52	0.2	1.17	0.3	46.76	1.6	1.53	0.2	11.65	1.3	22.75	2.5	0.23	0.0	21.40	0.8	-2.55	0.2	5.01	0.7
	S5	126.75	50.9	4.70	1.9	0.62	0.2	84.26	6.4	3.63	0.9	17.71	1.0	25.19	2.3	0.36	0.0	24.53	1.6	-1.79	0.4	6.86	0.9
	S6	49.27	3.1	1.20	0.2	1.01	0.2	49.45	1.3	1.20	0.2	12.91	1.4	26.53	2.2	0.20	0.0	23.78	1.1	-2.87	0.3	5.46	0.9
Fig. A2 Appendix	S1	81.25	1.6	0.25	0.0	1.29	0.3	83.29	0.7	0.28	0.0	39.13	3.6	66.28	1.2	0.11	0.0	81.05	3.1	-20.11	1.5	34.84	7.4
	S2	77.54	0.8	0.38	0.0	1.14	0.1	78.96	0.3	0.41	0.0	34.47	3.2	57.39	1.1	0.14	0.0	69.82	2.0	-16.09	0.9	31.94	6.9
	S3	167.77	209.3	3.07	5.0	0.40	0.3	77.16	2.9	0.97	0.2	29.44	1.3	41.78	1.3	0.27	0.0	46.88	2.0	-7.95	0.9	22.53	4.0
Fig. A3 Appendix	S1	81.26	3.6	2.72	0.4	1.96	0.3	107.27	9.6	2.57	0.6	30.74	1.2	34.24	4.5	0.43	0.1	38.47	5.8	-3.35	2.4	22.11	0.3
	S2	74.02	5.3	2.80	0.5	1.71	0.3	96.30	8.5	2.85	0.7	26.62	0.9	28.70	3.6	0.45	0.1	31.59	4.7	-2.15	2.0	18.61	0.7
	S3	70.21	5.8	2.96	0.4	1.52	0.3	89.58	6.9	3.17	0.6	23.79	0.7	24.75	2.7	0.48	0.1	26.65	3.7	-1.24	1.6	15.85	0.7
Fig. A4 Appendix	S4	152.65	55.0	3.91	1.8	0.48	0.1	68.13	2.3	1.25	0.2	24.53	0.8	31.32	0.5	0.34	0.0	35.30	0.8	-4.88	0.3	18.77	2.9
	S5	93.10	1.4	1.31	0.0	1.29	0.0	104.50	2.1	1.55	0.1	35.57	1.2	42.85	3.0	0.38	0.0	49.83	3.4	-6.46	1.5	27.55	3.0
	S6	93.70	7.4	2.26	0.3	1.07	0.1	98.40	2.7	2.39	0.2	29.33	0.6	30.93	2.0	0.47	0.0	33.30	2.8	-1.80	1.2	21.05	1.9
Fig. A5 Appendix	S4	73.12	2.6	3.85	0.2	1.46	0.1	92.09	4.4	3.88	0.5	22.09	0.5	22.85	2.2	0.48	0.1	24.46	2.7	-0.93	1.0	14.12	0.5
	S5	55.58	0.8	4.34	0.2	1.89	0.1	75.63	5.6	3.68	0.7	18.49	0.6	19.35	2.5	0.47	0.1	21.24	3.0	-1.08	1.2	12.08	0.4
	S6	44.84	0.3	5.45	0.3	2.50	0.1	63.54	6.5	3.39	0.9	15.99	0.7	17.12	2.8	0.46	0.1	19.26	3.3	-1.28	1.3	10.95	0.8
Fig. A6 Appendix	S10 (25 °C)	62.87	2.7	1.15	0.1	1.23	0.2	67.28	1.5	1.25	0.1	23.24	1.3	32.47	1.8	0.29	0.0	37.37	1.1	-5.95	0.5	16.92	2.3
	S10 (37 °C)	73.85	1.7	1.09	0.0	1.06	0.1	75.13	0.6	1.11	0.0	24.75	1.3	39.78	1.9	0.25	0.0	43.21	0.7	-6.96	0.5	17.85	2.5
	S11 (25 °C)	28.99	1.3	1.13	0.1	1.32	0.2	31.62	0.9	1.24	0.1	10.91	0.6	15.30	0.9	0.29	0.0	17.72	0.6	-2.87	0.3	8.03	1.1
	S11 (37 °C)	86.81	34.5	3.31	1.6	0.50	0.1	47.08	1.6	1.54	0.2	15.38	0.6	20.78	0.5	0.32	0.0	22.46	0.5	-2.92	0.2	10.35	1.5
Fig. A7 Appendix	S10 (25 °C)	96.12	11.5	5.79	1.0	1.65	0.3	152.27	23.8	6.54	1.8	28.78	1.2	22.95	3.2	0.64	0.1	20.56	5.4	3.56	2.3	15.63	0.3
	S10 (37 °C)	104.98	14.5	3.74	0.7	1.36	0.3	133.50	13.5	4.13	0.9	31.93	0.9	30.33	3.6	0.53	0.1	31.32	0.3	5.39	2.3	17.62	0.7
	S11 (25 °C)	127.37	52.0	8.00	3.1	0.95	0.2	115.01	9.6	7.34	1.1	20.42	0.6	15.99	1.0	0.65	0.0	13.76	1.8	2.88	0.8	10.79	0.6
	S11 (37 °C)	98.18	19.3	4.27	0.9	1.00	0.2	98.17	4.3	4.97	0.4	22.92	0.5	21.22	1.3	0.55	0.0	20.79	0.9	2.08	0.9	13.42	1.0

Table 4.6. Lack-of-fit (LOF) and R^2-adjusted values for the fittings of the work (cf. Figures A1–A7).

Figure No.	Carrier	Composition	Loading method (cargo)	*T* (ºC)	pH	Hill		Hill *n* = 1		Korsmeyers-Peppas		Alfrey		Higuchi		Zero-order	
						LOF	r^2-adj	LOF	r^2-adj	LOF	r^2-adj	LOF	r^2-adj	LOF	r^2-adj	LOF	r^2-adj
Fig. 4.12	S4	Chitosan	in situ (erioglaucine)	25	7.4	3.1	0.99	3.1	0.992	6.5	0.96	11.4	0.91	45.3	-0.14	100	0.33
	S5	Chitosan/silica				2.0	0.996	2.1	0.996	5.0	0.98	13.8	0.86	48.3	-0.37	100	0.4
	S6	Chitosan/silica				1.8	0.997	2.5	0.995	4.7	0.98	15.3	0.83	50.0	-0.48	100	0.33
Fig. A1 Appendix	S4	Chitosan	in situ (erioglaucine)	25	0.7	5.3	0.99	5.3	0.991	10.6	0.95	5.4	0.99	28.1	0.77	100	0.7
	S5	Chitosan/silica				7.0	0.98	9.3	0.97	7.7	0.98	7.2	0.98	15.4	0.94	100	0.77
	S6	Chitosan/silica				4.4	0.994	4.4		8.2	0.97	7.1	0.98	29.0	0.74	100	0.6
Fig. A2 Appendix	S1	Chitosan	post-loaded (erioglaucine)	25	7.4	1.0	0.9996	1.2	0.9996	2.5	0.998	4.3	0.994	22.3	0.83	100	0.76
	S2	Chitosan/silica				0.5	0.9999	0.6	0.9999	2.6	0.997	3.2	0.995	19.5	0.78	100	0.7
	S3	Chitosan/silica				2.9	0.996	4.2	0.993	2.9	0.996	3.3	0.995	11.8	0.94	100	0.82
Fig. A3 Appendix	S1	Chitosan	post-loaded (erioglaucine)	25	0.7	3.9	0.99	7.4	0.97	10.9	0.94	10.0	0.95	11.7	0.94	2.6	0.998
	S2	Chitosan/silica				4.7	0.98	6.9	0.978	10.0	0.95	9.4	0.95	10.6	0.95	5.9	0.991
	S3	Chitosan/silica				4.0		5.5	0.98	8.7	0.96	8.3	0.96	8.9	0.96	7.6	0.98
Fig. A4 Appendix	S4	Alginate	post-loaded (erioglaucine)	25	7.4	1.4	0.999	4.6	0.994	1.9	0.999	1.8	0.999	9.4	0.97	100	0.82
	S5	Alginate/silica				0.9	0.9998	2.9	0.998	8.3	0.98	6.7	0.991	10.0	0.97	100	0.92
	S6	Alginate/silica				2.7	0.998	2.9	0.998	7.1	0.99	6.8	0.992	6.9	0.99	100	0.94
Fig. A5 Appendix	S4	Alginate	post-loaded (erioglaucine)	25	0.7	1.9	0.997	3.8	0.992	7.5	0.97	7.2	0.97	7.6	0.97	5.9	0.991
	S5	Alginate/silica				1.3	0.999	6.1	0.98	10.1	0.94	9.6	0.95	10.2	0.95	5.9	0.991
	S6	Alginate/silica				1.1	0.999	8.9	0.96	12.9	0.91	12.2	0.92	13.2	0.92	11.8	0.97
Fig. A6 Appendix	S10	Chitosan	in situ (ephedrine)	25	7.4	2.5	0.996	3.1	0.995	7.0	0.97	3.2	0.993	15.9	0.88	100	0.77
				37	7.4	1.3	0.999	1.3	0.999	4.2	0.99	1.9	0.998	15.2	0.8859	25.2	0.81
	S11	Chitosan/silica	in situ (ephedrine)	25	7.4	3.1	0.992	4.0	0.99	7.9	0.95	3.9	0.98	16.6	0.83	100	0.7
				37	7.4	5.3	0.995	3.7	0.99	2.6	0.99	2.1	0.995	10.4	0.8972	26.6	0.51
Fig. A7 Appendix	S10	Chitosan	in situ (ephedrine)	25	0.7	5.2	0.98	7.1	0.97	9.5	0.96	10.0	0.96	16.1	0.95	3.9	0.996
				37	0.7	2.1	0.982	6.0	0.979	8.3	0.955	41.7	0.954	8.5	0.9596	8.3	0.98
	S11	Chitosan/silica	in situ (ephedrine)	25	0.7	3.5	0.994	3.5	0.995	4.3	0.992	4.8	0.992	10.0	0.97	10.1	0.97
				37	0.7	3.3	0.993	7.7	0.994	5.2	0.984	13.0	0.983	5.3	0.9826	13.1	0.90
LOF average						**2.9**		**4.5**		**6.8**		**8.6**		**17.5**		—	

As mentioned, the Korsmeyer–Peppas model fits the data reasonably better than Higuchi one. Since the latter is based on a purely diffusive theoretical model, we can conclude that the change in the carrier structure has a strong influence on the release kinetics of erioglaucine and ephedrine in most experiments. The inspection of Korsmeyer–Peppas exponent values (near to n = 0.5) suggest that that the diffusive phenomenon can be relevant for some experiments performed in an acidic environment (see Figure A3 and A5, and the corresponding values of n in Table 4.6.)

4.4 Conclusions

Chitosan and alginate were used as a polymer matrix for encapsulating erioglaucine sodium salt and ephedrine hydrochloride. Silica nanostructures, pre-formed in situ, were embedded in the polymer matrix during the physical cross-linking of the biopolymers with sodium triphosphate or calcium chloride solutions, for chitosan and alginate systems, respectively. Our results reveal that the formed silica nanostructures, homogeneously incorporated within the polymer matrix, play a significant role in both increasing the structural stability of the carrier and retarding the release behavior in both neutral and acidic environments. The work demonstrated that the prepared hybrid submillicarriers are efficient in entrapping hydrophilic substances, with high loading capacity in comparison with the systems without silica, but with a much slower release due to the strong adsorption.

4.5 Experimental Section

4.5.1 Materials

Low molecular weight chitosan (Sigma-Aldrich, M_v = 50,000–190,000 Da, 75–85% deacetylated), alginic acid sodium salt (powder, 15–25 cP, 1 % in H_2O), glacial acetic acid (Panreac-Quìmica), sodium tripolyphosphate (STP, Alfa-Aesar, ≥ 85%), calcium chloride dihydrate (Sigma-Aldrich, extra pure), tetraethyl orthosilicate (TEOS, Sigma-Aldrich, ≥ 98 %), hydrochloric acid 37% (J. T. Baker), ethanol (Merck, gradient grade for liquid chromatography), ephedrine hydrochloride (Sigma-Aldrich, ≥ 99%), erioglaucine disodium salt (Across Organics, pure), and phosphate buffer solution

(pH = 7.4) self-prepared with NaCl (Sigma-Aldrich, ≥ 99%), KCl (Sigma-Aldrich, ≥ 99%), $Na_2HPO_4 \cdot H_2O$ (Schlarlau, reagent grade), and KH_2PO_4 (Sigma-Aldrich, ≥ 99%). All chemicals and solvents were used as received. Ultrapure water was used through all the experiments.

4.5.2 Synthesis of Physically Cross-Linked Polysaccharide and Polysaccharide/Silica Submillispheres

Chitosan submillispheres were prepared through ionotropic gelation using sodium triphosphate (STP) as a physical cross-linker. An aqueous suspension of chitosan (3 wt%) was prepared by adding glacial acetic acid (overall concentration of 2 wt%) and magnetically stirring at 400 rpm for 24 h. For samples containing silica (and only for those, not for samples with chitosan alone), 200 µL of concentrated hydrochloric acid (37%) were added to 20 mL of the 3 wt% chitosan aqueous. Afterward, tetraethyl orthosilicate (TEOS) was added to the mixture at concentrations of 0.9 or 3.6 wt%. The chitosan/TEOS mixture was kept under stirring at 800 rpm for 2 h and then loaded in a plastic syringe provided with a 0.8 × 40 mm 21 G metallic needle (Braun Sterican). The inner diameter of the needle determines the size of the resulting particles. The chitosan solution (or the chitosan/TEOS mixture) was added dropwise using a syringe pump at a feeding rate of 0.5 mL/min to 100 mL of a sodium triphosphate solution (2.4 wt%) to obtain the submillispheres.

The resulting spheres were kept in triphosphate aqueous solution for 2 h under stirring to ensure complete cross-linking. Finally, the spheres were separated from the aqueous phase and successively washed with distilled water to remove the excess of unreacted triphosphate. The chitosan millispheres were dried under vacuum for 24 h at 50 ºC and stored at room temperature**.**

Alginate submillispheres were analogously prepared following the same procedure, but using $CaCl_2$ (final overall concentration of 4.76 wt%) as a physical cross-linker. For samples containing silica (and only for those, not for samples with alginate alone), 200 µL of concentrated NH_4OH were added to the alginate aqueous solution before the addition of TEOS. The concentrations of the components of all samples prepared in this work are listed in Table 4.7.

Table 4.7. Compositions of polysaccharide/silica submillicarriers

Sample	Polysaccharide	Sodium triphosphate (STP) (wt%)	$CaCl_2$ (wt%)	TEOS (wt%)	Cargo (wt%) [a]
S1	Chitosan	2.3	—		—
S2	Chitosan	2.3	—	0.9	—
S3	Chitosan	2.3	—	3.6	—
S4	Chitosan	2.3	—	—	1 (erioglaucine)
S5	Chitosan	2.3	—	0.9	1 (erioglaucine)
S6	Chitosan	2.3	—	3.6	1 (erioglaucine)
S7	Alginate	—	4.8	—	—
S8	Alginate	—	4.8	0.9	—
S9	Alginate	—	4.8	3.6	—
S10	Chitosan	2.3	—	—	10 (ephedrine)
S11	Chitosan	2.3	—	3.6	10 (ephedrine)

[a] Weight percent with respect to chitosan. In samples S1 to S3 and S7 to S9 the dye was post-loaded and not added during the particle synthesis (cf. section 4.4).

4.5.3 In Situ Loading of Hydrophilic Substances

Stock aqueous solutions of erioglaucine disodium salt (120 mg in 20 mL of water) and ephedrine hydrochloride (300 mg in 5 mL of water) were freshly prepared. From these stock solutions, 1 mL was added to 20 mL of the polysaccharide or polysaccharide/TEOS solution. The resulting loaded amount with respect to the polymer was 1 wt% for erioglaucine and 10 wt% for ephedrine. As in the unloaded particles, the whole volume of this solution was added dropwise to 100 mL of a sodium triphosphate solution (2.4 wt%). The hydrophilic substance is entrapped in the polymer matrix during the formation of the particles.

For determination of the loading efficiency, the loaded particles were separated by filtration from the cross-linker solution. The entrapped amount of the dye/drug in the particle was calculated by subtracting the amount in the filtered solution from the initially added to the polysaccharide solution. Concentrations were determined spectrophotometrically by measuring the maximum absorbance at 629 nm for erioglaucine sodium salt and at 256 nm for ephedrine hydrochloride (SECOMAM UVI Light UV-Visible spectrophotometer). The experiments were carried out in triplicate. The required calibration solutions contained the same concentration of sodium triphosphate as in the particle preparation (2.4 wt%).

4.5.4 Post-Loading of Erioglaucine Disodium Salt

Fixed amount of alginate or chitosan-based spheres (0.6 g) were immersed for 10 h in an aqueous solution of erioglaucine disodium salt (100 mL, 0.006 wt%). The entrapment of

the dye takes place by diffusion and adsorption during the swelling of the particles in the aqueous solution. Afterward, the particles were separated by filtration from the solution and dried under vacuum for 24 h at 50 ºC. Analogously to the described for the in-situ loading, the solution was assayed spectrophotometrically by measuring the maximum absorbance at 629 nm, which allowed us to determine the entrapped amount inside the particles. The experiments were also carried out in triplicate.

4.5.5 Swelling and Weight Loss

The swelling behavior of the submillispheres was evaluated at 25 ºC. The spheres were weighted and immersed in different aqueous solutions, either a nearly neutral medium (pH ≈ 7) or an acidic medium (HCl concentrations of 0.2 M or 0.4 M, corresponding to pH values of 0.7 and 0.4, respectively). After different times, the spheres were extracted from the solutions, carefully dried with a filter paper till the swelling equilibrium was attained, and weighted again. The mass swelling percentage was calculated according to the following equation:[163]

$$\text{Mass swelling (\%)} = \frac{w_\text{w}}{w_\text{d}} \times 100 \tag{4.1}$$

where w_w is weight of particles at a certain time and w_d is the initial weight of the dried particles. Data points are average of three measurements. The weight loss percentage was estimated with the expression

$$\text{Weight loss (\%)} = \frac{w_\text{i} - w_\text{d}}{w_\text{i}} \times 100 \tag{4.2}$$

where w_d is the dried weight of the spheres after swelling at different times and $w_\text{i:}$ is the initial weight of dried spheres.

4.5.6 Kinetic Release and Data Analysis

The release of the entrapped hydrophilic molecules was carried out at controlled temperature (25 °C for erioglaucine and 25 or 37 °C for ephedrine) by using a stirred beaker method. A known amount of the sub-millispheres (0.8 g) was immersed in suspended in a vessel containing 100 mL of the desired medium (either a phosphate buffer with pH = 7.4 or an acidic aqueous solution, [HCl] = 0.2 M), under constant stirring at 200 rpm with a Teflon-coated floating stirring bar. The experiments were

always conducted in triplicate. The amount of the hydrophilic substance entrapped within the particles used in each release experiment, calculated taking into account the entrapment efficiency, was between 1.2 and 2.7 mg for erioglaucine disodium salt and between 15 and 25 mg for ephedrine hydrochloride. Aliquots were extracted at different times and replaced with fresh solution. The concentrations were determined spectrophotometrically from the maximum of absorbance (629 nm for erioglaucine and 256 nm for ephedrine).

Chapter 5

A Chitosan/Silica Hybrid Scaffold for Simultaneous Entrapment of Two Different Hydrophilic Substances*

Having a hybrid organic/inorganic biomaterial with nontoxic properties, biocompatible, and able to encapsulate simultaneously two different hydrophilic substances was the main objective of the work explained in this chapter. Here, we present an in-situ strategy for the preparation of a hybrid chitosan/silica macroscaffold, applied for entrapping hydrophilic substances (erioglaucine disodium salt and ibuprofen sodium salt). The release of these substances was studied under neutral conditions. Chitosan is used to generate a scaffold network in which the formation of silica nanoparticles takes place in situ by a sol–gel process. The results demonstrate that the presence of nanostructured silica within the polymer matrix affects the release of both hydrophilic substances and increases the structural stability of the scaffold.

5.1 Introduction

Biodegradable polymers, which are biologically degraded to nontoxic components within the body, have been used in drug carriers because of their versatility and wide range of properties.[164] The incorporation of the drug into a biopolymer matrix enhances its protection against degradation and can control the release.[165] In addition, the ability to

* Chapter based on a manuscript with the same title by A. Elzayat, F. F. Pérez Pla, and R. Muñoz-Espí (in preparation for publication, 2021).

form hydrogels make biopolymers ideal candidates for encapsulation of therapeutic molecules.[151]

Silica nanoparticles in suspension can be formed by sol−gel process in the presence of polysaccharides, yielding the formation of a hybrid polymer structure with potential use in the delivery of therapeutic agents.[106, 108-109, 125, 157-160] Organic/inorganic hybrid structures are able to protect the encapsulated payloads from the surrounding environment and allow their release in a controlled manner.[112, 118, 161-162]

In this chapter, a loaded hybrid chitosan/silica microscaffold was prepared by ionotropic gelation, which minimizes the use of toxic organic solvents or chemical cross-linking agents.[154-156] Its efficiency for entrapping two different hydrophilic molecules was investigated. Chitosan was used as the main polymer component, and silica was used as a structuring additive. Finally, a release experiment was carried out in phosphate buffer (pH = 7.4) at 37 °C by using erioglaucine disodium salt and ibuprofen sodium salt as hydrophilic substances.

5.1.1 Preparation and Characterization of a Hybrid Scaffold

A chitosan/silica hybrid microscaffold was prepared by an ionotropic gelation occurring concurrently to a sol–gel process leading to the formation of silica in two steps, as schematically depicted in Figure 5.1. In the first step, analogously to the preparation strategy used in Chapter 4, tetraethyl orthosilicate (TEOS) was added to a polysaccharide solution, yielding silica nanostructures upon contact with water. Subsequently, biopolymer submillispheres were precipitated in a solution of the cross-linker agent. The forming silica is trapped in the biopolymer matrix, leading to hybrid chitosan/silica structures. The same strategy was carried out during the encapsulation of the first hydrophilic molecule (ibuprofen disodium salt). In the second step, the formation of the scaffold takes place through the gathering and sticking step of the formed hydrogel spheres with each other by using the same chitosan solution.

The second hydrophilic substance (erioglaucine disodium salt in our case) is entrapped within another chitosan solution, which was used to gather and collect the particles with each other in a form of a post-loading mechanism during the formation of the scaffold. The different compositions of the scaffolds prepared in this work are

summarized in Table 5.1. Chitosan samples were cross-linked with sodium triphosphate (STP) and loaded with erioglaucine disodium salt and ibuprofen sodium salt.

Table 5.1. Formulation of the prepared chitosan scaffolds.

Sample	System	Cross-linker	Polymer: cross-linker: TEOS weight ratio	Initial load (in-situ)	Post load (incubation)
SF1	Chitosan	STP	3:12:0	—	
SF2	Chitosan/silica	STP	3:12:4	—	
SF3	Chitosan	STP	3:12:0	Ibuprofen	Erioglaucine
SF4	Chitosan/silica	STP	3:12:4	Ibuprofen	Erioglaucine

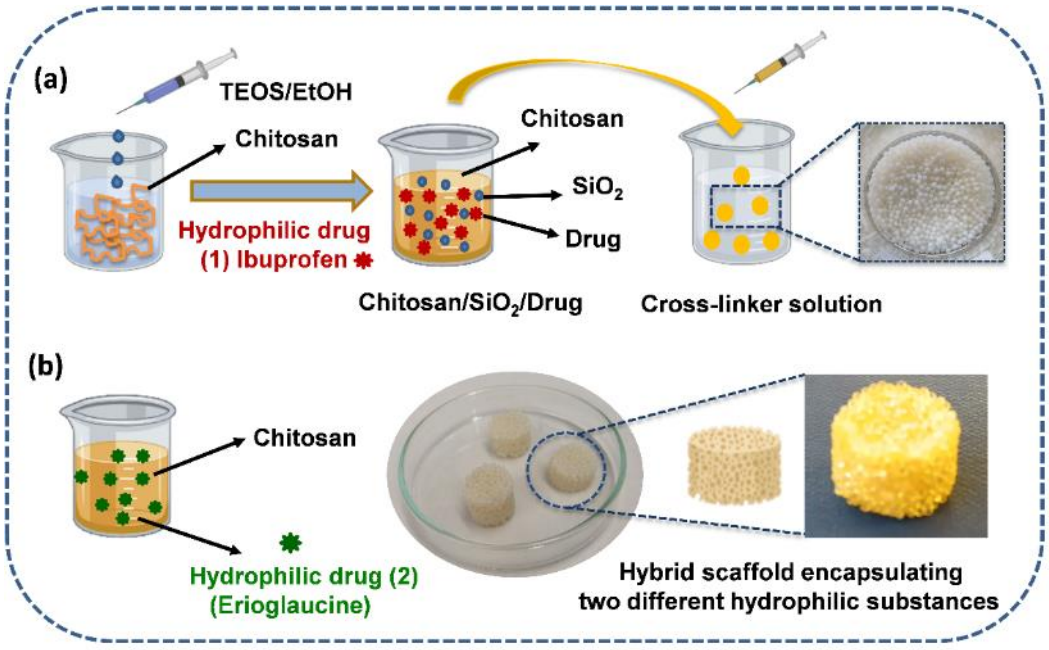

Figure 5.1. Schematic representation of the formation of chitosan scaffolds in two steps: (a) preparation of cross-linked chitosan/silica hybrid hydrogels encapsulating one hydrophilic substance by in situ loading, (b) collecting and adhesion process of these hydrogels to form the hybrid scaffold structure.

The swelling behavior with time of the prepared microscaffold, which relates to the ionic character of the polymer network, was evaluated in both phosphate buffer (pH = 7.4) and acidic buffer (pH = 3). Figure 5.2 represents the swelling behavior in different medium (in percentage with respect to the initial mass) at different times. The swelling percentage in acidic medium is higher than in the neutral one, which is related to the protonation of the amino groups in chitosan under acidic conditions. Under both conditions, the silica-containing macroscaffold decreases the swelling ability with

respect to the pristine chitosan ones. This result indicates that the presence of silica retards and even avoids the dissolution of the chitosan polymer network, increasing the structure stability of the scaffold.

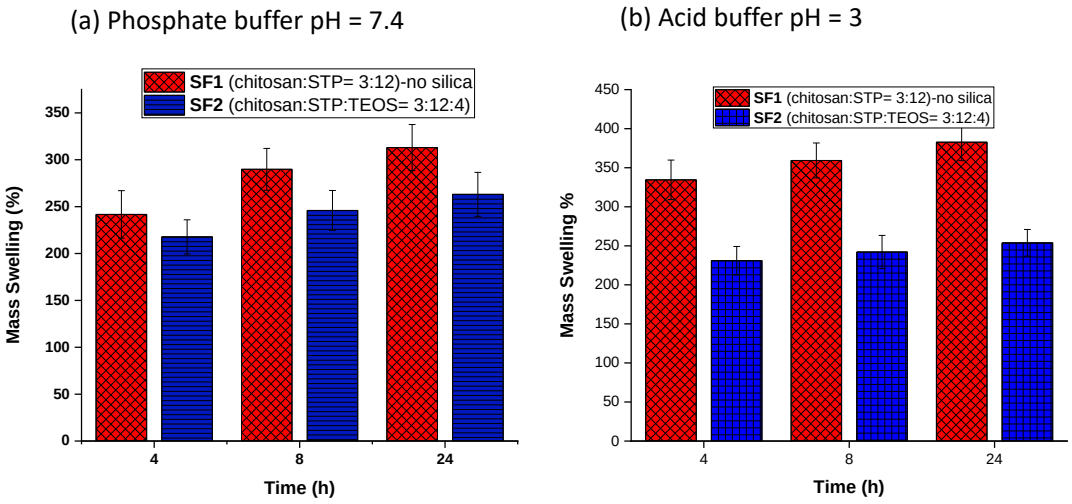

Figure 5.2. Swelling percentage at different times of chitosan and chitosan/silica scaffold with different polymer:cross-linker:TEOS weight ratio (3:12:0 and 3:12:4, respectively) in two different immersion media: (a) pH =7.4 and (b) pH = 3.

5.1.2 Surface Morphology

The morphology of the prepared chitosan scaffolds was compared to the hybrid chitosan/silica ones by means of optical microscopy and scanning electron microscopy (SEM). The corresponding micrographs are shown in Figure 5.3**.** The pure chitosan scaffold (sample **SF1**) presents a regular and spherical structure with a smooth surface, while chitosan/silica hybrid particles (sample **SF2,** polymer-to-TEOS ratio of 3:4) show a certain roughness, attributed to the presence of silica nanostructures embedded within the chitosan matrix during the formation process. The average size of the particles is 800 ± 50 µm, as statistically measured from SEM micrographs. The formation of silica takes place by a sol–gel process under acidic conditions. The alkoxide groups of TEOS are hydrolyzed to silanol groups in water, which can occur under acidic catalysis. A network of nanostructured silica is produced by polycondensation of silanol groups.

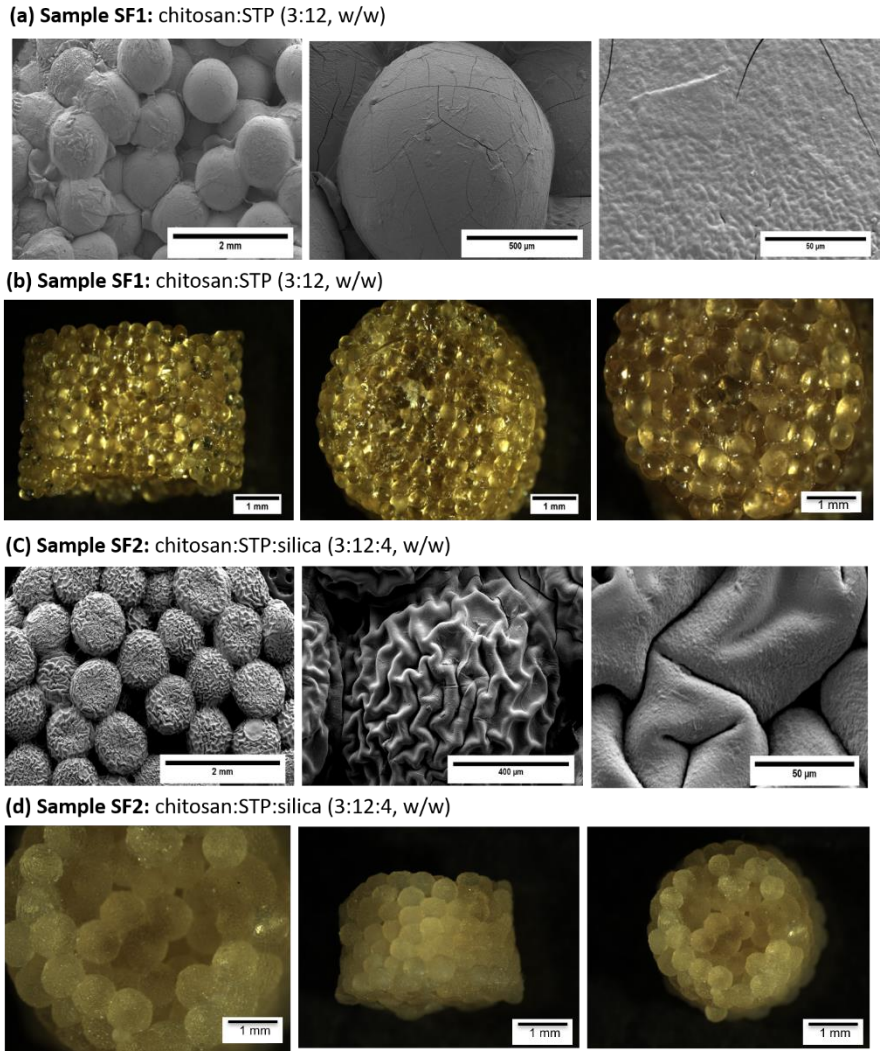

Figure 5.3. Micrographs of a chitosan and a chitosan/silica hybrid scaffold by SEM (a, c) and optical microscopy (b, d).

5.2 Release of Hydrophilic Substances

Two different hydrophilic substances were loaded within the polymer matrix by using the ionotropic gelation method. Ibuprofen sodium salt and erioglaucine were loaded simultaneously during the formation of the scaffold.

In an in-situ process, a definite amount of ibuprofen with respect to the polymer weight is mixed with a chitosan solution that contains silica nanostructured formed during the sol–gel process. The addition of this mixture to the cross-linker solution leads to the desired loaded spheres. The entrapment efficiency for systems with silica increases very significantly with respect to the systems without, as we described before in the

work presented in Chapter 4. Ibuprofen and erioglaucine showed different release profiles, but in both cases the presence of silica retards the release, when compared to samples without.

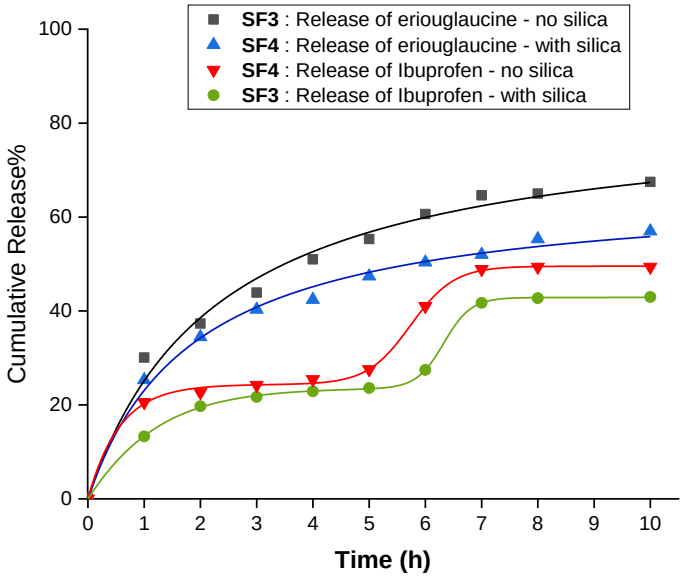

Figure 5.4. Cumulative release of both ibuprofen and erioglaucine disodium salt from the chitosan and hybrid chitosan scaffold in phosphate buffer pH = 7.4.

In the neutral buffer, the release of erioglaucine, loaded and entrapped on the surface and outer layer of the scaffold, is faster than the release of ibuprofen and it reaches a value of about 80% in less than 10 hours, as presented in Figure 5.4. Differently, ibuprofen which is embedded in situ within the chitosan/silica matrix, is liberated from the scaffold in two steps. This behavior appears to be related to the swelling of the scaffold, which allows the liberation of ibuprofen from the surface first and, afterward, the drug entrapped within the spheres is released. The incorporation of silica in the scaffold retards remarkably the release of both substances.

5.3 Conclusions

Chitosan was used as a polymer matrix for generating a hybrid polymer/silica scaffold encapsulating simultaneously two hydrophilic substances (erioglaucine sodium salt and ibuprofen sodium salt). Silica nanostructures, pre-formed in situ, were embedded in the polymer matrix during the physical cross-linking of the biopolymers with sodium

triphosphate. Our results reveal that the formed silica nanostructures, homogeneously incorporated within the polymer matrix, play a significant role in both increasing the structural stability of the scaffold and retarding the release behavior in neutral environments. In addition, the release behavior in case of the ibuprofen showed two different steps, which erioglaucine is released faster and in a single step.

5.4 Experimental Section

5.4.1 Synthesis of Chitosan and Chitosan/Silica Hybrid Scaffolds

Chitosan submillispheres were prepared by ionotropic gelation by using sodium triphosphate (STP) as a physical cross-linker, analogously to the method presented in Chapter 4.[166] An aqueous suspension of chitosan (3 wt%) was prepared by adding glacial acetic acid (overall concentration of 2 wt%) and stirring magnetically at 400 rpm for 24 h. For hybrid samples with silica, 200 µL of concentrated hydrochloric acid (37%) were added to a 20 mL of the chitosan suspension 3 wt%. Afterward, tetraethyl orthosilicate (TEOS) was dropped to that solution and stirred for 2 h. This mixture was dropped in the cross-linker receptor. Finally, the spheres were separated from the aqueous phase and washed several times with distilled water to remove the excess of unreacted triphosphate and the formation of the scaffold takes place during the adhesion and fusion of the particles with each other. The scaffolds were dried under vacuum for 24 h at 50 ºC and stored at room temperature.

5.4.2 Loading of Hydrophilic Substances

Stock aqueous solutions of erioglaucine disodium salt (120 mg in 20 mL of water) and ibuprofen (300 mg in 5 mL of water) were freshly prepared. From these stock solutions, 1 mL was added to 20 mL of the chitosan/TEOS solution. The resulting loaded amount with respect to the polymer was 1 wt% for erioglaucine and 10 wt% for ibuprofen.

5.4.3 Release Study

The release of the entrapped hydrophilic molecules was carried out by inserting the microscaffold in the desired medium (phosphate buffer with pH = 7.4). Aliquots were extracted at different times and assayed spectrophotometrically by measuring the

maximum absorbance at 629 nm for erioglaucine sodium salt and at 256 nm for the ibuprofen (SECOMAM UVI Light UV-visible spectrophotometer).

Chapter 6

Versatile Polysaccharide/Silica Microcapsules by Spray Drying: Application in Release of Hydrophilic Substances and Catalysis*

In this chapter, polysaccharide/silica hybrid microparticles were synthesized by using ionic cross-linking with sodium triphosphate (STP) followed by spray drying. This is a fast and continuous process, based on the transformation of a liquid feed into dry particles in three steps: atomization, mixing of fine droplets with a gas stream, and separation and collection of the dried powder. Chitosan and alginate were used as biopolymer matrices and in-situ prepared silica was used as a structuring additive. The prepared chitosan microparticles, taken as an example, were used in two very different applications. First, a model hydrophilic molecule (erioglaucine disodium salt) was encapsulated inside the microparticles, and the release behavior of this molecule in neutral media was investigated. Second, microparticles were used as a support for palladium nanoparticles and tested as catalysts for a model organic reaction, namely, the reduction reaction of *p*-nitrophenol by $NaBH_4$. As in previous chapters, the results indicate that the presence of silica nanostructures, incorporated within the polymer matrix, affect the morphology and the stability of the capsules and retard the release of the encapsulated substance. On the other hand, palladium-containing chitosan microparticles exhibited an excellent catalytic performance.

6.1 Introduction

Biopolymer-based microparticles have gained significant attention for drug delivery systems as a result of their wide range of properties and applications. The use of

* Chapter based on a manuscript with the same title by A. Elzayat, I. Adam-Cervera, M. Albus, A. Cháfer, J. D. Badia, F. F. Pérez-Pla, and R. Muñoz-Espí, R. (in preparation for publication, 2021).

microparticle-based therapy allows the drug release to be carefully targeted to the specific treatment site through the choice and formulation of various drug–polymer combinations. By using microencapsulation technologies and varying the formulation parameters, polymeric microspheres can be developed into an optimal drug delivery system, which should provide the desired release profile.[167-168]

Recently, spray drying has been widely used in the pharmaceutical and food industry for the preparation of microparticles, because it is a continuous process, it is easy to scale up, and it has relatively low processing cost.[169] It allows the transformation of a liquid feed into dry powders and it has also a possible control over particle size.[170-171] It starts with the atomization of the fluid feed inside a chamber at high temperature through a peristaltic pump to an atomizer or nozzle.[172] Afterward, atomization is performed by centrifugation, pressure or kinetic energy due to the force of the compressed air, disrupting the liquid into small droplets. The formation of fine droplets to dry particles takes place by the help of both heated gas stream and fast solvent evaporation, resulting in the separation and collection of the dried particles in a glass cyclone collector.[173-176] Polysaccharide microspheres prepared by spray-drying cannot be kept suspended in water because of their greater swelling and dissolution. Therefore, non-cross-linked microspheres are unsuitable for sustained delivery systems. Cross-linking agents are required to prepare stabilized microparticles.[177-178]

Chitosan is a hydrophilic polysaccharide and it can easily swell in aqueous media. It can form gels by interacting with different types of divalent and polyvalent anions to avoid undesired burst release, improve the mechanical properties, and obtain better shape microparticles while avoiding agglomeration.[179] To overcome certain disadvantages of chemical cross-linkers (such as toxicity), ionic cross-linking has also been explored.[180-181] Sodium triphosphate (STP) is generally recognized as safe by the Food and Drug Administration (FDA).[182] It is also a nontoxic polyanion that interacts with chitosan in acidic medium via electrostatic forces to form ionically cross-linked networks. Moreover, the unique polycationic structure of ionic cross-linkers allows an optimal use of chitosan for drug delivery.[183]

Nowadays, using polysaccharides as supports in heterogeneous catalysis is attracting an increasing research attention.[184-186] Palladium is a significant noble metal catalyst, which is widely used in different organic synthesis processes due to its high activity. It has been demonstrated that the material and structure of the support play a significant

role in the catalytic performance. In addition, the magnitude of the interaction between the support and the metal ions Pd^{2+} have a great influence on the catalytic activity of the metal nanoparticles.[187-188] For that, polymer supports usually have good interaction with Pd through the coordination between heteroatoms, such as N and O, on the branches of polymer molecules.[189-190] Chitosan offers strong chelating characteristics with metal ions.[191] The chelation is a kind of chemical interaction, which is considered to be stronger than physical adsorption between inorganic carrier and metal ions. Besides that, it has been reported that silica/chitosan hybrid materials exhibit enhanced mechanical properties compared with other hybrid materials.[192] Therefore, silica/chitosan hybrid materials are a good choice as a support for noble metal nanoparticles.

The aim of the work presented in this chapter was, in the first place, to prepare polysaccharide microparticles based on chitosan and alginate, containing silica nanostructures embedded within their matrix, by ionic gelation followed by a spray drying process. Various formulations were prepared to improve the structural stability of these particles. From the observed morphology, chitosan microparticles were selected for entrapping hydrophilic molecules and control the release behavior in neutral medium (pH = 7.4). On the other hand, they were also applied as a catalyst support for the reduction of *p*-nitrophenol by $NaBH_4$. The results indicated that microparticles prepared by this process exhibited great catalytic performance, long-term stability, and good mechanical strength.

6.2 Preparation of Polysaccharide Hybrid Microparticles by Spray Drying

Ionically cross-linked polysaccharide microcapsules were performed by spray drying in combination with ionic gelation to develop water resistant capsules. This method is simple, performed under mild conditions, and it can give a reproducible yield. The spontaneous reaction was based on the electrostatic attraction between the oppositely charged macromolecules of cationic chitosan with protonated amino groups ($–NH_3^+$) and the polyanion STP ($P_3O_{10}^{5-}$). A three-dimensional entanglement is precipitated from an aqueous solution in the form of hydrogel microcapsules as a drug controlled-release formulation. Alginate, in contrast, possesses carboxylate groups (COO^-), which are able to interact with Ca^{2+} ions.

To prepare chitosan/silica and alginate/silica hybrid microcapsules, tetraethyl orthosilicate (TEOS) was added to a polysaccharide solution, yielding silica nanostructures upon contact with water through a sol–gel process. The forming silica is trapped in the biopolymer matrix, leading to hybrid polymer/silica structures. After optimization experiments, the best experimental parameters for our system were found to be: inlet temperature, compressed air flow, liquid flow rate, and aspiration rate set at 110 °C, 1.2 m^3/min, 2 mL/min, and 80%, respectively. At the end of the process, the cross-linked polysaccharide microparticles were dried as schematically depicted in Figure 6.1. The same strategy was carried out during the encapsulation of a hydrophilic molecules (i.e., erioglaucine disodium salt) within the polymer/silica network structure.

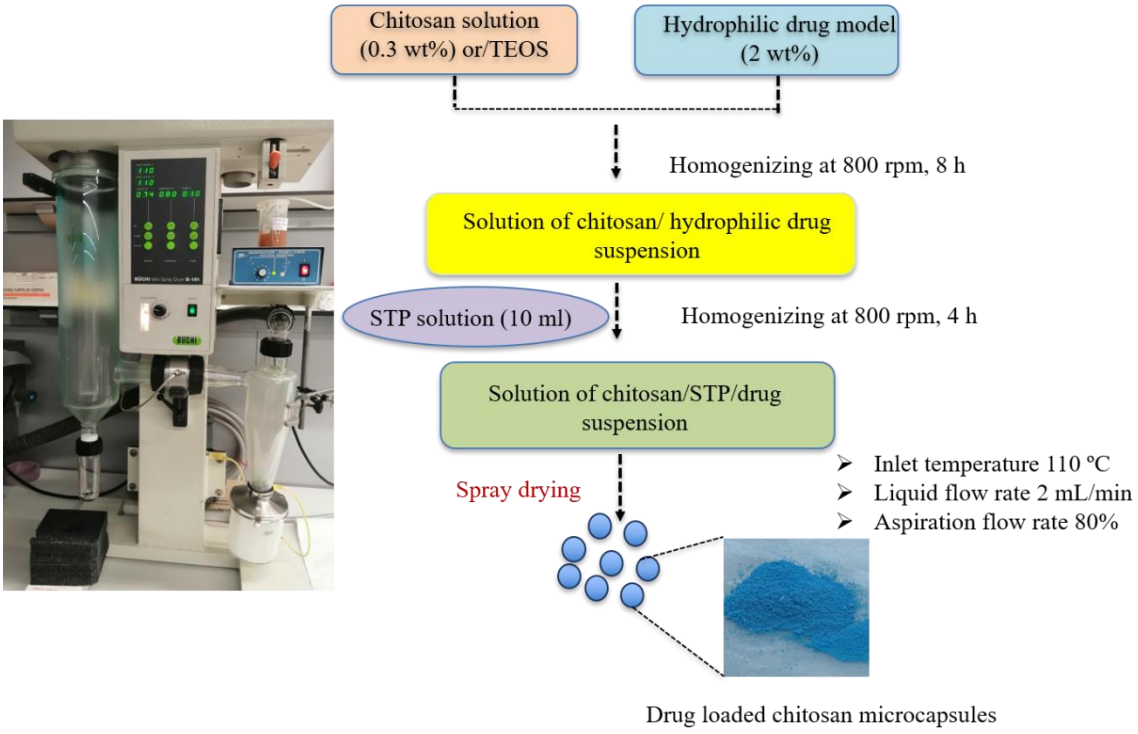

Figure 6.1. Synthesis of spray-dried chitosan/STP microcapsules loaded with a model drug (erioglaucine sodium salt).

The different compositions of the microcapsules prepared in this work are summarized in Table 6.1. Chitosan samples were cross-linked with sodium triphosphate (STP) and were prepared either without loading (for subsequent post-loading of palladium, samples **F1** and **F4**) or loaded in-situ with erioglaucine (samples **F5** to **F7**).

Alginate samples, labeled as **F8** to **F11**, were cross-linked with calcium chloride ($CaCl_2$). The hybrid polysaccharide/silica systems were prepared with a polymer-to-TEOS weight ratio of 3:4.

Table 6.1. Compositions of chitosan and alginate/silica microcapsules.

Sample	System	Cross-linker	Polymer cross-linker: TEOS weight ratio	Initial load (in situ) [a]
F1	Chitosan	—	4:0:0	—
F2	Chitosan/silica	—	4:0:5	—
F3	Chitosan	STP	4:1:0	—
F4	Chitosan/silica	STP	4:1:5	—
F5	Chitosan/silica	—	4:0:5	Erioglaucine
F6	Chitosan	STP	4:1:0	Erioglaucine
F7	Chitosan/silica	STP	4:1:5	Erioglaucine
F8	Alginate	—	4:0:0	—
F9	Alginate/silica	—	4:0:5	—
F10	Alginate	$CaCl_2$	4:1:0	—
F11	Alginate/silica	$CaCl_2$	4:1:5	—

[a] Samples **F3** and **F4** of chitosan were subsequently post-loaded with palladium.

The swelling of the spray-dried microparticles was studied in buffered media (pH = 7.4). The swelling results plotted as the percentage of mass swelling versus time are presented in Figure 6.2. In general, lower water uptake values were observed in the case of the hybrid polysaccharide containing silica nanoparticle inside their matrix. The presence of silica retards the dissolution of the polymeric material network and it supports the structural stability, which in turn decreases the swelling behavior. The swelling capacity of the cross-linked chitosan microparticles with STP (3 wt% aqueous solution) decreased considerably when compared with the non-cross-linked ones. The water uptake in hydrogels depends on the extent of the hydrodynamic free volume and the availability of hydrophilic functional groups for the water to establish hydrogen bonds. The results confirm the formation of rigid polysaccharide/silica hybrid cross-linked networks through the spray drying process.

The swelling behavior and the stability of alginate particles (**F8**–**F11**) showed the same trend of the chitosan ones, but the uptake values are lower even in the absence of silica, which may be related to the different chemistry of alginate and the strong interaction between Ca^{2+} ions and the carboxylic groups of alginate.

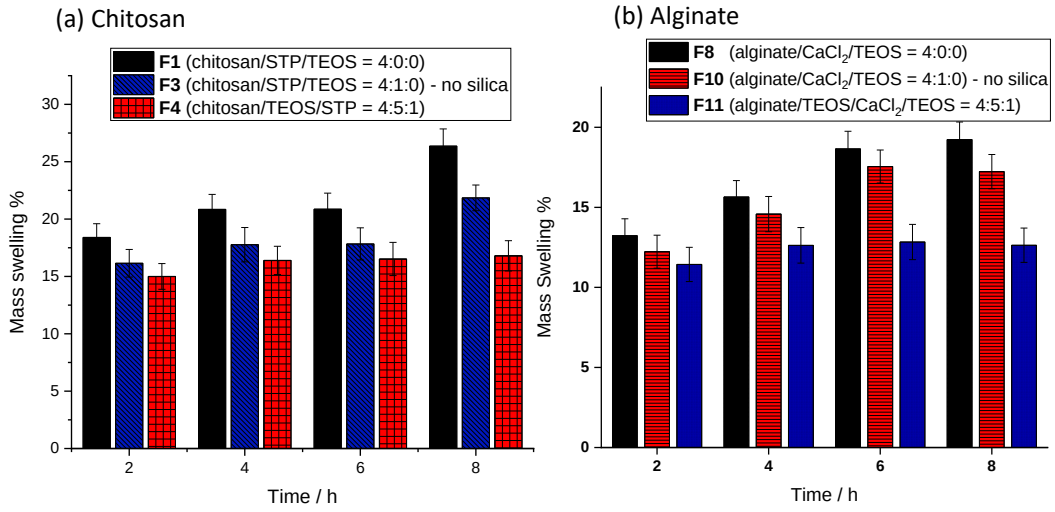

Figure 6.2. Swelling behavior at different times of polysaccharide and polysaccharide/silica microcapsules prepared by spray drying with polymer:cross-linker:TEOS weight ratio of 4:1:5 in neutral immersion media (pH = 7.4).

6.2.1 Surface Morphology

The morphology of the different formulations of polymer and polymer/silica hybrid microparticles prepared via spray drying was studied by means of scanning electron microscopy (SEM). The corresponding electron micrographs for chitosan and alginate particles are presented in Figures 6.3 and 6.4, respectively. It can be observed that non-cross-linked spray-dried chitosan microspheres (control sample **F1**) are irregular with wrinkles on their surface. Chitosan/silica and dye-loaded chitosan/silica hybrid microparticles (samples **F2** and **F5**) were prepared without adding the cross-linker generated well-formed spherical particles with a certain roughness on the surface, as a result of the presence of silica nanostructures embedded within the chitosan matrix. The formulation parameters, namely dye loading, concentration, and weight of chitosan, induced a remarkable change in the surface morphology of the microspheres. The cross-linked particles (samples **F3, F4,** and **F6**) show different morphologies when compared to the non-cross-linked ones. The addition of STP favored the formation of a shrunken morphology with partial roughness as a result of the higher amount of water content (moisture) inside the particles This morphology is attributed to the rapid evaporation during the first stages of the drying process.

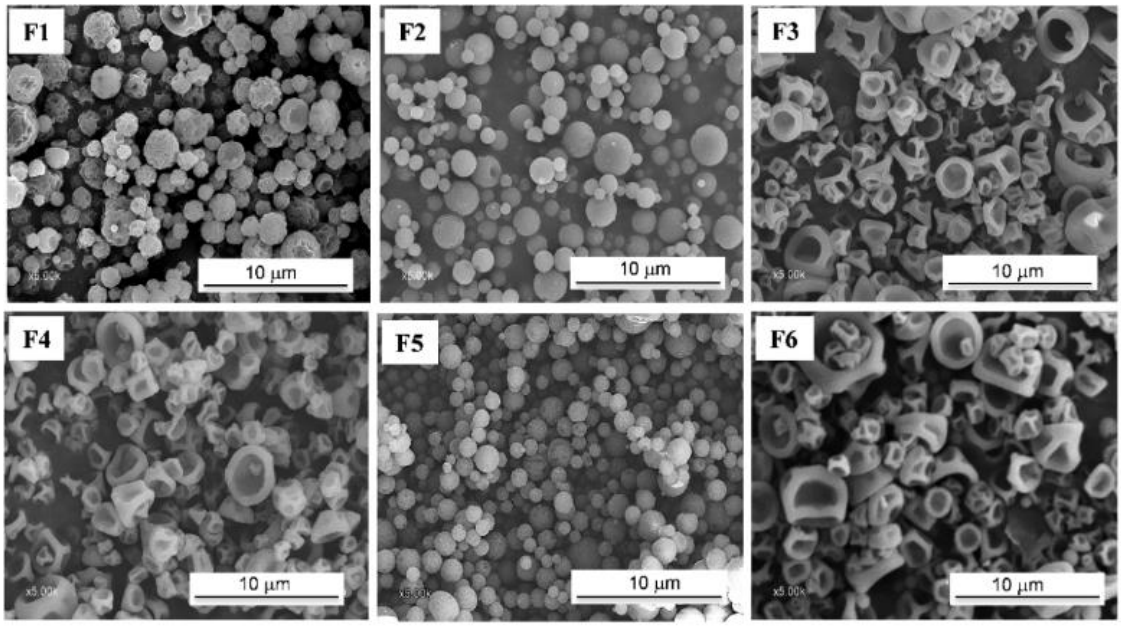

Figure 6.3. SEM images of spray dried chitosan microparticles in the presence of silica with a polymer:TEOS ratio 3:4 (samples **F2–F6**). Sample **F1** is the control sample prepared without cross-linker.

Alginate microparticles show a different morphological structure, when compared to the shrunken morphology of the cross-linked chitosan particles. Non-cross-linked spray-dried alginate microparticles (control sample **F8**) show an irregular, non-spherical structure. However, the microparticles get the spherical morphology in the presence of silica or dye loading (samples **F9** and **F12**) without addition of the cross-linker (calcium chloride in this case). After cross-linking (samples **F10** and **F11**), the morphology appears as a rather collapsed mass. This is attributed to the precipitation of calcium chloride ($CaCl_2$) after the saturation of the cross-linker with the polymer matrix. Calcium chloride crystals are observed in some micrographs. In contrast, the addition of the cross-linker in the presence of silica nanostructures within the polymer matrix allows the particles to get spherical structure with roughness on its surface (sample **F14**). As a general observation, chitosan microparticles show better defined capsules than the alginate ones under the similar operating conditions.

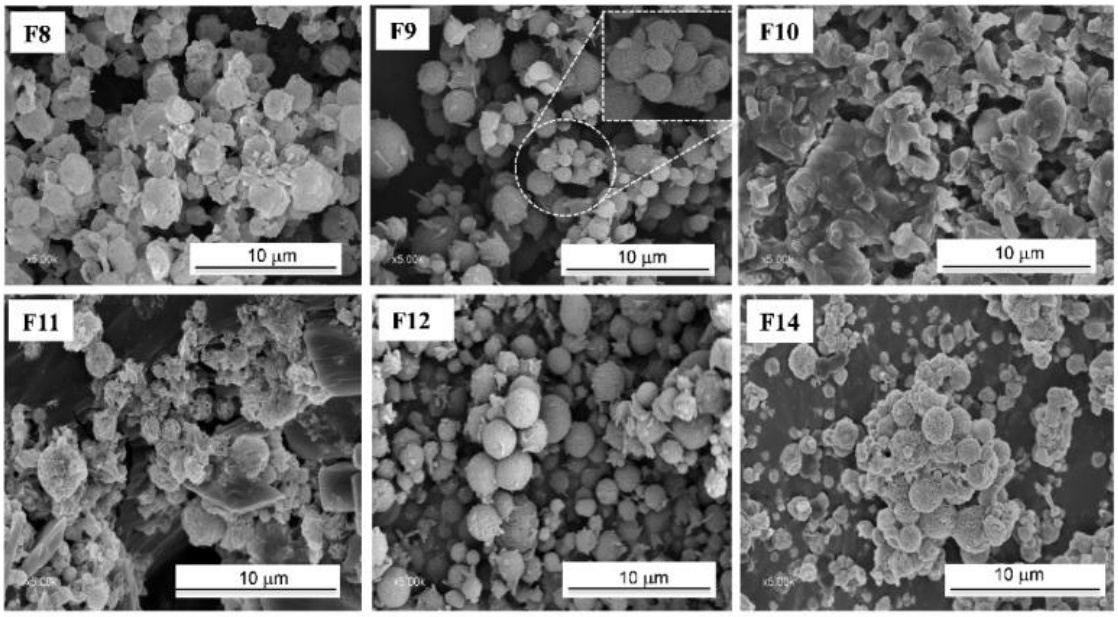

Figure 6.4. SEM images of spray dried alginate microparticles in the presence of silica with a polymer:TEOS, ratio of 3:4 (samples **F9–F14**). Sample **F8** is the control sample prepared without cross-linker.

6.2.2 Thermogravimetric Analysis of the Microcapsules

A thermogravimetric analysis (TGA) of the spray-dried microparticles was carried out to evaluate the decomposition behavior and to determine the silica content. The corresponding traces for chitosan and alginate samples are presented in Figure 6.5. In chitosan samples, an initial and progressive dehydration process corresponding to the evaporation of absorbed water is observed at low temperatures below 100 ºC, which is followed by two decomposition steps at 100–210 ºC and 220–450 ºC. Under the air atmosphere in which measurements were conducted, the cross-linked chitosan microparticles of sample **F3** (without silica) degrade completely to water and CO_2, and the final residue corresponds to sodium triphosphate, so that the percentage of polymer is of about 80%. The non-cross-linked sample, measured for comparison, exhibits approximately the same decomposition behavior. Silica-containing samples (samples **F2** and **F4**) show a lower mass loss, in correlation with the formation of silica. However, the final residue of cross-linked chitosan/silica particles (sample **F4)** is much lower than for sample **F2**. In addition, the final residues of the microparticles loaded with erioglaucine (sample **F5**) show higher mass loss in comparison to samples **F3** and **F4**, which can be attributed to the presence of payload molecule and the absence of silica.

In non-cross linked alginate particles (sample **F8**), the dehydration step is essentially absent, which indicates a very low moisture content. There is a quick thermal degradation at around 140 ºC to Na_2CO_3, with formation of a carbonized material that decomposes slowly from 230 to 500 ºC. A small residue of Na_2CO_3 is present at the end of heating cycle. The same behavior was observed for the alginate/silica hybrid (sample **F9**), but the sample shows a lower mass loss, which is indicative of the presence of silica. On the other hand, alginate cross-linked samples (**F10**, **F11** and **F13**) display a different thermal behavior at about 60 ºC: the cross-linked alginate sample exhibits a weight loss of approximately of 20%, followed by further dehydration step due to its water content. The results show that the materials start to decompose above 150 ºC through two different weights loss steps: a first degradation step observed in the range 150–410 ºC, resulting in the degradation of calcium alginate into $CaCO_3$ and carbonaceous materials, and a second step at 410–600 ºC. TGA results indicate that cross-linked alginate samples are thermally more stable than the non-cross-linked ones.

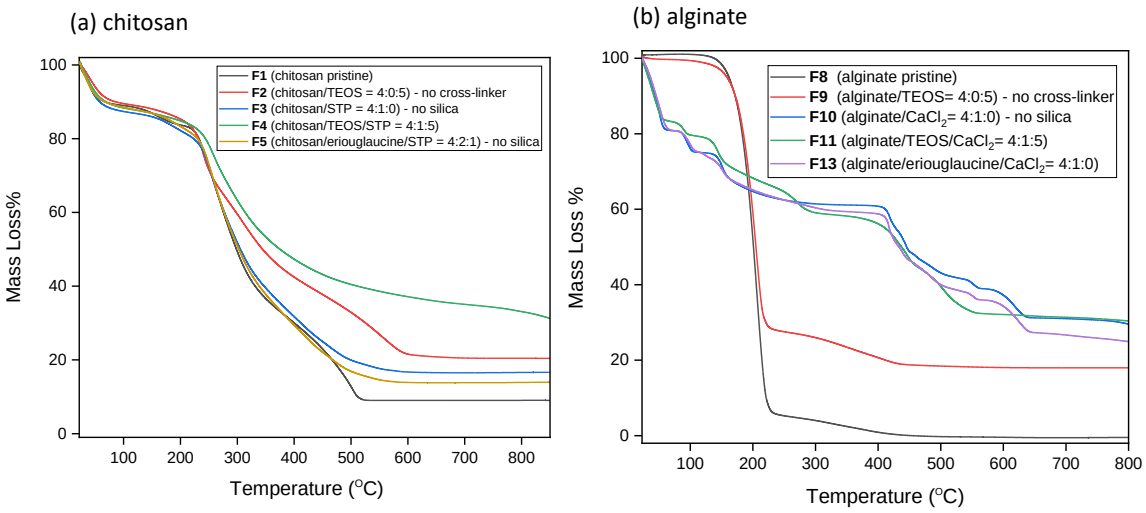

Figure 6.5. TGA traces of (a) chitosan and (b) alginate spray-dried microparticles with polymer:cross-linker:TEOS weight ratios of 4:1:5 (w/w). Spray-dried non-cross-linked samples are also shown for comparison (black lines).

6.2.3 Encapsulation and Release of a Model Hydrophilic Substance

The spray-dried chitosan microparticles were loaded with a model hydrophilic substance (erioglaucine disodium salt). A definite amount (2 wt%) with respect to the polymer weight was mixed to the chitosan solution, with or without presence of TEOS. After

dissolution of the dye, the cross-linker solution was added to these mixtures followed by spray drying, yielding the dye-loaded microparticles.

The hydrophilic molecules were encapsulated with different formulations in the presence (samples **S5** and **S7**) and in the absence of silica (sample **S6**) in order to estimate the effect of silica nanostructures on the release behavior in a comparison study with the non-cross-linked ones.

The release behavior was studied by performing dissolution studies in a phosphate buffer solution (pH = 7.4) at 37 ºC. Figure 6.6 presents the release process from spray-dried chitosan–STP microparticles. The overall release takes place rapidly during the first 3 h (approximately 40% to 60%), which can be attributed to the presence of a sufficient amount of the erioglaucine adhered to the microcapsules surface during the drying steps. Overall, the release is governed by the diffusion ability as a result of swelling process. The data are fitted to the Hill equation, analogously to Chapter 4.

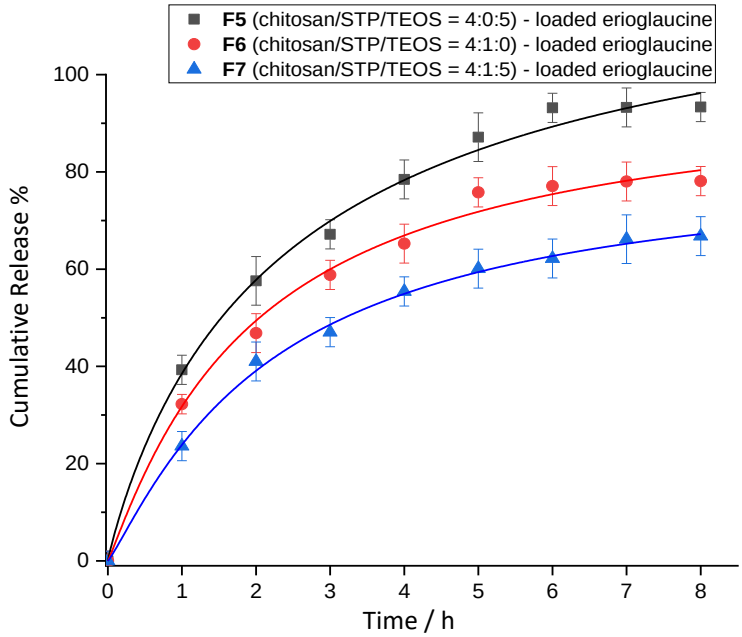

Figure 6.6. Cumulative release of erioglaucine loaded in sample **F5** (chitosan/silica hybrid spray-dried microparticles without cross-linker), sample **F6** (chitosan cross-linked spray-dried particles without silica), and sample **F7** (chitosan/silica hybrid cross-linked microparticles in phosphate buffer, pH = 7.4). The solid lines represent the theoretical fitting according to the Hill equation.

The release of the dye from the non-cross-linked microparticles was higher in the presence of silica (sample **F5**). It is clearly slower in the absence of silica for the cross-linked particles (sample **F6**). This behavior is mainly influenced by the cross-linking density of chitosan with the cross-linker (STP), which decreases the swelling ability of the particles due to the presence of a stronger matrix. On the other hand, chitosan/silica

hybrid cross-linked microparticles (sample **F7**) are more stable, and the release is much slower in comparison with the non-cross-linked ones under the same conditions. This is explained by both the strong complexation of the dye to the chitosan and the adsorption on silica. The results reveal that the hybrid chitosan/silica cross-linked microparticles are more efficient than the non-cross-linked ones in encapsulating erioglaucine as well as retarding its release.

6.3 Catalytic Activity of Microparticles and Comparison to Macroparticles

This part reports the results of the functionalization with Pd(0) of the previously synthetized cross-linked chitosan sub-millispheres of Chapter 4 (considered for comparison) and the spray-dried microparticles prepared in this chapter. The resulting palladium-containing samples are used catalysts for the reduction of 4-nitrophenol with $NaBH_4$. Here, a post-loading approach was chosen, meaning that the Pd(0) loading took place after the formation of the chitosan particles. To optimize this process, we developed two methods, differing in the pH value during the loading-process. In the first method (named in the following as "method A"), the particles were suspended into a hydrochloric acid solution of $PdCl_2$, and separated after stirring for a certain time. Pd(II) was then reduced to Pd(0) with $NaBH_4$. In the second method (named as "method B"), the pH value of the acidic $PdCl_2$ suspension was first increased from 1 to 12 before the separation and reduction processes. Obviously, the catalytic activity depends on the surface area of the catalyst and, therefore, on the diameter of the particles. To study the influence of particle size on activity, two catalysts of micrometer particle size were prepared. The microparticles were loaded with palladium using only method B. Table 6.2 summarizes the prepared catalysts.

Table 6.2. Overview of the conditions and carrier systems of the prepared catalysts.

Formulations	Before Loading	Method A	Method B
Macroparticles	**S1** (no silica)	**S1-Pd$_A$**	**S1-Pd$_B$**
	S3 (with silica)	**S3-Pd$_A$**	**S3-Pd$_B$**
Microparticles	**F3** (no silica)	—	**F3-Pd$_B$**
	F4 (with silica)	—	**F4-Pd$_B$**

6.3.1 Characterization of Surface Morphology and Compositions of the Prepared Catalysts (Macroparticles and Microparticles)

The morphology of the prepared catalyst was investigated by scanning electron microscopy (SEM). Figure 6.7 shows the SEM images of the different macrocatalysts prepared with macroparticles from Chapter 4 (labeled with **S**). The presence of silica and the post-loading method have a great impact on the surface morphology of the prepared catalysts. The surface of catalyst **S1-Pd$_A$**, (without silica) shown in Figure 6.7a–c is rather uneven, which may be explained by the effect of the presence of Pd nanoparticles. In contrast, catalyst **S3-Pd$_A$** (Figure 6.7d–f), which was post-loaded with Pd(0) with the same method but in the presence of silica, has an even although rough surface. As previously explained in this thesis, silica incorporation in the chitosan particles increases the structural stability. Hence the chitosan particles with incorporated silica are not as prone to damage during the post-loading process as particles without incorporated silica.

Catalyst **S1-Pd$_B$**, (without silica, Figure 6.7g–i,) shows some irregularities on its surface, but it is relatively smooth when compared to **S1-Pd$_A$**, (without silica) and **S3-Pd$_A$**. It seems that the raising of pH from 1 to 12 in method 2 has a positive impact on the particle stability. The surface morphology of catalyst **S3-Pd$_B$** (Figure 6.7j–l, with silica) differs notably from the other catalysts. The surface of the particles is streaked with cracks. The different surface morphologies could have an impact on the catalytic activity of the particles due to their different active surface areas during the reaction. The relative concentration of Pd was determined by energy dispersive X-ray analysis (EDX) and the obtained values are listed in Table 6.3.

Table 6.3. Pd concentration on the surface of the different catalysts determined by EDX.

Post-loading method	Catalyst	Relative Pd concentration [wt %]	Relative Pd concentration [at %]
Method A	**S1-Pd$_A$** (no silica)	4.49	0.62
	S3-Pd$_A$ (with silica)	3.77	0.52
Method B	**S1-Pd$_B$** (no silica)	14.8	2.25
	S3-Pd$_B$ (with silica)	15.8	2.41

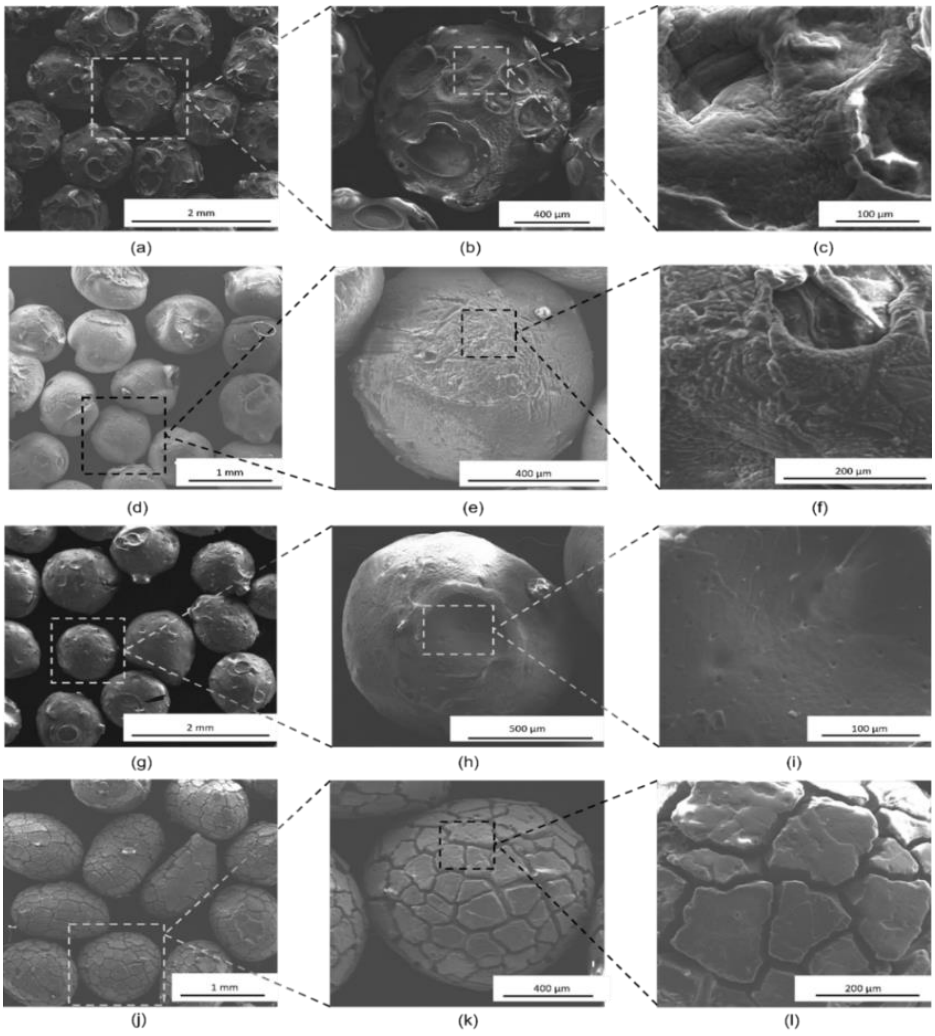

Figure 6.7. SEM images of macroparticle catalyst **S1-Pd$_A$** (no silica (a–c)), **S3-Pd$_A$** (with silica (d–f)), **S1-Pd$_B$** (no silica (g–i)), and **S3-Pd$_B$** (with silica (j–l)) at different magnifications.

The results of Table 6.3 suggest that method B increases the amount of Pd on the particle surface considerably. The determined amount of Pd is 3–4 times as high for **S1-Pd$_B$** (no silica) and **S3-Pd$_B$** (with silica) than for **S1-Pd$_A$** (no silica) and **S3-Pd$_A$** (with silica). On the other hand, the presence of silica in the particles has no significant effect on the amount of Pd fixed. Apparently, a high pH value during the post-loading process favors the attachment of Pd on the surface of the chitosan particles. It is well known that absorption of cations by chitosan is highly dependent on the availability and protonation state of the amino-groups.[193] In the basic medium provided by method B, Pd^{2+} is present in solution as tetrachloropalladate $[PdCl_4]^{2-}$, which can interact with the amino groups either by electrostatic attraction or complexation.[194-196] Since the pK_a value of chitosan is 6.4–6.5,[197] the amino-groups of chitosan are protonated at pH = 1 and, therefore, the main course of interaction will be electrostatic in nature. Nevertheless, the amino groups

remain unprotonated at pH = 12, acting as ligands that can replace the chloride anions of the tetrachloropalladate complex. The last mechanism seems to favor the aggregation of Pd on the particle surface. Furthermore, high pH values create favorable conditions for the reduction of Pd(II) with $NaBH_4$ during the second step of the post-loading process.

An elementary geometric calculation indicates that the ratio surface to volume increases as particle radius decreases. Higher surface to volume ratios is preferable in heterogeneous catalysis, since bigger surfaces mostly correspond to an enhanced accessibility of the active centers for reactants, which speeds up the reaction. The microparticles synthetized were post-loaded with Pd using a method similar in conditions to method B.

Figure 6.8 shows the SEM images of catalysts **F3-Pd$_B$** (without silica) and **F4-Pd$_B$** (with silica). The SEM images show that the chitosan microparticles (sample **F3**) stick together after the post-loading process rather than remain as separate entities. As in the case of macroparticles, the presence of silica seems to have an impact on the structure of the material. Thus, for catalysts **F4-Pd$_B$**, chitosan/silica hybrid microparticles (polymer-to-TEOS ratio of 3:4) individual particles are still distinguishable, in comparison with the images of **F3-Pd$_B$** (without silica). In addition to the SEM images, the relative concentration of Pd normed on the C-value was determined by EDX. The measured Pd quantities are listed in Table 6.4.

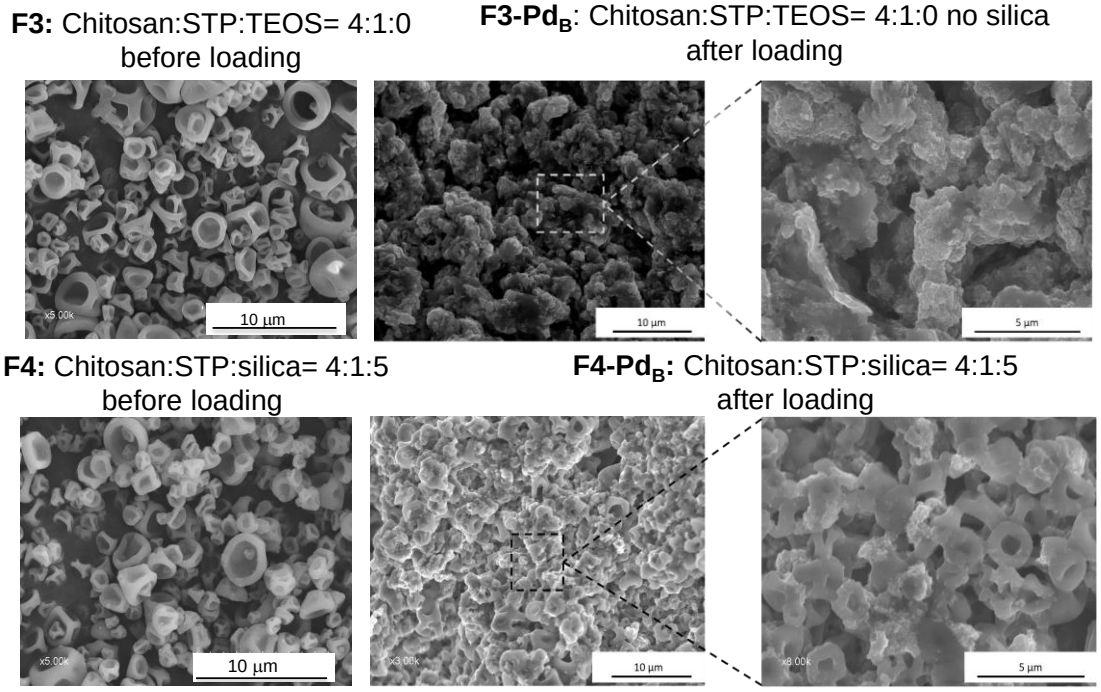

Figure 6.8. SEM images of (a) catalyst F3-Pd$_B$ (without silica), and (b) F4-Pd$_B$ (with silica) at different magnifications.

Table 6.4. Surface concentration of Pd for catalysts **F3-Pd$_B$** and **F4-Pd$_B$** determined by EDX**.**

Post-loading method	Catalyst	Relative Pd concentration (C normed) [wt %]	Relative Pd concentration (C normed) [at %]
Method B	**F3-Pd$_B$** (no silica)	66.41	19.3
	F4-Pd$_B$ (with silica)	49.38	11.6

Compared to samples post-loaded by method B, the relative amount of Pd on the surface of **F3-Pd$_B$** (no silica) and **F4-Pd$_B$** (with silica) resulted to be 3 to 4 times higher than in catalysts **S1-Pd$_B$** and **S3-Pd$_B$** Here, the particles without silica **F3-Pd$_B$** had a significantly higher proportion of Pd than those with silica. Because this high amount of Pd was not expected, the EDX mapping of Pd on the particles was recorded to investigate the surface distribution of Pd was on the material. Figure 6.9 shows the images of the EDX mapping.

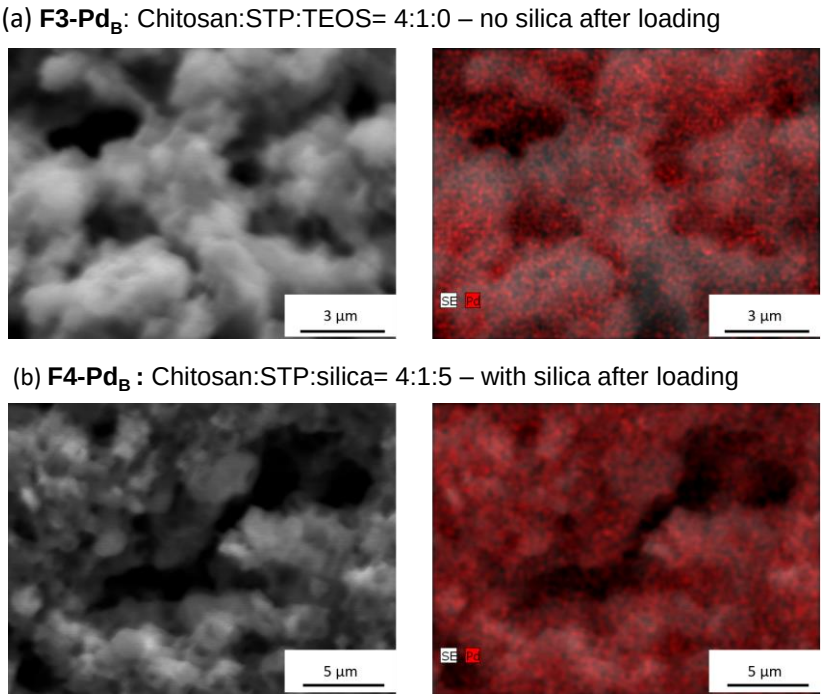

Figure 6.9. EDX mapping of Pd on catalysts **F3-Pd$_B$** (without silica, a) and **F4-Pd$_B$** (with silica, b). Pd is shown in red.

From the images, it is apparent that Pd covers not only the surface of the microparticles materials, but the metal is also found in the region where the microparticles are stuck together.

6.3.2 Catalytic Experiments

The catalytic activity of the materials was tested for the hydrogenation of 4-nitrophenol using $NaBH_4$ as the hydrogenating agent. Formally, the hydrogenation can be described in diluted solution by the simplified process shown in Figure 6.10, based on the model of Haber.[198-199] This pathway consists of three consecutive reactions leading to the formation of a 4-aminophenol from the *N*-(4-hydroxyphenyl)hydroxylamine through the corresponding nitroso derivative.

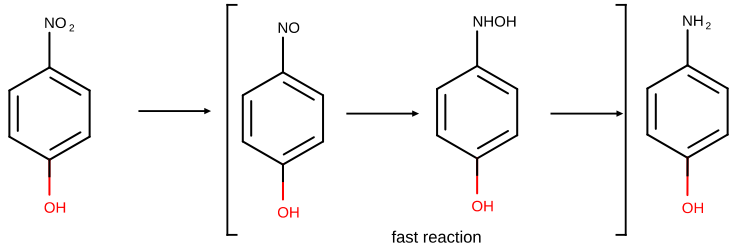

Figure 6.10. Direct Haber pathway for 4-nitrophenol.

The literature suggests that reduction of 4-nitrophenol with borohydride is simple enough to be used as a suitable model for activity comparison.[200-203] For this system, the intermediate products (i.e., *N*-(4-hydroxyphenyl)hydroxylamine and 4-nitrosophenol) reduce so rapidly that only 4-aminophenol is detected and, therefore, the overall reaction associated to the pathway is described by the reaction shown in Figure 6.11.

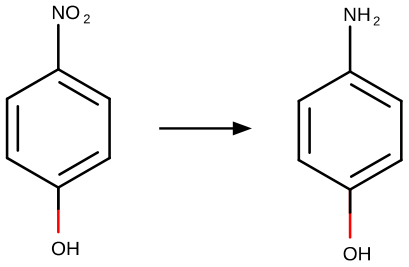

Figure 6.11. Overall reaction for reduction of 4-nitrophenol to 4-aminophenol.

Despite its apparent simplicity, the rate law for this heterogeneous reduction depends heavily on the catalyst used. In this regard, the reaction is usually described as first-order, but there is strong evidence that the rate law is more complicated due to the nitroarene and hydride adsorption phenomena on the Pd surface.[204-206]

Reactions were followed by taking aliquots at different reaction times and analyzed by HPLC with diode-array UV-vis detection. Chromatograms showed two main peaks,

the UV-vis-spectra of which over the reaction time are shown in Figure 6.12. The compounds were identified by comparison with pure standards as 4-nitrophenol (adsorption maximum at 317 nm, retention time R_t = 3 min) and 4-aminophenol (absorption maximum at 273 nm, retention time R_t = 1 min).[10,11]

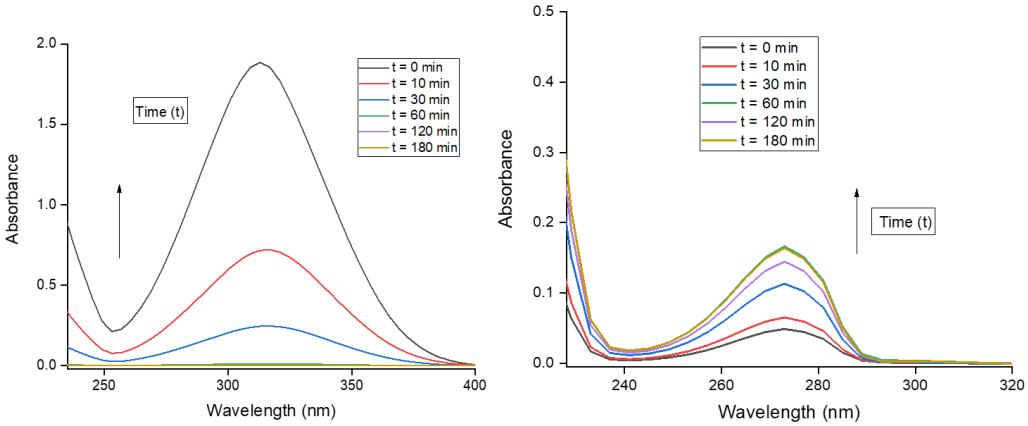

Figure 6.12. UV-vis spectra for 4-nitrophenol (a) and 4-aminophenol (b) recorded at different reaction times.

The conversion of 4-nitrophenol against the reaction time shown in Figure 6.10 and calculated according to Eq. 6.1,

$$M = 1 - \frac{[\mathrm{NP}]_t}{[\mathrm{NP}]_0} = 1 - \frac{A_t - A_\infty}{A_0 - A_\infty} \tag{6.1}$$

where NP stands for 4-nitrophenol, A_t stands for its absorbance at 317 nm, and A_0 and A_∞ are absorbance at zero time and by the end of reaction. Assuming a first-order kinetics, the change of x with time is given by Eq. 6.2,

$$x(t) = 1 - e^{-kt} \tag{6.2}$$

where k is the pseudo-first order rate constant for the direct conversion to 4-aminophenol. It should be noted that pseudo-first order conditions are achieved as reactions are conducted in a large $NaBH_4$ excess. Consequently, this coefficient depends on the reducing agent concentration. The k values were calculated by the non-linear least-squares fitting of experimental x data to those calculated from Eq. 6.2. Results of data analysis are collected in Figure 6.13 and Table 6.5.

To compare the activity of palladium deposited on different carriers using different post-loading methods, the turn over frequency (TOF) was calculated. TOF is defined as the quotient between the substrate disappearance rate and the active center concentration, in this case the quantity of Pd put in the reactor:

$$\mathrm{TOF} = -\frac{r_{\mathrm{NP}}}{[\mathrm{Pd}]} \tag{6.3}$$

Since the TOF value is time-dependent through r_{NP}, we will take the half-reaction time ($t_{1/2}$) as a reference. On the other hand, to avoid the use of a particular kinetic model, we will use for comparison the TOF time-average calculated at half-reaction:

$$\mathrm{TOF}_{1/2} = \frac{0.5[\mathrm{NP}]_0}{t_{1/2}[\mathrm{Pd}]} \tag{6.4}$$

The experimental half-life time $t_{1/2}$ was determined by reading it directly from the graph by extrapolating a straight line between data points. $TOF_{1/2}$ values are gathered in Table 6.5.

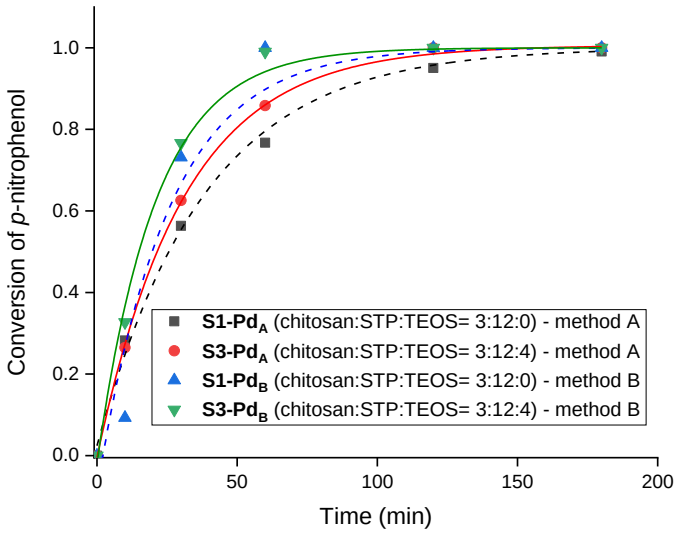

Figure 6.13. Experimental values of conversion of 4-nitrophenol (x) against the reaction time together with the fitting to the exponential plots given by Eq. 6.2. Catalysts post-loaded by method A are shown in black and red, catalysts post-loaded with method B in green and blue, particles with incorporated silica are shown with dashed lines, and particles without silica are shown with solid lines.

Catalysts post-loaded with method B (**S1-Pd$_B$, S3-Pd$_B$**) exhibit rate constant values slightly higher than those post-loaded with method A (**S1-Pd$_A$, S3-Pd$_A$**). For both

methods, the catalysts with incorporated silica (**S3-Pd$_A$, S3-Pd$_B$**) entail a faster reaction than ones without silica incorporated (**S1-Pd$_A$, S1-Pd$_B$**).

Table 6.5. Activity parameters for the macroparticles catalysts **S1-Pd** and **S3-Pd** by the two methods **A** and **B**.

Catalyst	$TOF_{1/2}$ / min^{-1}	k / min^{-1}	$t_{1/2}$ / min^{-1}
S1-Pd$_A$	0.13	0.026	25.3
S3-Pd$_A$	0.18	0.033	22.8
S1-Pd$_B$	0.05	0.040	22.5
S3-Pd$_B$	0.06	0.049	17.8

Let us now analyze the activity of the catalysts per mole of Pd used in its preparation through the TOF1/2 values. Catalysts **S1-Pd$_B$** and **S3-Pd$_B$** have a considerable higher Pd(0) load compared to **S1-Pd$_A$** and **S3-Pd$_A$** materials, so it is to be expected that the same amount of Pd will enhance the reaction rate. However, the $TOF_{1/2}$ values of **S1-Pd$_B$** and **S3-Pd$_B$** are significantly lower than those of **S1-Pd$_A$** and **S3-Pd$_A$**. This observation is unexpected since the reaction takes place faster (see *k* values) with the more Pd loaded **S1-Pd$_B$** and **S3-Pd$_B$** materials. An explanation would be that not all of the Pd(0) it is not accessible by the reactants due to the morphology of the carrier surface and the size of the crystallite size, which is related to the post-loading method. The catalysts with silica **S3-Pd$_A$** and **S3-Pd$_B$** have both higher TOFs than their equivalents without silica **S1-Pd$_A$** and **S1-Pd$_B$**. Hence the presence of silica in the particles has a positive effect on the reaction speed. Silica might have an influence on how the Pd agglomerates on the surface of the particles making it more accessible to the reactants during the reaction and hence increasing the reaction speed and TOF. However, this effect is relatively small.

The catalytic activity of the microparticles was tested with the method used for the macroparticles. Figure 6.14 shows the conversion of 4-nitrophenol against the reaction time, whereas Table 6.6 collects the activity parameters of **F3-Pd$_B$** (without silica) and **F4-Pd$_B$** (with silica) materials deduced from the data analysis.

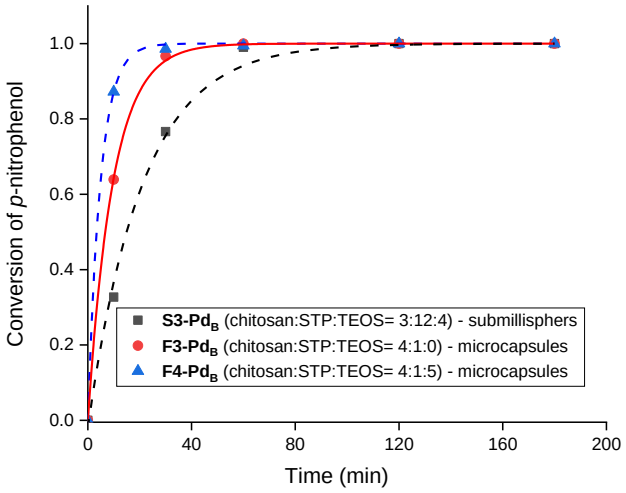

Figure 6.14. Conversion of 4-nitrophenol against reaction time together with the least-squares exponential plots to Eq. 2. Microparticles catalyzed conversions are displayed in blue and red, and **C4** catalyzed conversion in black (for comparison purposes). The conversions of particles incorporating silica are displayed with dashed lines, and solid lines were used for particles that did not contain silica.

Table 6.6. Activity parameters for catalysts **F3-Pd$_B$** (with**out s**ilica**)** and **F4-Pd$_B$** (with **s**ilica**)**.

Catalyst	TOF$_{1/2}$/min^{-1}	*k*/min^{-1}	$t_{1/2}$/ min^{-1}
F3-Pd$_B$ (without silica)	0.03	0.10	7.8
F4-Pd$_B$ (with silica)	0.06	0.21	5.8

As expected, the reaction catalyzed by microparticles exhibited significantly higher *k* values than that catalyzed by macroparticles, and as observed in the case of macroparticles catalysis microparticles containing silica presented lower half-life times. However, TOF$_{1/2}$ values were unexpected, as suggest that microparticles based catalysts are less active per mole of incorporated palladium than the corresponding macroparticulated materials. This observation possibly indicates that the Pd loading method leads to the formation of large Pd crystallites, strongly aggregated, having a poor catalytic activity. This phenomenon would be eventually compensated by the large amount of palladium deposited on the materials when the post-load method B is used on micrometric size chitosan cross-linked particles.

6.4 Conclusions

The present chapter demonstrates the feasibility of the spray-drying method for encapsulating hydrophilic molecule (erioglaucine sodium salt) into chitosan–STP microparticles. This method was selected because it is reproducible, rapid, and relatively easy to scale up. The applied preparation process favored the formation of shrunken microparticles (microcapsules) with some roughness on the surface, attributed to the higher amount of water content inside the particles. The samples showed a high encapsulation efficiency. The results indicated that the cross-linked hybrid chitosan/silica microparticles by this process retarded the release behavior in the neutral medium in comparison with the non-cross-linked ones. They showed as well an excellent catalytic performance for the reduction of *p*-nitrophenol by $NaBH_4$.

6.5 Experimental Section

6.5.1 Materials

Low molecular weight chitosan (Sigma-Aldrich, M_v = 50,000–190,000 Da, 75–85% deacetylated), alginic acid sodium salt (powder, 15–25 cP, 1% in H_2O), glacial acetic acid (Panreac-Química), sodium tripolyphosphate (STP, Alfa-Aesar, ≥ 85%), calcium chloride dihydrate (Sigma-Aldrich, extra pure), tetraethyl orthosilicate (TEOS, Sigma-Aldrich, ≥ 98 %), hydrochloric acid 37% (J. T. Baker), ethanol (Merck, gradient grade for liquid chromatography), erioglaucine disodium salt (Across Organics, pure), and phosphate buffer solution (pH = 7.4) self-prepared with NaCl (Sigma-Aldrich, ≥ 99%), KCl (Sigma-Aldrich, ≥ 99%), $Na_2HPO_4{\cdot}H_2O$ (Schlarlau, reagent grade), and KH_2PO_4 (Sigma-Aldrich, ≥ 99%), palladium(II) chloride (Sigma-Aldrich, 99%), sodium Borohydride (Sigma-Aldrich, 99%), *p*-nitrophenol (Doesder). All chemicals and solvents were used as received. Ultrapure water was used through all the experiments.

6.5.2 Synthesis of Chitosan Hydrogel Microcapsules

Chitosan microcapsules were synthesized by a spray-drying process combined with ionotropic method. A 0.3 wt% chitosan solution[†] was prepared by dissolving the

[†] As commonly done in literature, we speak here about "chitosan solution". However, as indicated in Section 2.1.1 (p. 7), some studies indicate that chitosan may not be fully soluble in acetic acid, even when clear "solutions" are obtained.[27] In that sense, such chitosan colloidal solutions should be strictly referred to as suspensions.

polymer in a 2 % v/v acetic acid aqueous solution. The solution was left under stirring for 24 h at room temperature. As in Chapter 4, for samples with silica (and only for those with silica), 100 μL of concentrated hydrochloric acid (37%) were added to 200 mL of the previously prepared chitosan solution and kept stirring for 1 h. Then, TEOS was added at a rate of 3:4 (wt/wt) in relation to chitosan. The resultant solution was left under stirring for 4 h at room temperature. Cross-linker solution was prepared in deionized water at a concentration of 3 wt%. Chitosan colloids were spontaneously fabricated after dropwise addition of the cross-linker to the chitosan solution at a chitosan-to-STP ratio of 2:1 (wt/wt), under magnetic stirring for 8 h at room temperature. This chitosan-to-STP ratio was selected based on our previous studies, since it provided an opalescent suspension, which is representative for the optimum cross-linking conditions. The chitosan or the chitosan/silica hybrid microparticles were hardened and dried using an equipment Büchi Mini Spray Dryer B-191. The operating parameters were set as follows: inlet air temperature in the range 110 °C, liquid flow rate between 150 and 200 mL/h and aspiration rate in the range 80%. The equipment operated in co-current flow mode. In order to maintain homogeneity, the colloidal solution was kept under magnetic stirring during the spray drying process.

The solid capsules were collected from the apparatus collector and stored under vacuum at room temperature. The production yield was expressed as the ratio between the weight percentage of the final product and the total amount of sprayed materials.

6.5.3 Swelling Study

The swelling behavior of the spray-dried polysaccharide and polysaccharide/silica hybrid cross-linked microspheres in the dissolution medium were determined. A known weight (100 mg) of spray-dried cross-linked microspheres were placed in phosphate buffer solution pH = 7.4 for a period of 8 h. The swollen microspheres were collected via centrifugation, and the wet weight of the swollen microspheres was determined by first blotting the particles with filter paper to remove absorbed water on the surface and then weighing immediately on an electronic balance. The weight of the swollen microspheres was recorded at a pre-determined time period (2, 4, 6, and 8 h). The percentage of swelling of the micro-spheres in the dissolution media was then calculated by using the expression

$$\text{Mass swelling (\%)} = \frac{w_w}{w_d} \times 100 \quad (6.5)$$

where w_w is weight of particles at a certain time and w_d is the initial weight of the dried particles. Data points are average of three measurements. The weight loss percentage was estimated with the expression

6.5.4 Preparation of Microcapsules Loaded with Hydrophilic Dye

Erioglaucine disodium salt was employed as a payload molecule to study the release profile from the chitosan-based microcapsules in phosphate buffer pH = 7.4 at 37 °C. Hydrophilic molecule (2 wt %) was added to the chitosan aqueous solution during the initial step with constant stirring at 800 rpm for 2 h. Spray drying was performed using an equipment Büchi Mini Spray Drier B-191. When the liquid was fed to the nozzle with peristaltic pump, atomization occurred by the force of the compressed air, disrupting the liquid into small droplets. The droplets, together with hot air, were blown into a chamber where the solvent in the droplets was evaporated and discharged out through an exhaust tube. The dry product was then collected in a collection glass path. The preparation process of drug loaded chitosan-STP microspheres by spray drying method is shown in Figure 6.1 Alginate submillispheres were analogously prepared following the same procedure, but using $CaCl_2$ as a physical cross-linker. The concentrations of the components of all samples prepared in this work are listed in Table 6.1.

6.5.5 Dye Release from the Loaded Microcapsules

The release of the entrapped hydrophilic molecule (erioglaucine) was assessed by using a dialysis membrane method. Physical separation of the dosage forms is achieved by usage of a dialysis membrane which allows for ease of sampling at periodic intervals. The loaded chitosan microparticles were placed inside a dialysis bag (regular dialysis) with a MWCO 14 kDa containing release media (inner media/compartment) that is subsequently sealed and placed in a larger vessel containing release media of volume 200 mL (buffer solution, pH = 7.4, outer media), the release cells consisted of cylindrical thermo jacketed glass vessels connected to a water bath set at 37 °C, the receptor solution was stirred by means of a magnetic stirrer at 300 rpm to homogenous all the unstirred buffer layers. The volume enclosed in a dialysis bag (inner media) was 5 mL of the phosphate buffer which is significantly smaller than the outer volume. Dye liberated

from the microcapsules diffuses through the dialysis membrane to the outer compartment which was mainly dependent on the dye solubility to transport across the dialysis membrane from where it is sampled for analysis. At prescribed time intervals, aliquots were extracted and replaced by the same fresh volume, then the samples monitored spectrophotometrically at 629 nm and the concentration of the dye was determined using the calibration curve. The fraction of the released amount can be calculated from the following equation:

$$\text{Fraction released} = \frac{\text{Amount released}}{\text{Amount entrapped}} \times 100 \tag{6.6}$$

6.5.6 Post-Loading of Chitosan Particles with **Pd**

To functionalize the prepared macroparticles with Pd(0) two different post loading methods were employed, which differed in the pH-value during the process.

1st Method (X Method)

$PdCl_2$ (0.004 mol/L) was dissolved in aqueous hydrochloric acid (0.1 mol/L, pH = 1). To the solution the prepared particles were added and then stirred overnight. Afterwards the particles were separated by filtration and washed with distilled water. They were then placed in an aqueous solution of $NaBH_4$ (0.075 mol/L, 25 mL), which was stirred until the reduction of Pd(II) was completed. The particles were then separated again by filtration, washed with distilled water and dried at 50 °C under reduced pressure.

2nd Method (Y Method)

$PdCl_2$ (0.004 mol/L) was dissolved in aqueous hydrochloric acid (0.1 mol/L, pH = 1). To the solution the prepared particles were added and then stirred for 3 h. Then NaOH pellets were added to the solution until the pH value raised to approximately pH = 12. The solution was then stirred overnight. Afterwards the particles were separated by filtration and washed with distilled water. They were then placed in an aqueous solution of $NaBH_4$ (0.075 mol/L, 25 mL), which was stirred until the reduction of Pd(II) was completed. The particles were then separated again by filtration, washed with distilled water and dried at 50 °C under reduced pressure.

Post Loading of Microparticles

The prepared microparticles of chitosan and chitosan/silica hybrid microparticles were post loaded with Pd through these steps: a $PdCl_2$ (0.004 mol/L) was dissolved in an aqueous hydrochloric acid (0.1 mol/L, pH = 1) to the solution specific amount of microparticles (50 mg) were added. The acidic solution was stirring for 3 h at 800 rpm, then it was raised to a basic pH = 12 by adding NaOH pellets and kept stirring overnight at room temperature. Afterwards, the particles were separated by centrifugation (10,000 rpm, 10 min). They were then placed in an aqueous solution of $NaBH_4$ (0.075 mol/L, 25 mL), which was stirred until the reduction of Pd(II) was completed. The particles were then separated again by centrifugation, washed with distilled water and dried at 50 °C under reduced pressure.

6.5.7 Test of Catalytic Activity

All catalysis experiments were done under a protective Ag atmosphere with overpressure. Before the experiments, an aqueous stock solution of *p*-nitrophenol (0.001 M) was flushed with Ag for 30 min at 25 °C in an ultrasound bath to expel any solved oxygen in the solution. Afterwards the *p-n*itrophenol solution (5 mL, 0.005 mmol) was added to $NaBH_4$ (~1.5 mmol, 0.3 M) and the respective catalyst (~ 5 mg). The reaction mixture was then stirred at 700 rpm at 25 °C in a thermoshaker (Double block Thermomixer MHL23, Hettich). To follow the reaction progress, aliquots of 100 µL were taken after 0, 10, 30, 60, 120 and 180 min. The aliquots were diluted in 1 mL of distilled water and then frozen immediately to stop any on-going reactions in the samples. They were stored at −20 °C for further investigation.

6.5.8 Separation with HPLC and Detection with UV-vis

The educt *p*-nitrophenol and the product *p*-aminophenol of the catalytic tests were detected by UV/vis after they were separated by HPLC. For the HPLC a reverse phase phenyl-hexyl column (100×4.6 mm, 2.6 µm particle size) was used. As an eluent a 30/70 mixture of acetonitrile/HCl_{aq} (0.05 mmol/L) was used. The detection was done with a Photodiode Array Detector (MD-2018 Plus, Jasco).

6.5.9 Surface Morphology

The surface morphology of the microcapsules was investigated through analysis by scanning electron microscopy (SEM) (Hitachi, model S4800). The powders were previously fixed on a brass stub using double-sided adhesive tape and then were made electrically conductive by coating, in a vacuum, with a thin layer of platinum (approximately 3–5 nm), for 3 min and at 30 W. Images were taken by applying an electron beam decelerating voltage of 0.5 kV and magnifications of 3k or 3.5k or 5k or 7k.

Chapter 7

Chitosan/Silica Hybrid Nanogels by Inverse Nanoemulsion for Encapsulation of Hydrophilic Substances*

In this chapter, we describe a strategy for the synthesis of hybrid chitosan/silica nanohydrogels by combination of the gelation of chitosan in a miniemulsion system with a sol–gel process to produce silica. Two different methods were used and their efficiency for entrapping a hydrophilic substance (erioglaucine disodium salt) was investigated by studying the release in a neutral medium (phosphate buffer, pH = 7.4). As in the rest of the thesis, chitosan was also used here as a biopolymer matrix and in-situ prepared silica was used as a structuring additive. The formulation of hydrogel nanocapsules based on chitosan was obtained by ionic interaction of the cationic groups of the polymer with the anionic groups of the cross-linker. The size of the obtained nanocapsules ranges from 50 to 200 nm, as determined by DLS and electron microscopy. The stability of the nanoemulsion was evaluated with a multiple light scattering apparatus that combines transmission and back-scattering measurements (Turbiscan). For both preparation methods, the release behavior of erioglaucine was retarded when silica was present in the systems.

7.1 Introduction

The synthesis of nanocarriers has attracted much attention in recent years for being applied in medical diagnostic and drug release research. Nanocarriers can significantly improve therapeutic efficiency while limiting possible undesirable effects. Different

* Chapter based on a manuscript with the same title by A. Elzayat, K. Landfester, and R. Muñoz-Espí (in preparation for publication, 2021).

types of nanocarriers are used for drug delivery, including liposomes, micelles, microspheres, solid lipid nanoparticles (SLN), and hydrogel nanoparticles.[106, 207-208]

Over recent years, biodegradable nanoparticles (BNPs) have been used as drug nanocarriers. BNPs play a vital role in increasing the stability of therapeutic agents by protecting them against degradation or oxidation, and they possess a useful control release performance. The major goal in designing these nanoparticles as drug carriers are controlling the particle size, surface properties, and release behavior of pharmaceutical substances to reach the specific site of action with an optimal rate.[79, 209] The drug can be dissolved, encapsulated, entrapped or attached to the nanoparticle matrix.[210-211]

Biopolymers have been used as nanocontainers in the drug release field. By entrapping the drug inside them, they can effectively deliver the drug to the specific site of action.[212-213]

Hydrogels are three-dimensional, cross-linked networks that can absorb and retain significant amounts of water, without dissolving or losing their structures.[5] Thus, considerable research efforts have been directed towards the developing of polymeric nanohydrogels, especially attractive materials for drug delivery. First, their inner network structure can be used for entrapping drugs. Second, their surface functional groups can be easily conjugated to receptor-specific molecules to achieve a targeting ability.[163, 214] Moreover, due to their open network structure, they can undergo swelling–deswelling transitions in response to the changes in pH, ionic strength or temperature.[215-217] Therapeutic efficiency could be dramatically improved as well by the engineering of a targeted release system for a drug, which is loaded inside the network of the hydrogel nanoparticles.[218]

Emulsion techniques are commonly used for producing nanoparticles aiming at high encapsulation efficiency. The formation of the nanoparticles using miniemulsion system was previously studied by Landfester and coworkers.[219-223] The utilization of miniemulsion process offers the possibility of creating stable nanocapsules with a size range from 50 to 500 nm.[82] The synthesis of nanocapsules can be accomplished by different procedures using a variety of materials as a core or hybrid the polymer matrix with inorganic fillers such as silica or magnetic nanoparticles.[109, 114, 224]

Silica is one of the most studied materials with respect to polymer-based hybrid systems for drug delivery.[108, 125, 158, 225] It has been demonstrated that it provides significant enhancement in the mechanical properties when combined into a polymeric

matrix and hence, it has also an effect on the drug release mechanism.[161-162, 226] However, encapsulation of hydrophilic compounds with high loading efficiency remains a challenge. The formation of hybrid systems with the presence of silica nanostructures are useful with that respect.[227]

In this study, cross-linked chitosan hydrogel nanoparticles are prepared by an inverse (water-in-oil, W/O) nanoemulsion technique by using sodium triphosphate (STP) as a cross-linking agent. The gels are formed through electrostatic interactions between the opposite charges of the polymer and the cross-linker in an ionically gelation reaction.[154-156, 228-229]

7.2 Synthesis of Chitosan and Chitosan/Silica Hybrid Nanocapsules

Physically cross-linked chitosan and chitosan/silica hybrid nanocapsules were synthesized by an inverse nanoemulsion (i.e., water-in-oil) combined with ionotropic method, which allowed us to encapsulate hydrophilic substances. An electrostatic interaction between polyelectrolyte and an oppositely charged cross-linking agent, STP, takes place during the nanoemulsion process, as schematically depicted in Figure 7.1. Tetraethyl orthosilicate (TEOS) was added to a chitosan solution in the pre-emulsified step, yielding silica nanostructures upon contact with water, which is trapped in the biopolymer matrix, leading to a hybrid chitosan/silica network structure.

Two different methods based on the nanoemulsion process were carried out. In the first, named as “one-nanoemulsion” method, is a nanoemulsion/gelation process in which the preparation of chitosan nanoparticles takes place by adding the cross-linking agent directly to a nanoemulsion that contains an aqueous solution of chitosan in the disperse phase. The physical cross-linking takes place after an additional ultrasonication step, which leads to gelation and formation of the nanoparticles. The second strategy, named as “two-nanoemulsion” method, consists in mixing two independent nanoemulsions, the first containing the chitosan and the second containing the cross-liker. The gelation and the nanoparticles formation take place by fusion of the droplets of the two nanoemulsion.

In both strategies, TEOS was added to incorporate silica in the polymer matrix during the particle formation. The compositions of the nanoparticles prepared in this

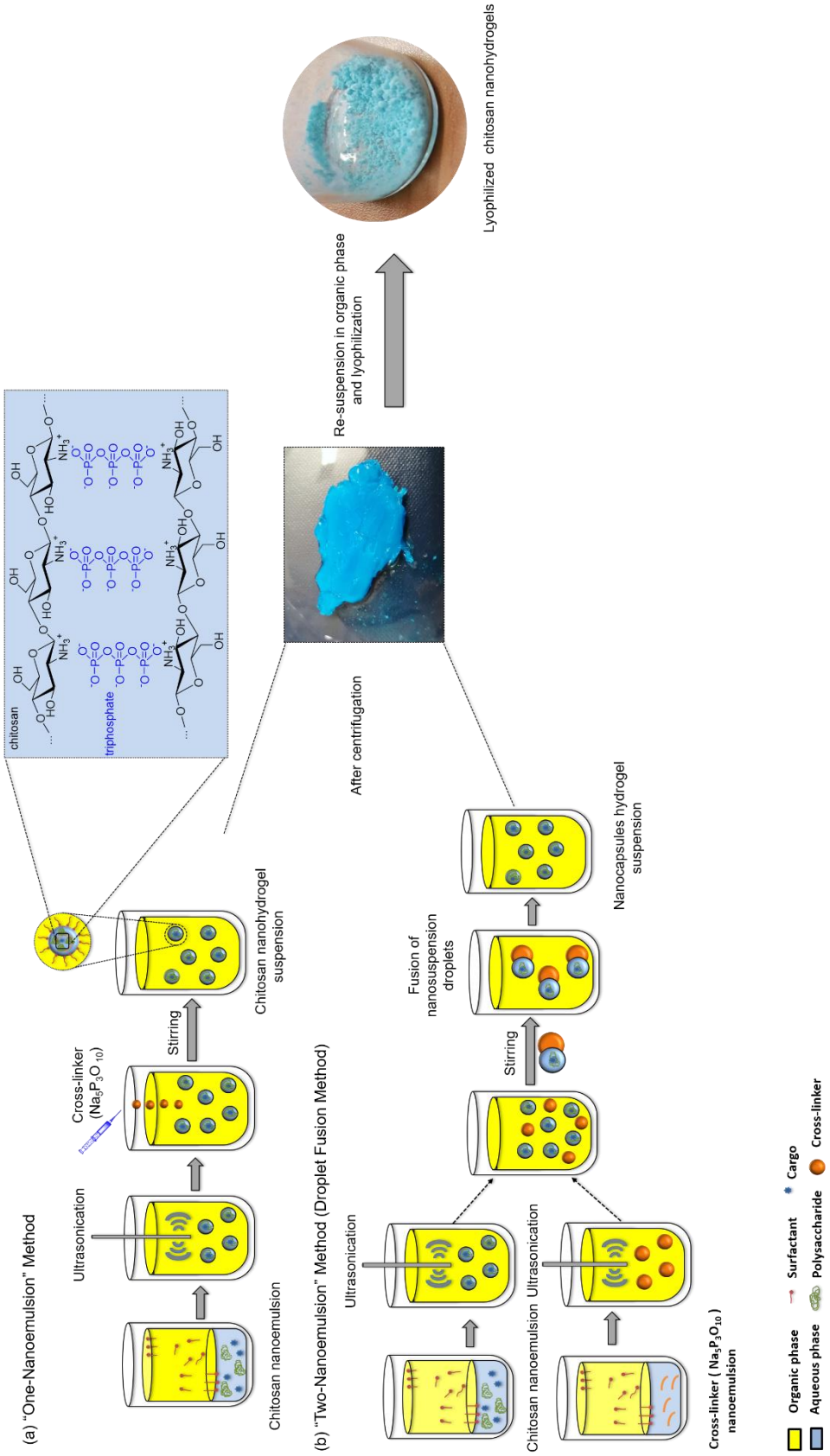

Figure 7.1. Schematic representation of the formation of cross-linked chitosan nanohydrogel encapsulating active hydrophilic molecule through different nanoemulsion mechanisms (a) "one-nanoemulsion" method (b) "two-nanoemulsion" method (droplet-fusion method).

work are summarized in Table 7.1. Chitosan nanoparticles were cross-linked with STP and loaded with erioglaucine disodium salt, taken as model hydrophilic molecule (samples **E3**, **E4**, **E7**, and **E8**). The hybrid chitosan/silica systems were prepared with a polymer-to-TEOS weight ratio of 3:4.

Table 7.1. Compositions of chitosan and chitosan/silica hybrid hydrogel nanocapsules

Sample	System	Preparation Method	Polymer: cross-linker: TEOS weight ratio	Initial load (in situ)
E1	Chitosan	One-nanoemulsion	3:1:0	—
E2	Chitosan/silica	One-nanoemulsion	3:1:4	—
E3	Chitosan	One-nanoemulsion	3:1:0	Erioglaucine
E4	Chitosan/silica	One-nanoemulsion	3:1:4	Erioglaucine
E5	Chitosan	Two-nanoemulsion	3:1:0	—
E6	Chitosan/silica	Two-nanoemulsion	3:1:4	—
E7	Chitosan	Two-nanoemulsion	3:1:0	Erioglaucine
E8	Chitosan/silica	Two-nanoemulsion	3:1:4	Erioglaucine

7.3 Characterization of Chitosan and Chitosan/Silica Hybrid Nanocapsules

7.3.1 Particle Size and Morphology

Particle sizes in the nanogel dispersions after preparation were determined by dynamic light scattering (DLS). The results obtained for the two methods are listed in Table 7.2. The hydrodynamic diameter of the hybrid nanoparticles with silica are smaller than for nanoparticles without silica, which is attributed to the effect of silica to decrease the swelling of the gel.

Table 7.2. Hydrodynamic diameters (D_h) of nanoparticles without loading prepared by the two different nanoemulsion methods.

Sample	Preparation method	Polymer:cross-linker:TEOS weight ratio	Hydrodynamic diameter (D_h) before redispersion (nm)
E1	One-nanoemulsion	3:1:0	185 ± 50
E2	One-nanoemulsion	3:1:4	175 ± 65
E5	Two-nanoemulsion	3:1:0	170 ± 70
E6	Two-nanoemulsion	3:1:4	155 ± 70

With the “one-nanoemulsion” method, electron micrographs by SEM and TEM confirm the formation of nanoparticles of nearly spherical shape with a smooth surface and a mean diameter of 120–150 nm for both chitosan and hybrid chitosan/silica systems. Consistent with the DLS results, the sample with silica shows slightly smaller particle sizes than the sample without. As expected, the sizes observed are smaller than the hydrodynamic diameters obtained by DLS, because the particle are able to swell in a liquid medium. TEM images of the particles prepared by the “two-nanoemulsion” method, presented in Figure 7.3, indicate a significantly smaller size than with the “one-nanoemulsion” method, with a very evident capsule morphology proven by darker shells in the micrographs. As a result of the small sizes, SEM images were not representative for the samples Figure 7.2, and only TEM images are shown. The capsule formation can be explained by the cross-linking of the polymer by STP at the water/oil interface of the inverse nanoemulsion. Interestingly, the capsules appear to assemble to form multicapsular structures (see Figure 7.3c2), which can be an indication of the formation of multiple emulsion during the process. The structures formed are in the range 50–100 nm.

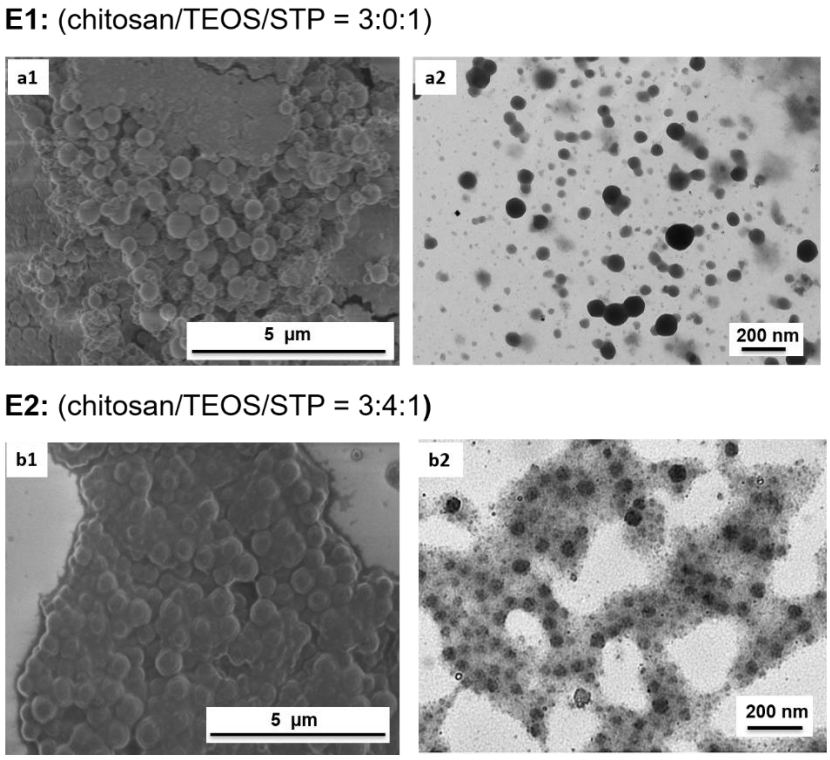

Figure 7.2. Surface morphology by both scanning electron microscopy (SEM) and transmission electron microscopy (TEM) micrographs of (a1, a2) cross-linked chitosan and (b1, b2) chitosan/silica nanohydrogel by “one-nanoemulsion” method (polymer: cross-linker: TEOS weight ratios (3:1:4)).

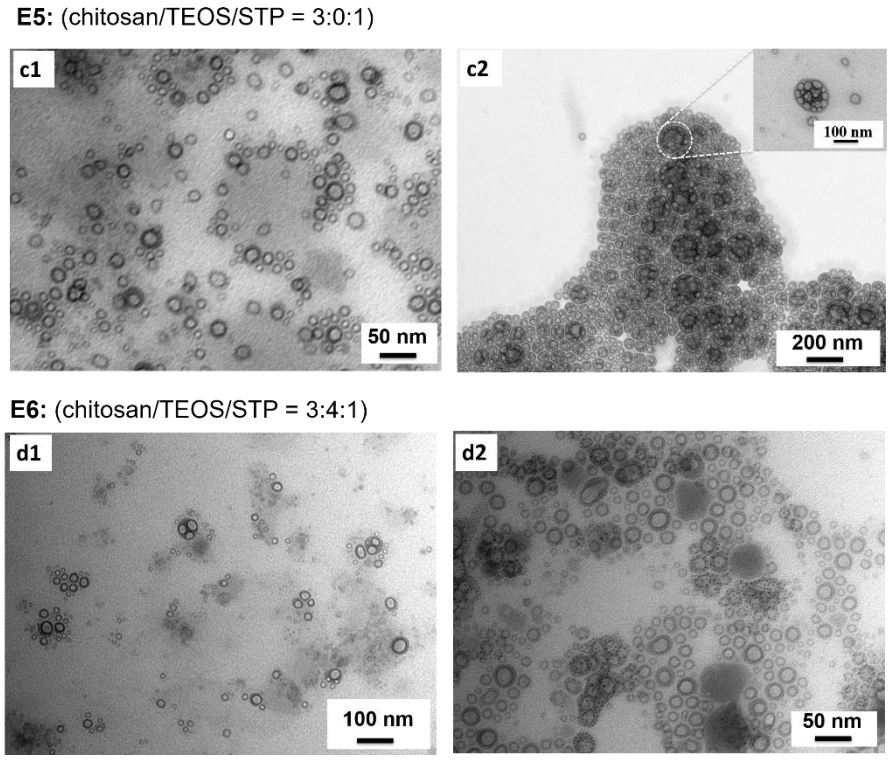

Figure 7.3. Transmission electron microscopy (TEM) micrographs of (c1, c2) cross-linked chitosan and (d1, d2) chitosan/silica hybrid nanohydrogel by "two-nanoemulsion" method (droplets fusion method) (polymer: cross-linker: TEOS weight ratios (3:1:4))

7.3.2 Evaluation of the Stability of Nanoemulsion

The stability of the inverse nanoemulsions was evaluated with a multiple light scattering commercial apparatus that combines transmission and back-scattering measurements (Turbiscan, IESMAT). The measurements of the recorded intensity as a function of time are plotted in Figure 7.4. This technique provides information of the stability of a dispersion or emulsion by assessing any modification concerning sedimentation, droplet migration, or size change. As representative cases, we studied samples **E1** and **E5**, prepared with the "one-nanoemulsion" and the "two-nanoemulsion" method, respectively. The results indicate that the "two-nanoemulsion" method (blue curve, less intensity, less sedimentation) yields a more stable system upon mixing of the two emulsions than the "one-emulsion" system (red curve) after addition of the cross-linker. In the "one-emulsion" system, the cross-linker is in a different phase (aqueous) than the continuous phase (cyclohexane). After re-sonication step affects significantly the system and its stability. In contrast, in the "two-nanoemulsion" method, the system starts with two metastable (kinetically stabilized) emulsions, so it is not surprising that the stability is higher.

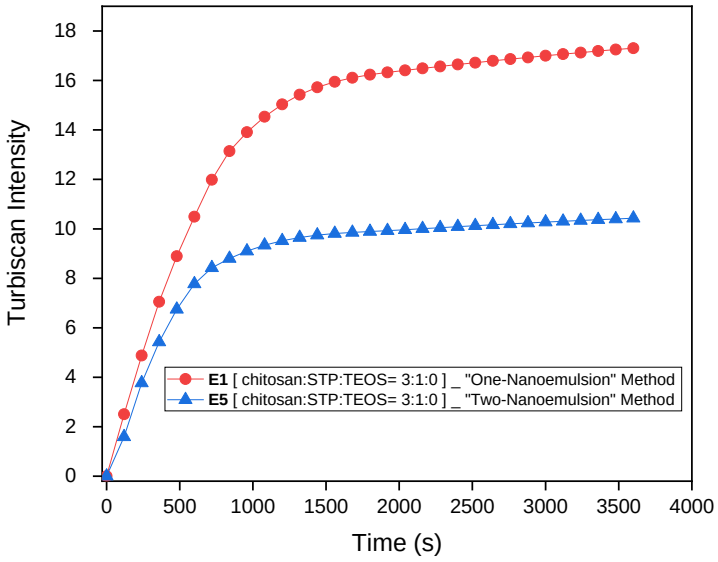

Figure 7.4. Turbiscan stability of cross-linked chitosan nanohydrogel by two different nanoemulsion methods **E1: "**one-nanoemulsion" method and **E2:** "two-nanoemulsion" method**.**

7.3.3 Thermogravimetric Analysis (TGA)

Thermogravimetric analysis (TGA) of the prepared nanocapsules was carried out to evaluate the thermal degradation and to determine the amount of silica. Figure 7.5 presents the TGA traces of both cross-linked chitosan nanoparticles and hybrid ones with silica. The pristine non-cross-linked polymer (in bulk) is also shown as a reference. All the samples show a first decomposition step corresponding to the evaporation of water at temperatures below 100 ºC, followed by the thermal degradation of the polymer between 200 and 300 ºC. Under the air atmosphere of the measurements, the polymer present in sample **E1** (without silica) degrades completely to water and CO_2, and the final residue (about 11%) corresponds to sodium triphosphate. Silica-containing sample **E2** shows a lower mass loss (about 25%), which is related to the silica content.

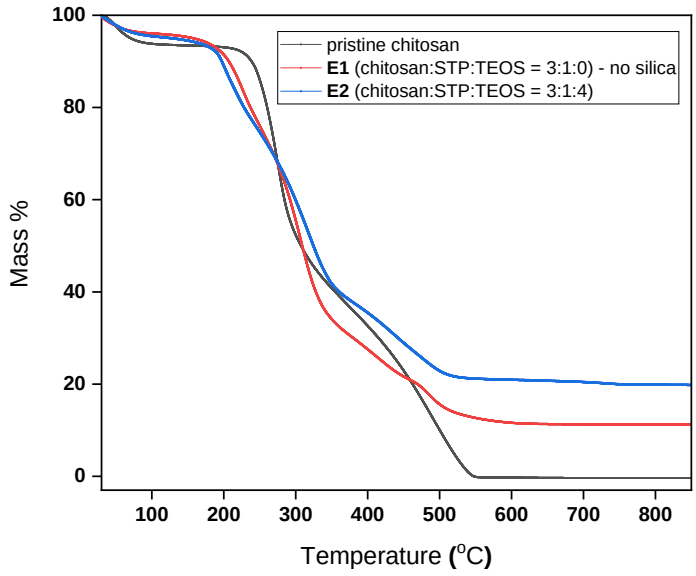

Figure 7.5. TGA traces of chitosan and hybrid chitosan/silica nanogel with polymer:cross-linker:TEOS weight ratios of 3:1:0 and 3:1:4, respectively. Pristine non-cross-linked chitosan is also shown as a reference (black line).

7.3.4 Fourier-Transform Infrared Spectroscopy (FTIR)

The prepared materials were also characterized by FTIR spectroscopy. The corresponding spectra are presented in Figure 7.6, together with the spectra of pure sodium triphosphate and chitosan as references. The spectrum of pure sodium triphosphate shows characteristic bands at 1218 (P=O stretching), 1156 cm^{-1} (symmetrical and asymmetric stretching vibration of the PO_2 groups), 1097 cm^{-1} (symmetric and asymmetric stretching vibration of the PO_3 groups) and 889 cm^{-1} (P–O–P asymmetric stretching).[230-231] The FTIR spectrum of pure chitosan, (Figure 7.6.b) shows three main characteristic bands: at 1650 cm^{-1} (C=O); at 1480 cm^{-1}, attributed to N–H of amine group; and at 1380 cm^{-1}, assigned to C–H. The band in the region 3400–3200 cm^{-1} is attributed to $–NH_2$ and –OH groups stretching vibrations. In the spectrum of the cross-linked nanoparticles, the weak bands at 1218 cm^{-1} can be assigned to the P=O stretching vibration, and the band at 889 cm^{-1} is attributed to P–O–P asymmetric stretching. These signals indicate the presence of phosphate groups in the chitosan-STP nanoparticles. The absorption band at 1530 cm^{-1} could be attributed to the protonation of amine groups $N–H^+$.[231-232] The absorption band of C=O that appears in the spectrum for chitosan is shifted to 1740 cm^{-1} for the cross-linked nanoparticles. New bands, absent in

the spectrum of chitosan, appear at 2850 and 2924 cm^{-1}. FTIR spectra confirm that the cross-linking of chitosan was effective.

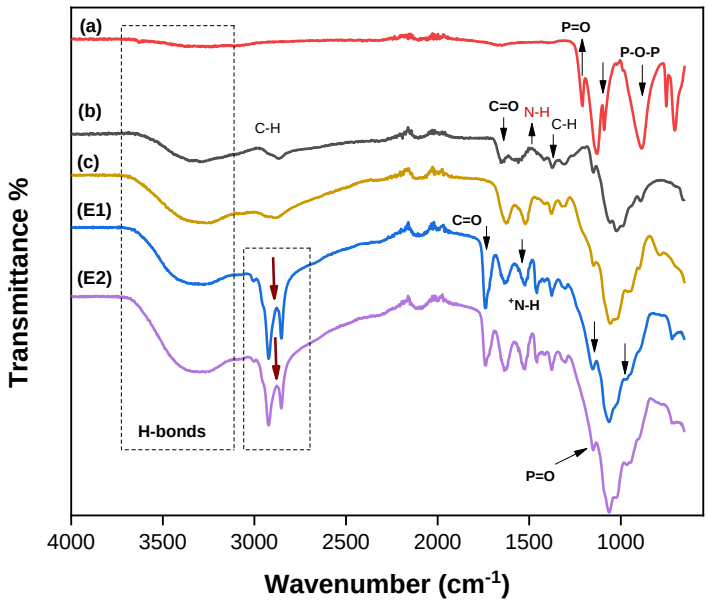

Figure 7.6. FTIR spectra of (a) sodium triphosphate (STP), (b) chitosan, (c) chitosan:STP:TEOS (3:0:4 w/w), (**E1**) chitosan:STP:TEOS=3:1:0, and (**E2**) chitosan:STP:TEOS=3:1:4. nanohydrogel by nanoemulsion method.

7.4 Release of Hydrophilic Substance from the Nanogels

The cumulative release of a definite amount of erioglaucine, entrapped during an in-situ process, was evaluated in phosphate buffer pH = 7.4 in two different ways: a direct "sample and separation" method and an indirect method using a dialysis membrane. The results obtained are presented in Figure 7.7. By using the sample and separation method**,** the release of erioglaucine reaches a plateau of approximately 80 % after 10 h for sample **E3**. This value is attributed to the easy release of the dye to the immersion medium, which is mainly affected by the swelling of the formed nanohydrogel nanoparticles formed by the "one-nanoemulsion" method. For the "two-nanoemulsion" method (sample **E4**), the release after 10 h is slightly lower, of about 70 %. The incorporation of silica nanostructure within the nanocapsules retarders very significantly the release rate by the two different nanoemulsion methods (cumulative release values of 45% and 39% after 10 h for the first and the second, respectively). In addition, the

release continues after 10 h, and no plateau is reached. As in all the systems presented in this thesis, the retardation of the release is attributed to the higher stability of the hybrid nanocapsules, which decreases the swelling and affects the diffusion of the dye to the immersion medium.

By using the dialysis, in which the nanoparticles are introduced in a dialysis membrane placed in the immersion medium (see details in the Experimental Section), the release behavior for both nanoemulsion methods is considerably different. In all cases, in comparison with the direct measurement, the calculated release is lower and no plateau is reached for any sample after 10 h. This different behavior can be mainly attributed to the effect of the diffusion process through the dialysis membrane and to the possible re-adsorption of the dye to the particles (even more important in samples with silica) within the confined space of the dialysis bag. In any case, the general trend for the different samples is the same as the one found with the direct measurements. The experimental curves are empirically fitted to the Hill equation, following the arguments given in Chapter 4.

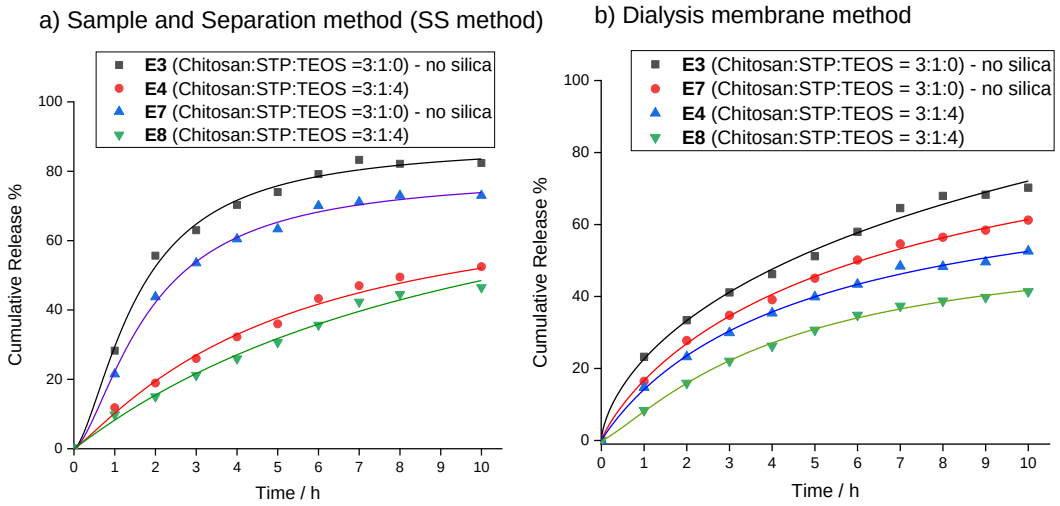

Figure 7.7. Cumulative release in phosphate buffer (pH = 7.4) of erioglaucine, loaded in-situ within chitosan and chitosan/silica hybrid nanohydrogel by two different nanoemulsion processes: a "one-emulsion" method (**E3** and **E4)** and a "two-nanoemulsion" method (**E7** and **E8)**. The release is evaluated by two different strategies: (a) "sample and separation" method and (b) indirect dialysis membrane method.

7.5 Conclusions

Chitosan and hybrid chitosan/silica nanohydrogel capsules with diameters down to less than 100 nm were generated by using the nanoemulsion technique combined with the

ionotropic method. Two different processes were evaluated for the synthesis of these nanohydrogel structures using sodium-triphosphate (STP) as a physical cross-linking agent. The results indicated that the preparation method ("one-nanoemulsion" or "two-nanoemulsion" method) has a significant effect on the nanostructure morphology of final product, allowing the formation of chitosan hydrogel nanoparticles or nanocapsules. The release behavior from chitosan based-hybrid nanohydrogel in neutral surrounding medium of pH = 7.4 was significantly retarded as a result of the incorporation of the silica nanostructured within the polymer matrix

7.6 Experimental Section

7.6.1 "One-Nanoemulsion" Method

In this procedure, a solution of chitosan (3 wt%) was prepared in water acidified with glacial acetic acid (overall concentration of 2 wt%), under magnetic stirring at 400 rpm for 24 h. From this solution, 2 g were added to 8 g of a solution of Span 80 in cyclohexane (1.0 wt%). The mixture was pre-emulsified with the vortex and ultrasonicated (Branson W450 digital Sonifier) using a ½" sonication tip for 3 min with a pulse sequence (10 s on, 2 s off, and nominal intensity of 90 %). After stirring of the emulsion, 1.0 g of an aqueous solution of sodium triphosphate (3 wt%) was added dropwise directly to the emulsified chitosan solution with the help of a plastic syringe provided with a 0.8 × 40 mm 21 G metallic needle (Braun Sterican), as shown in Figure 7.1 The formation and solidification of the cross-linked hydrogel nanoparticles were allowed by stirring at 800 rpm during 24 h. Alternatively, for the hybrid/silica nanoparticles, tetraethyl orthosilicate (TEOS) dissolved in ethanol (proportion of 1:1 in weight) was added to the chitosan solution (0.8 g of TEOS/ethanol mixture to 20 g of chitosan solution). For hybrid samples with silica, 200 µL of concentrated hydrochloric acid (37%) were added to the chitosan solution before dropping the TEOS to ensure the acidic catalysis of the sol−gel process. The mixture was left for stirring during 4 hours. From this chitosan/silica mixture, 2 g were added to 8 g of a solution of Span 80 in cyclohexane (1.0 wt%). The mixture was pre-emulsified with the vortex and ultrasonified using the same previous steps and the emulsion process following the same manner.

Purification of Chitosan Nanoparticles. Chitosan hydrogel nanoparticles were purified by centrifugation. The emulsion after 24 h of cross-linking was transferred to polycarbonate centrifugation tubes. The emulsion was centrifuged at 10,000 rpm for 30 minutes. The supernatant was discarded and the solid was washed three times with distilled water and sonicated for 2 minutes (sonication bath) to remove non-reacted cross-linker. Chitosan nanoparticles were re-dispersed in cyclohexane, lyophilized, and then at 50 ºC for 24 h (Figure 7.8).

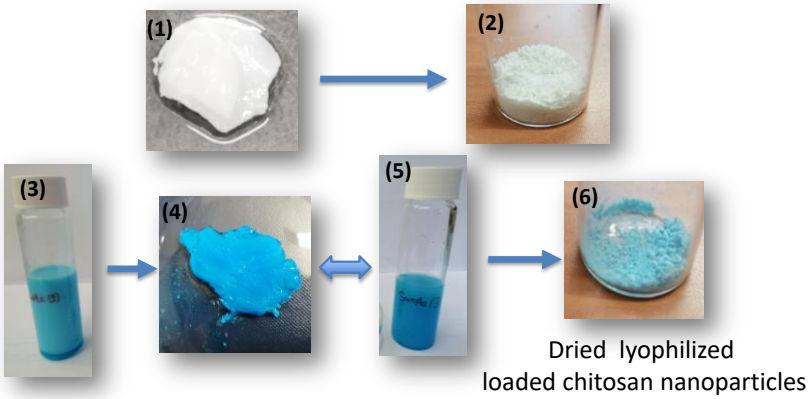

Figure 7.8. Schematic representation of the separation and purification steps of the nanoparticles prepared by inverse nanoemulsion process. (1–2); centrifugation and lyophilization of the solution of chitosan nanoemulsion suspension, (3–5): encapsulating hydrophilic molecule (erioglaucine) followed by ultrasonication step to prepare a solution of chitosan nanoemulsion suspension which is resuspended again in the organic phase and then lyophilized to get dried loaded chitosan nanoparticles.

7.6.2 "Two-Nanoemulsion" Method (Droplet Fusion)

In this process, two separated nanoemulsions for both chitosan and sodium triphosphate were prepared. The chitosan nanoemulsion was analogously prepared as in the "one-nanoemulsion" method, with the same water/oil (cyclohexane and Span 80 solution) ratio. For the cross-linker (STP) miniemulsion, a defined amount (1.0 g) of an aqueous solution of sodium triphosphate (3 wt%) was added to 8 g of a solution of Span 80 in cyclohexane (1.0 wt%). The mixture was pre-emulsified with the vortex and ultrasonified (Branson W450 digital Sonifier) using ½" sonication tip for 3 min with a pulse sequence (10 s on, 2 s off, and 90 % intensity). Finally, the nanoemulsion of the cross-linker (STP) was added dropwise directly to the nanoemulsion of chitosan solution by a plastic syringe provided with a 0.8 × 40 mm 21 G metallic needle (Braun Sterican) and stirred vigorously at 800 rpm for 24 h. The samples were purified as in the previous method.

7.6.3 Encapsulation of Erioglaucine Disodium Salt

Erioglaucine disodium salt was employed as "payload" molecule to study the release profile from the chitosan-based nanoparticles in phosphate buffer pH = 7.4 at 37 ºC. Hydrophilic molecule was loaded into the chitosan nanoparticles during the pre-emulsified step. Stock aqueous solutions of erioglaucine disodium salt (60 mg in 50 mL of water) was freshly prepared. From these stock solutions, 500 µL form both stocks were added to 2 g of the chitosan or chitosan/TEOS solution by mixing vigorously for 2 h. The resulting load amount with respect to the polymer was 1 wt%. The entrapment efficiency of the hydrophilic molecules is significantly high since the inverse miniemulsion (W/O) takes place and hindering the release of the hydrophilic substance to the surrounding (outer phase)**.**

7.6.4 Dye Release from the Nanoparticles

The release of the entrapped hydrophilic molecule (erioglaucine) was assessed by two different methods, described below: "sample and separate" and "dialysis membrane" methods.

1st method "Sample and Separate" Method. This method provides a direct approach to monitor the release of the loaded substance. The lyophilized loaded chitosan nanoparticles are introduced into a large volume (200 mL) of the release media (phosphate buffer, pH = 7.4), which is maintained at a constant temperature (37 ºC). Drug release is monitored by physically separating the nanoparticles from the release media, followed by analysis of the supernatant by centrifugation. Syringe filters (0.2 µm) were used to separate the particles from the release medium. The samples were tested spectrophotometrically at 629 nm. At prescribed time intervals, aliquots were extracted and replaced by the same fresh volume.

2nd method "Dialysis Membrane" Method. The dialysis method was used for studying the release behavior as explained in Chapter 6, section 6.1.4. At prescribed time intervals, aliquots were extracted and replaced by the same fresh volume. Then, the samples were monitored spectrophotometrically at 629 nm, and the concentration of the dye was determined by using a calibration curve.

Chapter 8

General Conclusions and Outlook

This thesis presents the preparation of organic–inorganic biopolymer-based hydrogel carriers by three different methods, which lead to different size scales: macrometric beads are obtained by ionotropic gelation, microparticles are obtained by spray drying, and nanoparticles are obtained by using the nanoemulsion (or miniemulsion) technique. Along the work chitosan and alginate were used as polysaccharides and silica was used as a structuring additive. The ability and efficiency of the different systems to entrap hydrophilic molecules (i.e., erioglaucine disodium salt, ephedrine hydrochloride, and ibuprofen sodium salt) was investigated.

The formation of polysaccharide/silica hybrid sub-millispheres containing silica nanostructures, formed in-situ and embedded within the polymer matrix, was addressed in Chapter 4. The method is simple and forms rapidly hydrogels by extrusion of an aqueous solution in the form of droplets into the cross-linking agent receptor. It also minimizes the use of toxic organic solvents or cross-linking agents. On the basis of the prepared hybrid sub-millispheres, the strategy was further extended to the incorporation of two different hydrophilic substances simultaneously through the preparation of a hybrid 3D macroscaffold (Chapter 5).

Spray drying was used in Chapter 6 to prepare chitosan and alginate microparticles ranging from 1 to 5 μm. The process is reproducible, rapid, and relatively easy to scale up. The use of lower inlet temperatures (110 ºC) significantly favored the production yield and resulted in a good encapsulation efficiency of the hydrophilic substances. To demonstrate the versatility in the applicability of the materials, in addition to the release studies, spray-dried chitosan microparticles were also used as supports for palladium catalysts. Pd(II) ions are complexed by the amino groups present in chitosan and subsequently reduced to Pd(0). The resulting heterogeneous catalysts showed an

excellent performance in the reduction of *p*-nitrophenol by $NaBH_4$, taken as a model reaction.

Finally, in Chapter 7, the preparation of ionically a cross-linked chitosan nanohydrogel was approached through two nanoemulsion strategies. The first method allows us to produce chitosan nanoparticles by adding the cross-linking agent directly to the chitosan nanoemulsion, re-sonifying to allow the diffusion to the droplets. In the second method, two independent nanoemulsions containing the cross-linker and chitosan are mixed together. The fusion of the droplets leads to the formation of a nanocapsular morphology, as proven by electron microscopy, which suggests that the cross-linking takes mainly place at the oil–liquid interface in the nanoemulsion droplets.

In contrast to cytotoxic chemical cross-linkers (e.g., glutaraldehyde), the physical cross-linking agents (such as phosphate ions for chitosan or calcium ions for alginate) are highly biocompatible, which is a great advantage for biological applications.

For all the systems prepared in this thesis, macroparticles, microparticles, and nanoparticles, the presence of silica nanostructures always increases the structural stability of the carriers, influencing the swelling and, consequently, retarding the release of the encapsulated substances. The analysis of the samples by electron microscopy confirmed the presence of silica on the surface of the particles.

Taking into account the diversity in the chemistry of polysaccharides, the work presented here opens a wide range of possibilities to prepare a large variety of biopolymer/inorganic hybrid particles of different materials and sizes, ranging from macroscopic to nanosized systems, depending on the specific desired application. Further research could extend the work to hydrophobized polysaccharides in order to encapsulate not only hydrophilic, but also hydrophobic drugs. The combination of different materials could lead to hierarchical multifunctional materials able to address simultaneously different therapeutical applications. On the other hand, the surface functionalization of the particles with specific ligands could help in the specific migration of the carriers to the action site.

As proven in this work with the catalytic examples, the versatility of polysaccharide hydrogels goes beyond the applications in biomedicine. They offer biocompatible materials able to bind heavy metals, which is of interest not only for catalysis, but also for sustainable applications in water treatment. The addition of magnetic components (magnetite or maghemite), which is feasible for any of the methods proposed in the

thesis, is a line of research to be studied in future. The methodology established here is believed to be extendable to the preparation of magnetic hydrogels, a topic that has started to attract much research attention in recent years.

Appendix

Additional Fitting Data for Release Profiles of Macroscopic Systems (from Chapter 4)

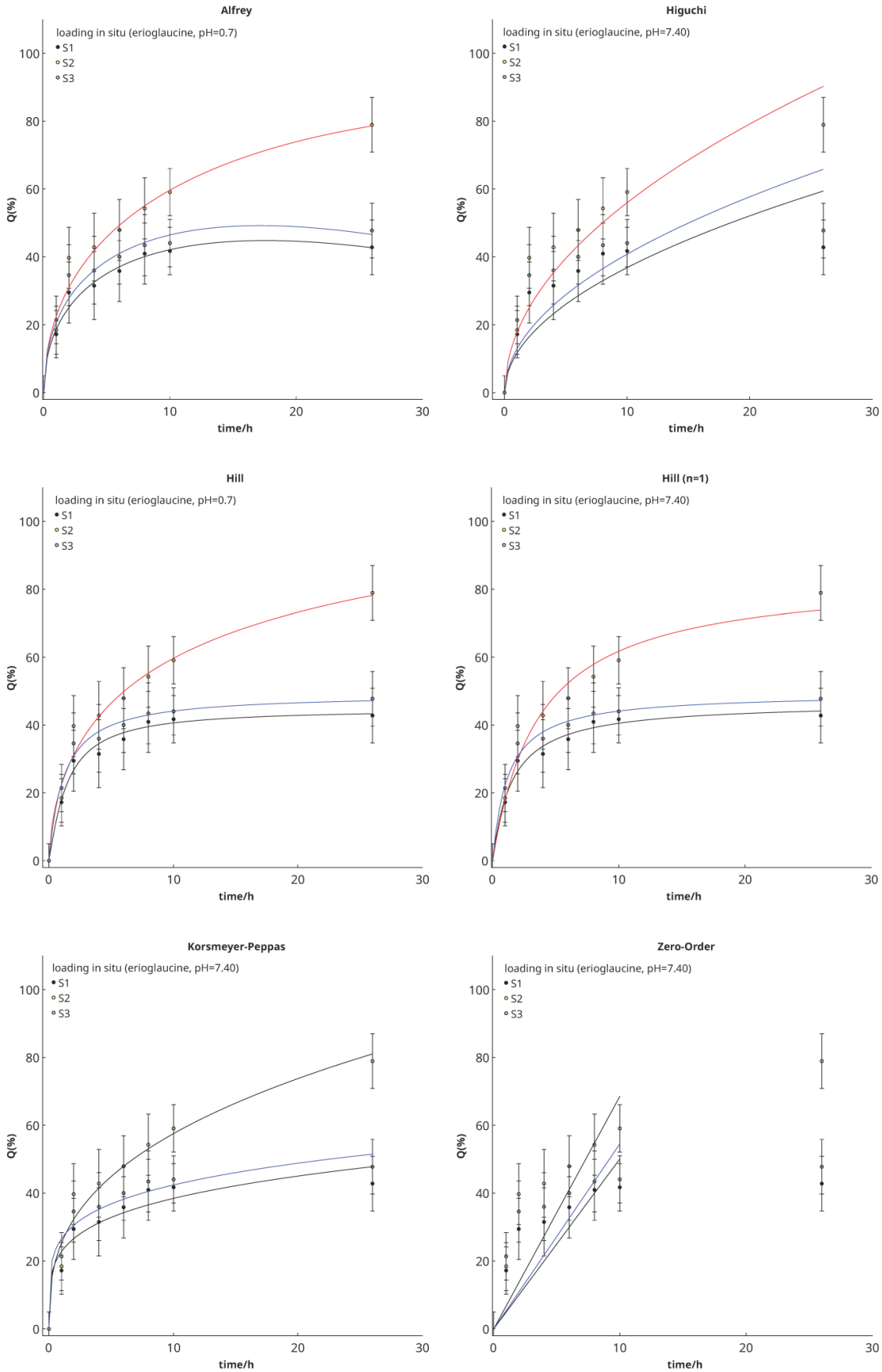

Figure A1. Fittings to the different models corresponding to Figure 4.8b in Chapter 4.

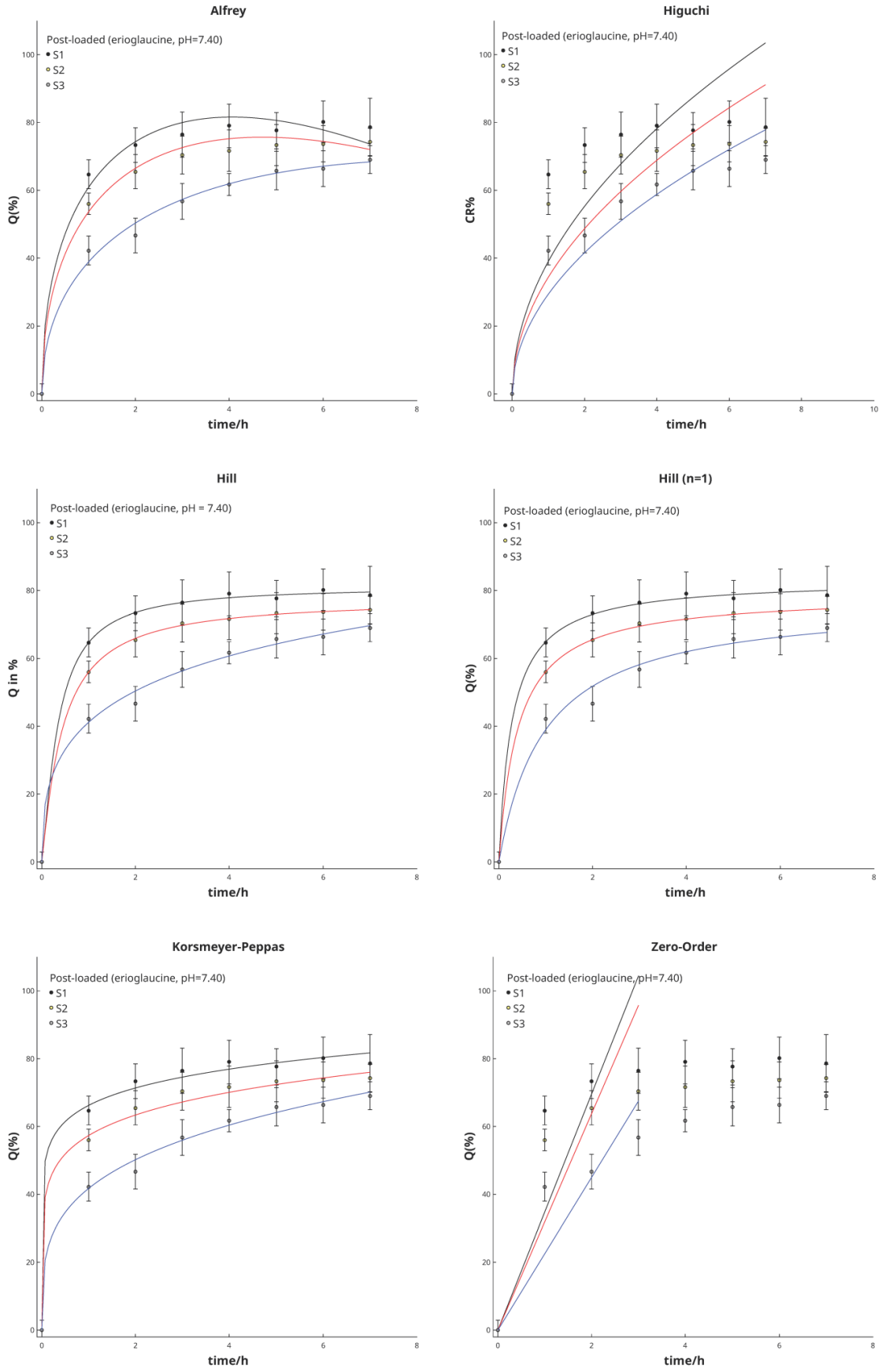

Figure A2. Fittings to the different models corresponding to Figure 4.9a1 in Chapter 4.

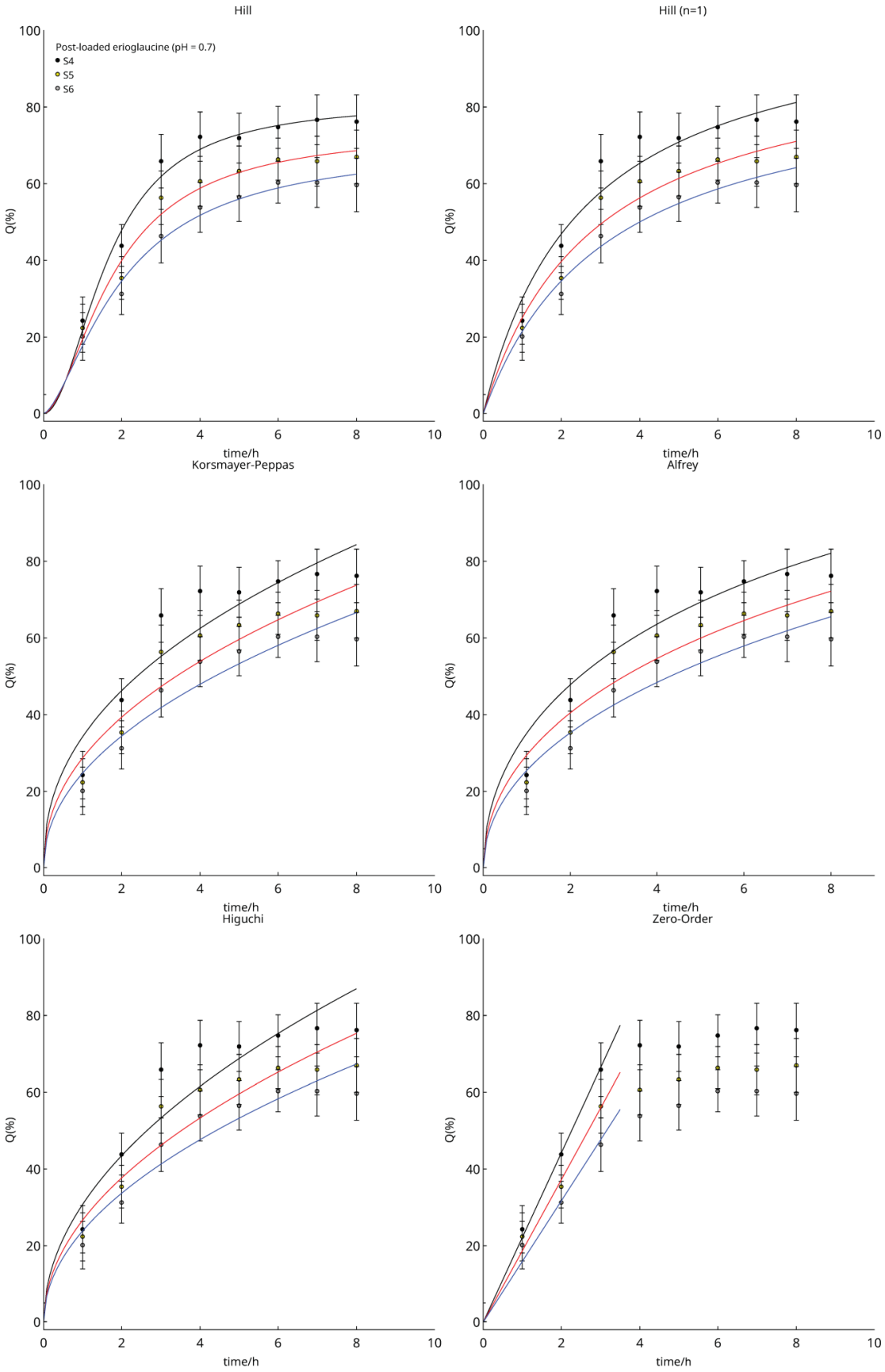

Figure A3. Fittings to the different models corresponding to Figure 4.9a2 in Chapter 4.

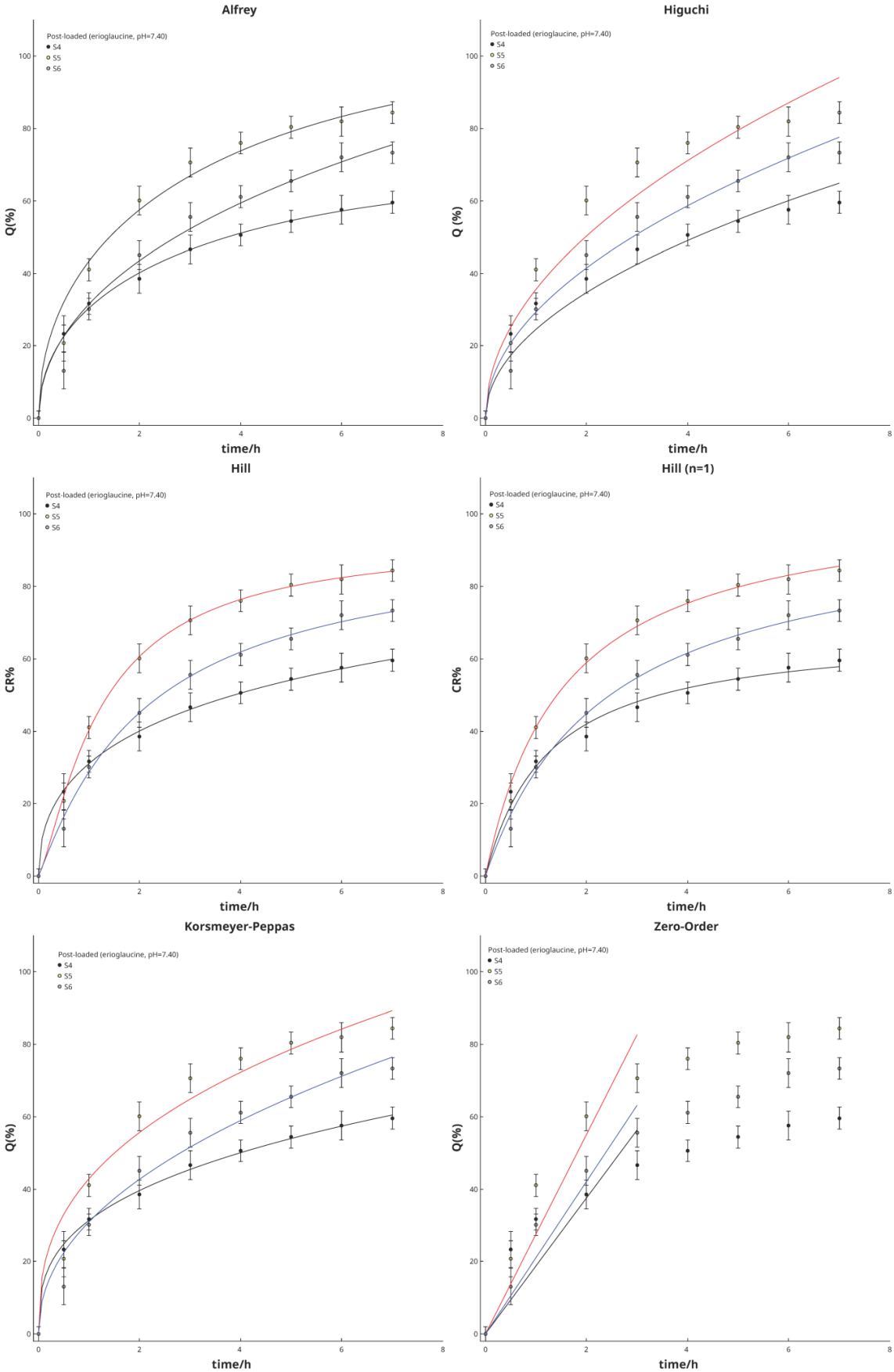

Figure A4. Fittings to the different models corresponding to Figure 4.9b1 in Chapter4.

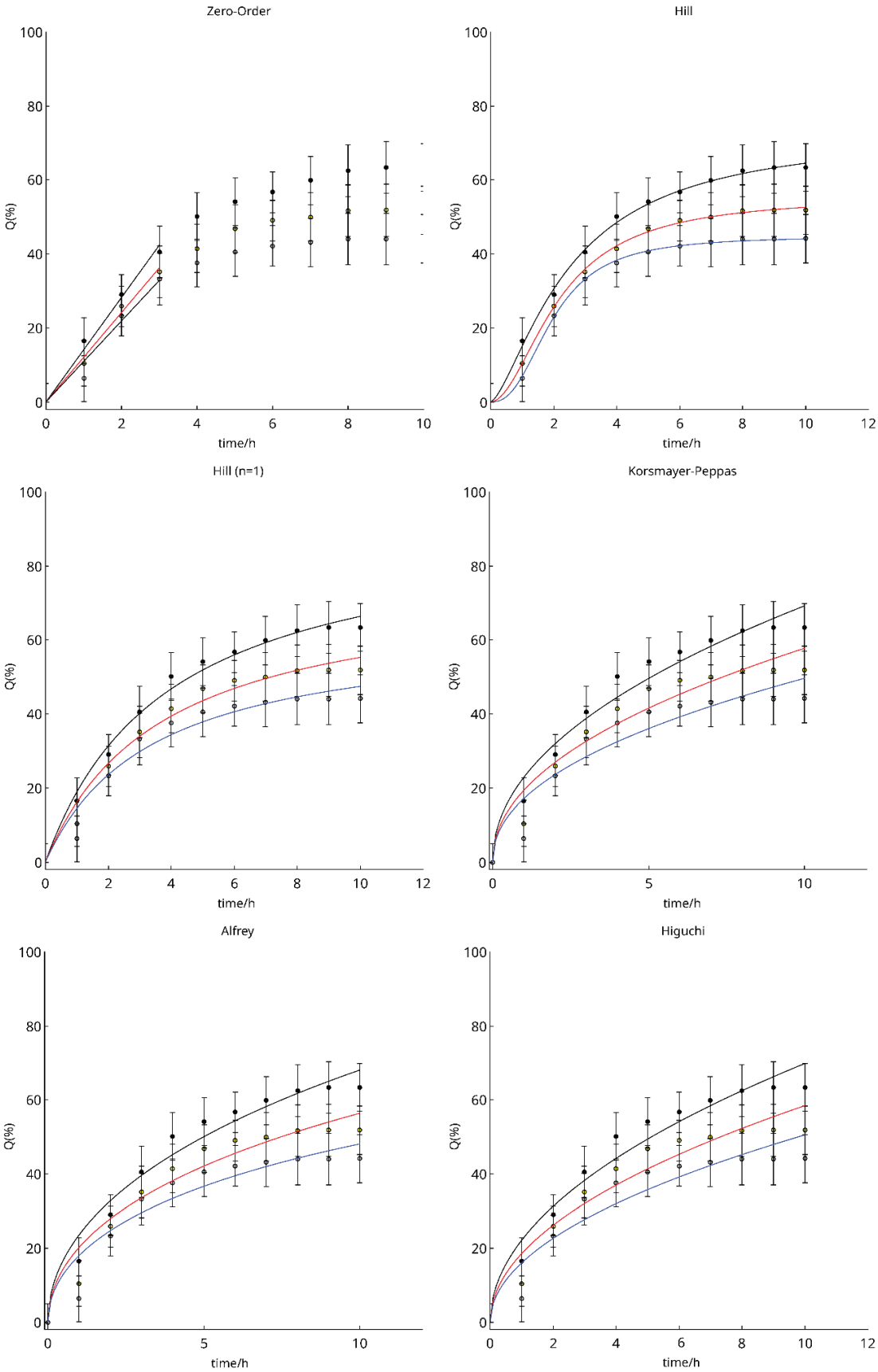

Figure A5. Fittings to the different models corresponding to Figure 4.9b2 in Chapter 4.

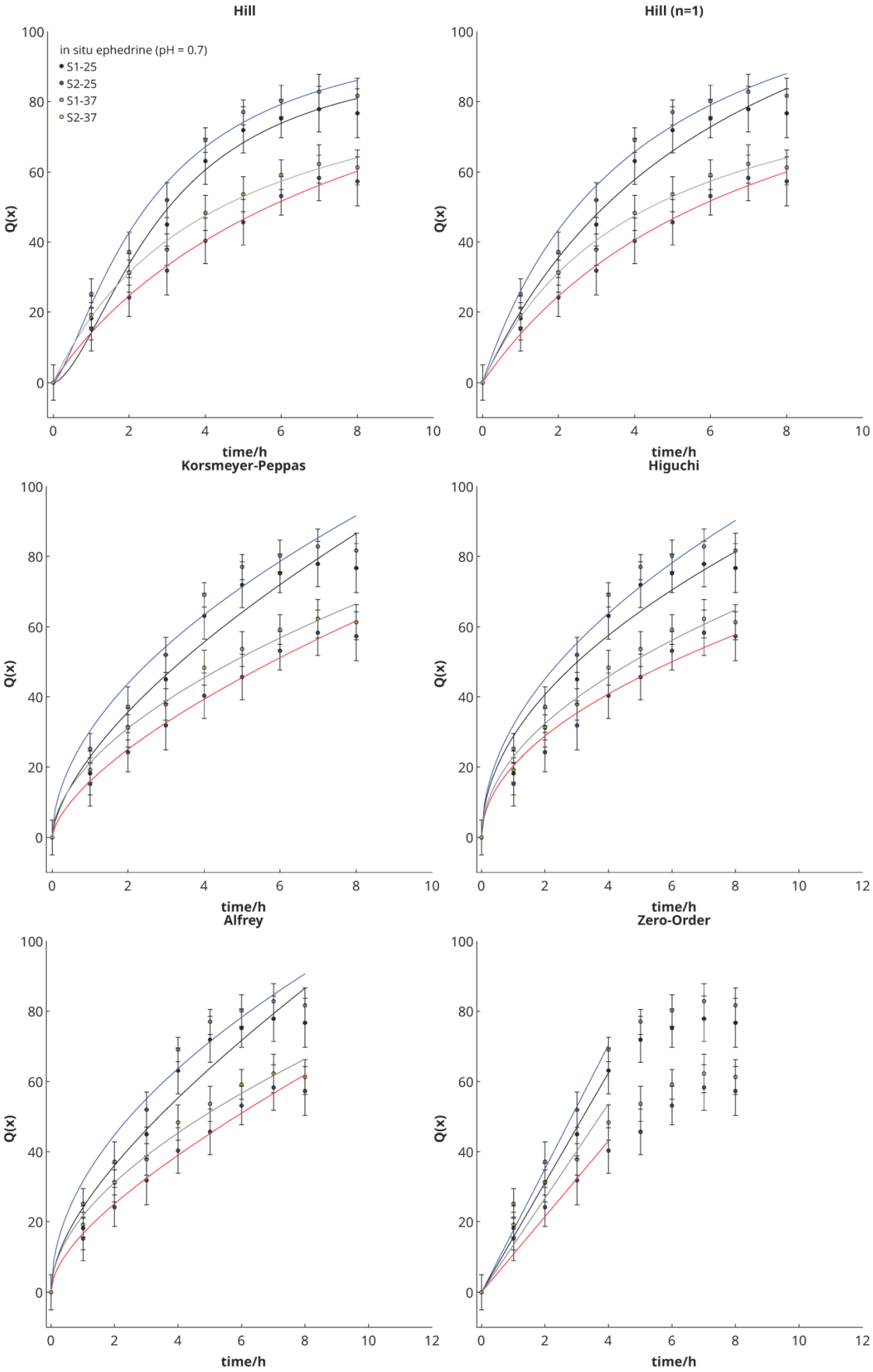

Figure A6. Fittings to the different models corresponding to Figure 4.10a in Chapter 4.

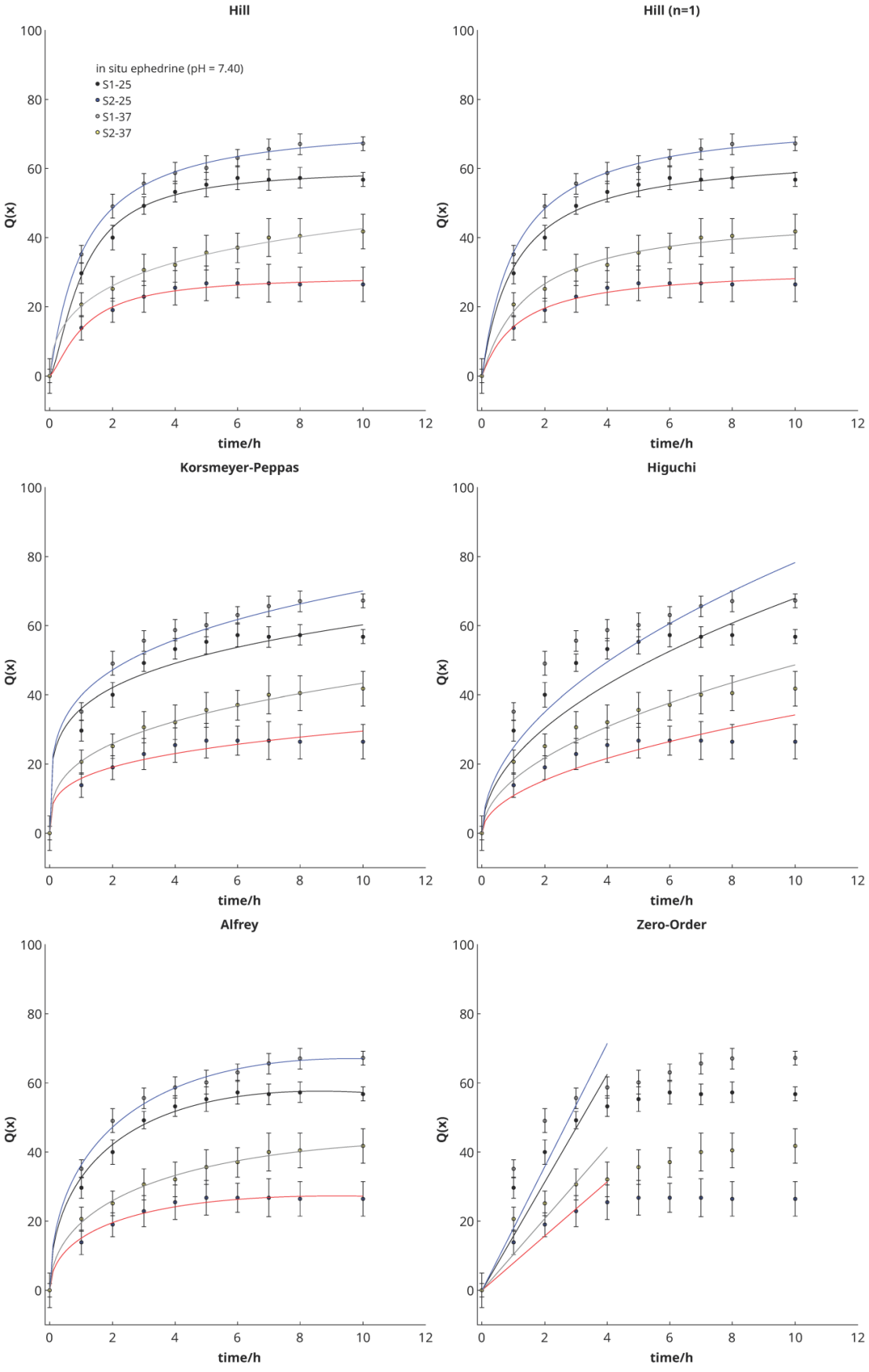

Figure A7. Fittings to the different models corresponding to Figure 4.10b in Chapter 4.

References

1. Zamani, F.; Jahanmard, F.; Ghasemkhah, F.; Amjad-Iranagh, S.; Bagherzadeh, R.; Amani-Tehran, M.; Latifi, M. Nanofibrous and nanoparticle materials as drug-delivery systems. In *Nanostructures for Drug Delivery*, Elsevier: 2017; pp 239-270.
2. Vong, L. B.; Kimura, S.; Nagasaki, Y. Newly Designed Silica-Containing Redox Nanoparticles for Oral Delivery of Novel TOP2 Catalytic Inhibitor for Treating Colon Cancer. *Advanced Healthcare Materials* **2017,** *6* (20), 1700428.
3. Couvreur, P.; Vauthier, C. Nanotechnology: intelligent design to treat complex disease. *Pharmaceutical Research* **2006,** *23* (7), 1417-1450.
4. Prabaharan, M.; Mano, J. Chitosan-based particles as controlled drug delivery systems. *Drug Delivery* **2004,** *12* (1), 41-57.
5. Hamedi, H.; Moradi, S.; Hudson, S. M.; Tonelli, A. E. Chitosan based hydrogels and their applications for drug delivery in wound dressings: A review. *Carbohydrate Polymers* **2018,** *199*, 445-460.
6. Fernando, I. P. S.; Lee, W.; Han, E. J.; Ahn, G. Alginate-based nanomaterials: Fabrication techniques, properties, and applications. *Chemical Engineering Journal* **2019**, 123823.
7. Boi, S.; Rouatbi, N.; Dellacasa, E.; Di Lisa, D.; Bianchini, P.; Monticelli, O.; Pastorino, L. Alginate microbeads with internal microvoids for the sustained release of drugs. *International Journal of Biological Macromolecules* **2020,** *156*, 454-461.
8. Silva, B.; Marto, J.; Braz, B. S.; Delgado, E.; Almeida, A. J.; Gonçalves, L. New nanoparticles for topical ocular delivery of erythropoietin. *International Journal of Pharmaceutics* **2020,** *576*, 119020.
9. Nayak, A. K.; Ahmad, S. A.; Beg, S.; Ara, T. J.; Hasnain, M. S. 12 - Drug delivery: Present, past, and future of medicine. In *Applications of Nanocomposite Materials in Drug Delivery*, Inamuddin; Asiri, A. M.; Mohammad, A., Eds. Woodhead Publishing: 2018; pp 255-282.
10. Nayak, A. K.; Hasnain, M. S. Plant Polysaccharides in Drug Delivery Applications. In *Plant Polysaccharides-Based Multiple-Unit Systems for Oral*

Drug Delivery, Nayak, A. K.; Hasnain, M. S., Eds. Springer Singapore: Singapore, 2019; pp 19-23.

11. Hasnain, M. S.; Ahmed, S. A.; Alkahtani, S.; Milivojevic, M.; Kandar, C. C.; Dhara, A. K.; Nayak, A. K. Biopolymers for Drug Delivery. In *Advanced Biopolymeric Systems for Drug Delivery*, Nayak, A. K.; Hasnain, M. S., Eds. Springer International Publishing: Cham, 2020; pp 1-29.
12. Hasnain, M. S.; Nayak, A. K. Targeted Delivery with Carbon Nanotubes. In *Carbon Nanotubes for Targeted Drug Delivery*, Hasnain, M. S.; Nayak, A. K., Eds. Springer Singapore: Singapore, 2019; pp 37-50.
13. Hasnain, M. S.; Nayak, A. K. 21 - Recent progress in responsive polymer-based drug delivery systems. In *Stimuli Responsive Polymeric Nanocarriers for Drug Delivery Applications*, Makhlouf, A. S. H.; Abu-Thabit, N. Y., Eds. Woodhead Publishing: 2019; pp 569-595.
14. Nayak, A. K.; Hasnain, M. S. Background: Multiple Units in Oral Drug Delivery. In *Plant Polysaccharides-Based Multiple-Unit Systems for Oral Drug Delivery*, Nayak, A. K.; Hasnain, M. S., Eds. Springer Singapore: Singapore, 2019; pp 1-17.
15. Nair, L. S.; Laurencin, C. T. Biodegradable polymers as biomaterials. *Progress in Polymer Science* **2007,** *32* (8), 762-798.
16. Farrugia, C. A.; Groves, M. J. Gelatin Behaviour in Dilute Aqueous Solution: Designing a Nanoparticulate Formulation. *Journal of Pharmacy and Pharmacology* **1999,** *51* (6), 643-649.
17. Caraballo, I. Critical points in the formulation of pharmaceutical swellable controlled release dosage forms—Influence of particle size. *Particuology* **2009,** *7* (6), 421-425.
18. Miranda, A.; Millán, M.; Caraballo, I. Investigation of the Influence of Particle Size on the Excipient Percolation Thresholds of HPMC Hydrophilic Matrix Tablets. *Journal of Pharmaceutical Sciences* **2007,** *96* (10), 2746-2756.
19. Caraballo, I. Factors affecting drug release from hydroxypropyl methylcellulose matrix systems in the light of classical and percolation theories. *Expert Opinion on Drug Delivery* **2010,** *7* (11), 1291-1301.
20. Aguilar-de-Leyva, Á.; Campiñez, M. D.; Jost, F.; Gavira, M.; Caraballo, I. Study of the critical points in combined matrix tablets containing both inert and swelling excipients. *Journal of Drug Delivery Science and Technology* **2019,** *52*, 885-894.

21. Aguilar-De-Leyva, Á.; Campiñez, M.; Casas, M.; Caraballo, I. Critical points and phase transitions in polymeric matrices for controlled drug release. *Handbook of Polymers for Pharmaceutical Technologies* **2015,** *1*, 101-142.
22. Huynh, C. T.; Lee, D.-S. Controlled Release. *Encyclopedia of Polymeric Nanomaterials, 2014* **2014**, 1-12.
23. Nayak, A. K.; Pal, D. Chitosan-based interpenetrating polymeric network systems for sustained drug release. *Advanced Theranostics Materials* **2015**, 183-208.
24. Rasoulzadeh, M.; Namazi, H. Carboxymethyl cellulose/graphene oxide bio-nanocomposite hydrogel beads as anticancer drug carrier agent. *Carbohydrate Polymers* **2017,** *168*, 320-326.
25. De, A.; Nayak, A. K.; Kundu, A.; Das, B.; Samanta, A. Chapter 7 - Gum arabic-based nanomaterials in drug delivery and biomedical applications. In *Biopolymer-Based Nanomaterials in Drug Delivery and Biomedical Applications*, Bera, H.; Hossain, C. M.; Saha, S., Eds. Academic Press: 2021; pp 165-182.
26. Hasnain, M. S.; Nayak, A. K. 21 - Chitosan as responsive polymer for drug delivery applications. In *Stimuli Responsive Polymeric Nanocarriers for Drug Delivery Applications, Volume 1*, Makhlouf, A. S. H.; Abu-Thabit, N. Y., Eds. Woodhead Publishing: 2018; pp 581-605.
27. Thevarajah, J. J.; Bulanadi, J. C.; Wagner, M.; Gaborieau, M.; Castignolles, P. Towards a less biased dissolution of chitosan. *Analytica Chimica Acta* **2016,** *935*, 258-268.
28. Jana, S.; Saha, A.; Nayak, A. K.; Sen, K. K.; Basu, S. K. Aceclofenac-loaded chitosan-tamarind seed polysaccharide interpenetrating polymeric network microparticles. *Colloids and Surfaces B: Biointerfaces* **2013,** *105*, 303-309.
29. Fu, J.; Yang, F.; Guo, Z. The chitosan hydrogels: from structure to function. *New Journal of Chemistry* **2018,** *42* (21), 17162-17180.
30. Ghaffarian, R.; Pérez-Herrero, E.; Oh, H.; Raghavan, S. R.; Muro, S. Chitosan–Alginate Microcapsules Provide Gastric Protection and Intestinal Release of ICAM-1-Targeting Nanocarriers, Enabling GI Targeting In Vivo. *Advanced Functional Materials* **2016,** *26* (20), 3382-3393.
31. Anal, A. K.; Stevens, W. F. Chitosan–alginate multilayer beads for controlled release of ampicillin. *International Journal of Pharmaceutics* **2005,** *290* (1-2), 45-54.

32. Anal, A. K.; Stevens, W. F.; Remunan-Lopez, C. Ionotropic cross-linked chitosan microspheres for controlled release of ampicillin. *International Journal of Pharmaceutics* **2006,** *312* (1-2), 166-173.
33. Bernkop-Schnürch, A.; Dünnhaupt, S. Chitosan-based drug delivery systems. *European Journal of Pharmaceutics and Biopharmaceutics* **2012,** *81* (3), 463-469.
34. Prabaharan, M.; Mano, J. F. Chitosan-Based Particles as Controlled Drug Delivery Systems. *Drug Delivery* **2004,** *12* (1), 41-57.
35. Davidson, P. M.; Taylor, T. M.; Schmidt, S. E. Chemical Preservatives and Natural Food Antimicrobials. In: Doyle, M. P.; Diez-Gonzalez, F.; Hill, C., Eds. *Food Microbiology: Fundamentals and Frontiers*, Wiley: 2019,
36. Gades, M. D.; Stern, J. S. Chitosan Supplementation and Fecal Fat Excretion in Men. *Obesity Research* **2003,** *11* (5), 683-688.
37. Li, K.; Wang, Y.; Huang, M.; Yan, H.; Yang, H.; Xiao, S.; Li, A. Preparation of chitosan-graft-polyacrylamide magnetic composite microspheres for enhanced selective removal of mercury ions from water. *Journal of Colloid and Interface Science* **2015,** *455*, 261-270.
38. Nasirimoghaddam, S.; Zeinali, S.; Sabbaghi, S. Chitosan coated magnetic nanoparticles as nano-adsorbent for efficient removal of mercury contents from industrial aqueous and oily samples. *Journal of Industrial and Engineering Chemistry* **2015,** *27*, 79-87.
39. Miretzky, P.; Cirelli, A. F. Hg(II) removal from water by chitosan and chitosan derivatives: A review. *Journal of Hazardous Materials* **2009,** *167* (1), 10-23.
40. Nayak, A. K.; Ara, T. J.; Saquib Hasnain, M.; Hoda, N. 32 - Okra gum–alginate composites for controlled releasing drug delivery. In *Applications of Nanocomposite Materials in Drug Delivery*, Inamuddin; Asiri, A. M.; Mohammad, A., Eds. Woodhead Publishing: 2018; pp 761-785.
41. Pal, D.; Saha, S.; Nayak, A. K.; Hasnain, M. S. Marine-derived polysaccharides: pharmaceutical applications. In *Natural polymers for pharmaceutical applications*, Apple Academic Press: 2019; pp 1-36.
42. Das, B.; Dutta, S.; Nayak, A. K.; Nanda, U. Zinc alginate-carboxymethyl cashew gum microbeads for prolonged drug release: Development and optimization. *International Journal of Biological Macromolecules* **2014,** *70*, 506-515.

43. Malakar, J.; Nayak, A. K.; Das, A. Modified starch (cationized)–alginate beads containing aceclofenac: Formulation optimization using central composite design. *Starch - Stärke* **2013,** *65* (7-8), 603-612.
44. Tripathi, R.; Mishra, B. "Development and Evaluation of Sodium Alginate–Polyacrylamide Graft–Co-polymer-Based Stomach Targeted Hydrogels of Famotidine". *AAPS Pharmceutical Scientist Technology* **2012,** *13* (4), 1091-1102.
45. Nayak, A. K.; Pal, D. Alginates, blends and microspheres: controlled drug delivery. In *Encyclopedia of Biomedical Polymers and Polymeric Biomaterials, 11 Volume Set*, CRC Press: 2016; pp 89-98.
46. Nayak, A. K.; Hasnain, M. S.; Pal, D. *Natural Polymers for Pharmaceutical Applications: Volume 2: Marine-and Microbiologically Derived Polymers*. CRC Press: 2019.
47. Pal, D.; Nayak, A. K. Plant polysaccharides-blended ionotropically-gelled alginate multiple-unit systems for sustained drug release. *Handbook of composites from renewable materials* **2017,** *6*, 399-400.
48. Salisu, A.; Sanagi, M. M.; Abu Naim, A.; Wan Ibrahim, W. A.; Abd Karim, K. J. Removal of lead ions from aqueous solutions using sodium alginate-graft-poly(methyl methacrylate) beads. *Desalination and Water Treatment* **2016,** *57* (33), 15353-15361.
49. Nayak, A.; Pal, D. Plant-derived polymers: Ionically gelled sustained drug release systems. *Encyclopedia of biomedical polymers and polymeric biomaterials* **2015,** *8*, 6002e17.
50. Anumolu, S. S.; Singh, Y.; Gao, D.; Stein, S.; Sinko, P. J. Design and evaluation of novel fast forming pilocarpine-loaded ocular hydrogels for sustained pharmacological response. *Journal of Controlled Release* **2009,** *137* (2), 152-159.
51. Hoffman, A. S. Hydrogels for biomedical applications. *Advanced Drug Delivery Reviews* **2012,** *64*, 18-23.
52. Peppas, N. A.; Bures, P.; Leobandung, W.; Ichikawa, H. Hydrogels in pharmaceutical formulations. *European Journal of Pharmaceutics and Biopharmaceutics* **2000,** *50* (1), 27-46.
53. Saka, R.; Sathe, P.; Khan, W. 11 - Brain local delivery strategy. In *Brain Targeted Drug Delivery System*, Gao, H.; Gao, X., Eds. Academic Press: 2019; pp 241-286.

54. Caldorera-Moore, M.; Peppas, N. A. Micro- and nanotechnologies for intelligent and responsive biomaterial-based medical systems. *Advanced Drug Delivery Reviews* **2009,** *61* (15), 1391-1401.
55. Singh, A.; Peppas, N. A. Hydrogels and Scaffolds for Immunomodulation. *Advanced Materials* **2014,** *26* (38), 6530-6541.
56. Harner, J. M.; Hoagland, D. A. Thermoreversible Gelation of an Ionic Liquid by Crystallization of a Dissolved Polymer. *The Journal of Physical Chemistry B* **2010,** *114* (10), 3411-3418.
57. Ravi Kumar, M. N. V. A review of chitin and chitosan applications. *Reactive and Functional Polymers* **2000,** *46* (1), 1-27.
58. Wichterle, O.; LÍM, D. Hydrophilic Gels for Biological Use. *Nature* **1960,** *185* (4706), 117-118.
59. Peppas, N. A.; Wood, K. M.; Blanchette, J. O. Hydrogels for oral delivery of therapeutic proteins. *Expert Opinion on Biological Therapy* **2004,** *4* (6), 881-887.
60. Park, H.; Park, K.; Shalaby, W. S. *Biodegradable hydrogels for drug delivery*. CRC Press: 1993.
61. El-Sherbiny, I. M.; Yacoub, M. H. Hydrogel scaffolds for tissue engineering: Progress and challenges. *Global Cardiology Science and Practice* **2013,** *2013* (3), 38.
62. Jin, S.; Liu, M.; Zhang, F.; Chen, S.; Niu, A. Synthesis and characterization of pH-sensitivity semi-IPN hydrogel based on hydrogen bond between poly(N-vinylpyrrolidone) and poly(acrylic acid). *Polymer* **2006,** *47* (5), 1526-1532.
63. Okano, T.; Katayama, M.; Shinohara, I. The influence of hydrophilic and hydrophobic domains on water wettability of 2-hydroxyethyl methacrylate-styrene copolymers. *Journal of Applied Polymer Science* **1978,** *22* (2), 369-377.
64. Lankalapalli, S.; Kolapalli, V. R. M. Polyelectrolyte Complexes: A Review of their Applicability in Drug Delivery Technology. *Indian Journal of Pharmaceutical Science* **2009,** *71* (5), 481-487.
65. Anal, A. K.; Stevens, W. F. Chitosan–alginate multilayer beads for controlled release of ampicillin. *International Journal of Pharmaceutics* **2005,** *290* (1), 45-54.
66. Tığlı Aydın, R. S.; Pulat, M. 5-Fluorouracil Encapsulated Chitosan Nanoparticles for pH-Stimulated Drug Delivery: Evaluation of Controlled Release Kinetics. *Journal of Nanomaterials* **2012,** *2012*, 313961.

67. Alam, S.; Khan, Z. I.; Mustafa, G.; Kumar, M.; Islam, F.; Bhatnagar, A.; Ahmad, F. J. Development and evaluation of thymoquinone-encapsulated chitosan nanoparticles for nose-to-brain targeting: a pharmacoscintigraphic study. *Int J Nanomedicine* **2012,** *7*, 5705-5718.
68. Meng, J.; Sturgis, T. F.; Youan, B.-B. C. Engineering tenofovir loaded chitosan nanoparticles to maximize microbicide mucoadhesion. *European Journal of Pharmaceutical Sciences* **2011,** *44* (1), 57-67.
69. Nanjwade, B. K.; Singh, J.; Parikh, K. A.; Manvi, F. V. Preparation and evaluation of carboplatin biodegradable polymeric nanoparticles. *International Journal of Pharmaceutics* **2010,** *385* (1), 176-180.
70. Bhattarai, N.; Ramay, H. R.; Chou, S.-H.; Zhang, M. Chitosan and lactic acid-grafted chitosan nanoparticles as carriers for prolonged drug delivery. *International Journal of Nanomedicine* **2006,** *1* (2), 181-187.
71. Pan, Y.; Li, Y.-j.; Zhao, H.-y.; Zheng, J.-m.; Xu, H.; Wei, G.; Hao, J.-s.; Cui, F.-d. Bioadhesive polysaccharide in protein delivery system: chitosan nanoparticles improve the intestinal absorption of insulin in vivo. *International Journal of Pharmaceutics* **2002,** *249* (1), 139-147.
72. Ngan, L. T. K.; Wang, S.-L.; Hiep, Đ. M.; Luong, P. M.; Vui, N. T.; Đinh, T. M.; Dzung, N. A. Preparation of chitosan nanoparticles by spray drying, and their antibacterial activity. *Research on Chemical Intermediates* **2014,** *40* (6), 2165-2175.
73. Sinsuebpol, C.; Chatchawalsaisin, J.; Kulvanich, P. Preparation and in vivo absorption evaluation of spray dried powders containing salmon calcitonin loaded chitosan nanoparticles for pulmonary delivery. *Drug Design Development and Therapy* **2013,** *7*, 861-873.
74. Nienhaus, K.; Wang, H.; Nienhaus, G. U. Nanoparticles for biomedical applications: exploring and exploiting molecular interactions at the nano-bio interface. *Materials Today Advances* **2020,** *5*, 100036.
75. Reinholz, J.; Landfester, K.; Mailänder, V. The challenges of oral drug delivery via nanocarriers. *Drug Delivery* **2018,** *25* (1), 1694-1705.
76. Lima, A. C.; Alvarez-Lorenzo, C.; Mano, J. F. Design Advances in Particulate Systems for Biomedical Applications. *Advanced Healthcare Materials* **2016,** *5* (14), 1687-1723.

77. Muñoz-Espí, R.; Álvarez-Bermúdez, O. Chapter 15 - Application of Nanoemulsions in the Synthesis of Nanoparticles. In *Nanoemulsions*, Jafari, S. M.; McClements, D. J., Eds. Academic Press: 2018; pp 477-515.
78. Landfester, K. Miniemulsion Polymerization and the Structure of Polymer and Hybrid Nanoparticles. *Angewandte Chemie International Edition* **2009,** *48* (25), 4488-4507.
79. Landfester, K.; Musyanovych, A.; Mailänder, V. From polymeric particles to multifunctional nanocapsules for biomedical applications using the miniemulsion process. *Journal of Polymer Science Part A: Polymer Chemistry* **2010,** *48* (3), 493-515.
80. Landfester, K.; Mailänder, V. Nanocapsules with specific targeting and release properties using miniemulsion polymerization. *Expert Opinion on Drug Delivery* **2013,** *10* (5), 593-609.
81. Iyisan, B.; Landfester, K. Modular Approach for the Design of Smart Polymeric Nanocapsules. *Macromolecular Rapid Communications* **2019,** *40* (1), 1800577.
82. Jenjob, R.; Phakkeeree, T.; Seidi, F.; Theerasilp, M.; Crespy, D. Emulsion Techniques for the Production of Pharmacological Nanoparticles. *Macromolecular Bioscience* **2019,** *19* (6), 1900063.
83. Sharma, A. K.; Garg, T.; Goyal, A. K.; Rath, G. Role of microemuslsions in advanced drug delivery. *Artificial Cells, Nanomedicine, and Biotechnology* **2016,** *44* (4), 1177-1185.
84. Boscán, F.; Barandiaran, M. J.; Paulis, M. From miniemulsion to nanoemulsion polymerization of superhydrophobic monomers through low energy phase inversion temperature. *Journal of Industrial and Engineering Chemistry* **2018,** *58*, 1-8.
85. Shakirova, J. R.; Shevchenko, N. N.; Baigildin, V. A.; Chelushkin, P. S.; Khlebnikov, A. F.; Tomashenko, O. A.; Solomatina, A. I.; Starova, G. L.; Tunik, S. P. Eu-Based Phosphorescence Lifetime Polymer Nanothermometer: A Nanoemulsion Polymerization Approach to Eliminate Quenching of Eu Emission in Aqueous Media. *ACS Applied Polymer Materials* **2020,** *2* (2), 537-547.
86. Siebert, J. M.; Baumann, D.; Zeller, A.; Mailänder, V.; Landfester, K. Synthesis of Polyester Nanoparticles in Miniemulsion Obtained by Radical Ring-Opening of

BMDO and Their Potential as Biodegradable Drug Carriers. *Macromolecular Bioscience* **2012,** *12* (2), 165-175.

87. Feuser, P. E.; Gaspar, P. C.; Ricci-Júnior, E.; Silva, M. C. S. d.; Nele, M.; Sayer, C.; H. H. de Araújo, P. Synthesis and Characterization of Poly(Methyl Methacrylate) PMMA and Evaluation of Cytotoxicity for Biomedical Application. *Macromolecular Symposia* **2014,** *343* (1), 65-69.
88. Preiss, L. C.; Werber, L.; Fischer, V.; Hanif, S.; Landfester, K.; Mastai, Y.; Muñoz-Espí, R. Amino-Acid-Based Chiral Nanoparticles for Enantioselective Crystallization. *Advanced Materials* **2015,** *27* (17), 2728-2732.
89. Preiss, L. C.; Wagner, M.; Mastai, Y.; Landfester, K.; Muñoz-Espí, R. Amino-Acid-Based Polymerizable Surfactants for the Synthesis of Chiral Nanoparticles. *Macromolecular Rapid Communications* **2016,** *37* (17), 1421-1426.
90. Yamala, A. K.; Nadella, V.; Mastai, Y.; Prakash, H.; Paik, P. Poly-N-acryloyl-(l-phenylalanine methyl ester) hollow core nanocapsules facilitate sustained delivery of immunomodulatory drugs and exhibit adjuvant properties. *Nanoscale* **2017,** *9* (37), 14006-14014.
91. Farazi, S.; Chen, F.; Foster, H.; Boquiren, R.; McAlpine, S. R.; Chapman, R. Real time monitoring of peptide delivery in vitro using high payload pH responsive nanogels. *Polymer Chemistry* **2020,** *11* (2), 425-432.
92. Malzahn, K.; Jamieson, W. D.; Dröge, M.; Mailänder, V.; Jenkins, A. T. A.; Weiss, C. K.; Landfester, K. Advanced dextran based nanogels for fighting Staphylococcus aureus infections by sustained zinc release. *Journal of Materials Chemistry B* **2014,** *2* (15), 2175-2183.
93. An, H. Z.; Helgeson, M. E.; Doyle, P. S. Nanoemulsion Composite Microgels for Orthogonal Encapsulation and Release. *Advanced Materials* **2012,** *24* (28), 3838-3844.
94. Hemingway, M. G.; Gupta, R. B.; Elton, D. J. Hydrogel Nanopowder Production by Inverse-Miniemulsion Polymerization and Supercritical Drying. *Industrial & Engineering Chemistry Research* **2010,** *49* (20), 10094-10099.
95. Solomko, N.; Budishevska, O.; Voronov, S.; Landfester, K.; Musyanovych, A. pH-Sensitive Chitosan-based Hydrogel Nanoparticles through Miniemulsion Polymerization Mediated by Peroxide Containing Macromonomer. *Macromolecular Bioscience* **2014,** *14* (8), 1076-1083.

96. Vadlamudi, S.; Nichols, D.; Papavasiliou, G.; Teymour, F. Phosphate-Loaded Hydrogel Nanoparticles for Sepsis Prevention Prepared via Inverse Miniemulsion Polymerization. *Macromolecular Reaction Engineering* **2019,** *13* (1), 1800066.
97. Borges, F. T. P.; Papavasiliou, G.; Teymour, F. Synthesis of Polyphosphate-Loaded Nanoparticles Using Inverse Miniemulsion Polymerization for Sustained Delivery to the Gastrointestinal Tract. *Macromolecular Reaction Engineering* **2019,** *13* (2), 1800068.
98. Peres, L. B.; dos Anjos, R. S.; Tappertzhofen, L. C.; Feuser, P. E.; de Araújo, P. H. H.; Landfester, K.; Sayer, C.; Muñoz-Espí, R. pH-responsive physically and chemically cross-linked glutamic-acid-based hydrogels and nanogels. *European Polymer Journal* **2018,** *101*, 341-349.
99. Oh, J. K.; Bencherif, S. A.; Matyjaszewski, K. Atom transfer radical polymerization in inverse miniemulsion: A versatile route toward preparation and functionalization of microgels/nanogels for targeted drug delivery applications. *Polymer* **2009,** *50* (19), 4407-4423.
100. Staff, R. H.; Landfester, K.; Crespy, D. Recent Advances in the Emulsion Solvent Evaporation Technique for the Preparation of Nanoparticles and Nanocapsules. In *Hierarchical Macromolecular Structures: 60 Years after the Staudinger Nobel Prize II*, Percec, V., Ed. Springer International Publishing: Cham, 2013; pp 329-344.
101. Iqbal, M.; Zafar, N.; Fessi, H.; Elaissari, A. Double emulsion solvent evaporation techniques used for drug encapsulation. *International Journal of Pharmaceutics* **2015,** *496* (2), 173-190.
102. Alexandrino, E. M.; Ritz, S.; Marsico, F.; Baier, G.; Mailänder, V.; Landfester, K.; Wurm, F. R. Paclitaxel-loaded polyphosphate nanoparticles: a potential strategy for bone cancer treatment. *Journal of Materials Chemistry B* **2014,** *2* (10), 1298-1306.
103. Höcherl, A.; Dass, M.; Landfester, K.; Mailänder, V.; Musyanovych, A. Competitive Cellular Uptake of Nanoparticles Made From Polystyrene, Poly(methyl methacrylate), and Polylactide. *Macromolecular Bioscience* **2012,** *12* (4), 454-464.
104. Baier, G.; Cavallaro, A.; Friedemann, K.; Müller, B.; Glasser, G.; Vasilev, K.; Landfester, K. Enzymatic degradation of poly(l-lactide) nanoparticles followed by

the release of octenidine and their bactericidal effects. *Nanomedicine: Nanotechnology, Biology and Medicine* **2014,** *10* (1), 131-139.

105. Taheri, S.; Baier, G.; Majewski, P.; Barton, M.; Förch, R.; Landfester, K.; Vasilev, K. Synthesis and surface immobilization of antibacterial hybrid silver-poly(l-lactide) nanoparticles. *Nanotechnology* **2014,** *25* (30), 305102.
106. Niyom, Y.; Phakkeeree, T.; Flood, A.; Crespy, D. Synergy between polymer crystallinity and nanoparticles size for payloads release. *Journal of. Colloids and Interfaces. Science.* **2019,** *550*, 139-146.
107. Staff, R. H.; Schaeffel, D.; Turshatov, A.; Donadio, D.; Butt, H.-J.; Landfester, K.; Koynov, K.; Crespy, D. Particle Formation in the Emulsion-Solvent Evaporation Process. *Small* **2013,** *9* (20), 3514-3522.
108. Doan-Nguyen, T. P.; Natsathaporn, P.; Jenjob, R.; Niyom, Y.; Ittisanronnachai, S.; Flood, A.; Crespy, D. Regulating Payload Release from Hybrid Nanocapsules with Dual Silica/Polycaprolactone Shells. *Langmuir* **2019,** *35* (35), 11389-11396.
109. Blin, J.-L.; Stébé, M.-J.; Lebeau, B. Hybrid/porous materials obtained from nano-emulsions. *Current Opinion in Colloid & Interface Science* **2016,** *25*, 75-82.
110. Riachy, P.; Roig, F.; García-Celma, M.-J.; Stébé, M.-J.; Pasc, A.; Esquena, J.; Solans, C.; Blin, J. L. Hybrid Hierarchical Porous Silica Templated in Nanoemulsions for Drug Release. *European Journal of Inorganic Chemistry* **2016,** *2016* (13-14), 1989-1997.
111. Fickert, J.; Schaeffel, D.; Koynov, K.; Landfester, K.; Crespy, D. Silica nanocapsules for redox-responsive delivery. *Colloid and Polymer Science* **2014,** *292* (1), 251-255.
112. Behzadi, S.; Steinmann, M.; Estupiñán, D.; Landfester, K.; Crespy, D. The pro-active payload strategy significantly increases selective release from mesoporous nanocapsules. *Journal of Controlled Release* **2016,** *242*, 119-125.
113. Wang, S.; Chen, M.; Wu, L. One-Step Synthesis of Cagelike Hollow Silica Spheres with Large Through-Holes for Macromolecule Delivery. *ACS Applied Materials & Interfaces* **2016,** *8* (48), 33316-33325.
114. Jiang, S.; Mottola, M.; Han, S.; Thiramanas, R.; Graf, R.; Lieberwirth, I.; Mailänder, V.; Crespy, D.; Landfester, K. Versatile Preparation of Silica Nanocapsules for Biomedical Applications. *Particle & Particle Systems Characterization* **2020,** *37* (4), 1900484.

115. Thiramanas, R.; Jiang, S.; Simon, J.; Landfester, K.; Mailänder, V. Silica Nanocapsules with Different Sizes and Physicochemical Properties as Suitable Nanocarriers for Uptake in T-Cells. *International Journal of Nanomedicine* **2020,** *15*, 6069-6084.
116. Hood, M. A.; Encinas, N.; Vollmer, D.; Graf, R.; Landfester, K.; Muñoz-Espí, R. Controlling hydrophobicity of silica nanocapsules prepared from organosilanes. *Colloids and Surfaces A: Physicochemical and Engineering Aspects* **2017,** *532*, 172-177.
117. Jo, S.-M.; Wurm, F. R.; Landfester, K. Oncolytic Nanoreactors Producing Hydrogen Peroxide for Oxidative Cancer Therapy. *Nano Letters* **2020,** *20* (1), 526-533.
118. Hajir, M.; Dolcet, P.; Fischer, V.; Holzinger, J.; Landfester, K.; Muñoz-Espí, R. Sol–gel processes at the droplet interface: hydrous zirconia and hafnia nanocapsules by interfacial inorganic polycondensation. *Journal of Materials Chemistry* **2012,** *22* (12), 5622-5628.
119. Hood, M. A.; Mari, M.; Muñoz-Espí, R. Synthetic Strategies in the Preparation of Polymer/Inorganic Hybrid Nanoparticles. *Materials* **2014,** *7* (5).
120. Berger, J.; Reist, M.; Mayer, J. M.; Felt, O.; Gurny, R. Structure and interactions in chitosan hydrogels formed by complexation or aggregation for biomedical applications. *European Journal of Pharmaceutics and Biopharmaceutics* **2004,** *57* (1), 35-52.
121. Xu, Y.; Du, Y.; Huang, R.; Gao, L. Preparation and modification of N-(2-hydroxyl) propyl-3-trimethyl ammonium chitosan chloride nanoparticle as a protein carrier. *Biomaterials* **2003,** *24* (27), 5015-5022.
122. Mi, F.-L.; Chen, C.-T.; Tseng, Y.-C.; Kuan, C.-Y.; Shyu, S.-S. Iron(III)-carboxymethylchitin microsphere for the pH-sensitive release of 6-mercaptopurine. *Journal of Controlled Release* **1997,** *44* (1), 19-32.
123. Calvo, P.; Vila-Jato, J. L.; Alonso, M. a. J. Evaluation of cationic polymer-coated nanocapsules as ocular drug carriers. *International Journal of Pharmaceutics* **1997,** *153* (1), 41-50.
124. Ehlerding, E. B.; Chen, F.; Cai, W. Biodegradable and Renal Clearable Inorganic Nanoparticles. *Advanced Science* **2016,** *3* (2), 1500223.

125. Zhang, Y.; Hsu, B. Y. W.; Ren, C.; Li, X.; Wang, J. Silica-based nanocapsules: synthesis, structure control and biomedical applications. *Chemical Society Reviews* **2015,** *44* (1), 315-335.
126. Li, F.-Q.; Ji, R.-R.; Chen, X.; You, B.-M.; Pan, Y.-H.; Su, J.-C. Cetirizine dihydrochloride loaded microparticles design using ionotropic cross-linked chitosan nanoparticles by spray-drying method. *Archives of Pharmacal Research* **2010,** *33* (12), 1967-1973.
127. Ohya, Y.; Shiratani, M.; Kobayashi, H.; Ouchi, T. Release Behavior of 5-Fluorouracil from Chitosan-Gel Nanospheres Immobilizing 5-Fluorouracil Coated with Polysaccharides and Their Cell Specific Cytotoxicity. *Journal of Macromolecular Science, Part A* **1994,** *31* (5), 629-642.
128. Grenha, A. Chitosan nanoparticles: a survey of preparation methods. *Journal of Drug Targeting* **2012,** *20* (4), 291-300.
129. Tokumitsu, H.; Ichikawa, H.; Fukumori, Y. Chitosan-Gadopentetic Acid Complex Nanoparticles for Gadolinium Neutron-Capture Therapy of Cancer: Preparation by Novel Emulsion-Droplet Coalescence Technique and Characterization. *Pharmaceutical Research* **1999,** *16* (12), 1830-1835.
130. "Guidance for industry dissolution testing of immediate release solid oral dosage forms" U.S. Department of Health and Human Services, Food and Drug Administration, Center for Drug Evaluation and Research (CDER), August 1997.
131. Higuchi, T., Rate of release of medicaments from ointment bases containing drugs in suspensions. Journal of. Pharmceutical. Science. 1961, 50, 874-875
132. Siepmann, J.; Peppas, N. A. Higuchi equation: derivation, applications, use and misuse. *International Journal of Pharmaceutics* **2011,** *418* (1), 6-12.
133. Korsmeyer, R. W.; Gurny, R.; Doelker, E.; Buri, P.; Peppas, N. A. Mechanisms of solute release from porous hydrophilic polymers. *International Journal of Pharmaceutics* **1983,** *15* (1), 25-35.
134. Bruschi, M. L. *Strategies to modify the drug release from pharmaceutical systems*. Woodhead Publishing: 2015.
135. Alfrey Jr, T.; Gurnee, E.; Lloyd, W. In *Diffusion in glassy polymers*, Journal of Polymer Science Part C: Polymer Symposia, Wiley Online Library: 1966; pp 249-261.

136. Fu, Y.; Kao, W. J. Drug release kinetics and transport mechanisms of non-degradable and degradable polymeric delivery systems. *Expert Opinion on Drug Delivery* **2010,** *7* (4), 429-444.
137. Narasimhan, B. Mathematical models describing polymer dissolution: consequences for drug delivery. *Advanced Drug Delivery Reviews* **2001,** *48* (2-3), 195-210.
138. Goutelle, S.; Maurin, M.; Rougier, F.; Barbaut, X.; Bourguignon, L.; Ducher, M.; Maire, P. The Hill equation: a review of its capabilities in pharmacological modelling. *Fundamental & Clinical Pharmacology* **2008,** *22* (6), 633-648.
139. Murzin, D. Y.; Heikkilä, T. Modeling of drug dissolution kinetics with sigmoidal behavior from ordered mesoporous silica. *Chemical Engineering Communications* **2014,** *201* (5), 579-592.
140. Marquardt, D. W. An algorithm for least-squares estimation of nonlinear parameters. *Journal of the society for Industrial and Applied Mathematics* **1963,** *11* (2), 431-441.
141. Perez, J.; Francois, N.; Maroniche, G. A.; Borrajo, M. P.; Pereyra, M.; Creus, C. M. A novel, green, low-cost chitosan-starch hydrogel as potential delivery system for plant growth-promoting bacteria. *Carbohydrate Polymers* **2018,** *202*, 409-417.
142. Maestrelli, F.; Jug, M.; Cirri, M.; Kosalec, I.; Mura, P. Characterization and microbiological evaluation of chitosan-alginate microspheres for cefixime vaginal administration. *Carbohydrate Polymers* **2018,** *192*, 176-183.
143. Hood, M. A.; Landfester, K.; Muñoz-Espí, R. Chitosan nanoparticles affect polymorph selection in crystallization of calcium carbonate. *Colloids and Surfaces A: Physicochemical and Engineering Aspects* **2018,** *540*, 48-52.
144. Mukwaya, V.; Wang, C.; Dou, H. Saccharide-based nanocarriers for targeted therapeutic and diagnostic applications. *Polymer International* **2019,** *68* (3), 306-319.
145. Perez, J. J.; Francois, N. J. Chitosan-starch beads prepared by ionotropic gelation as potential matrices for controlled release of fertilizers. *Carbohydrate Polymers* **2016,** *148*, 134-142.
146. Cevher, E.; Orhan, Z.; Mülazımoğlu, L.; Şensoy, D.; Alper, M.; Yıldız, A.; Özsoy, Y. Characterization of biodegradable chitosan microspheres containing vancomycin and treatment of experimental osteomyelitis caused by methicillin-

resistant Staphylococcus aureus with prepared microspheres. *International Journal of Pharmaceutics* **2006,** *317* (2), 127-135.

147. Peniche, H.; Peniche, C. Chitosan nanoparticles: a contribution to nanomedicine. *Polymer International* **2011,** *60* (6), 883-889.
148. Fernández-Gutiérrez, M.; Bossio, O.; Gómez-Mascaraque, L. G.; Vázquez-Lasa, B.; Román, J. S. Bioactive Chitosan Nanoparticles Loaded with Retinyl Palmitate: A Simple Route Using Ionotropic Gelation. *Macromolecular Chemistry and Physics* **2015,** *216* (12), 1321-1332.
149. Lee, K. Y.; Mooney, D. J. Alginate: properties and biomedical applications. *Progress in Polymer Science* **2012,** *37* (1), 106-126.
150. Vicini, S.; Castellano, M.; Mauri, M.; Marsano, E. Gelling process for sodium alginate: New technical approach by using calcium rich micro-spheres. *Carbohydrate Polymers* **2015,** *134*, 767-774.
151. Caetano, L. A.; Almeida, A. J.; Gonçalves, L. Effect of experimental parameters on alginate/chitosan microparticles for BCG encapsulation. *Marine Drugs* **2016,** *14* (5), 90.
152. Unagolla, J. M.; Jayasuriya, A. C. Drug transport mechanisms and in vitro release kinetics of vancomycin encapsulated chitosan-alginate polyelectrolyte microparticles as a controlled drug delivery system. *European Journal of Pharmaceutical Sciences* **2018,** *114*, 199-209.
153. Dash, M.; Chiellini, F.; Ottenbrite, R. M.; Chiellini, E. Chitosan—A versatile semi-synthetic polymer in biomedical applications. *Progress in Polymer Science* **2011,** *36* (8), 981-1014.
154. Antoniou, J.; Liu, F.; Majeed, H.; Qi, J.; Yokoyama, W.; Zhong, F. Physicochemical and morphological properties of size-controlled chitosan–tripolyphosphate nanoparticles. *Colloids and Surfaces A: Physicochemical and Engineering Aspects* **2015,** *465*, 137-146.
155. Nguyen, S.; Escudero, C.; Sediqi, N.; Smistad, G.; Hiorth, M. Fluoride loaded polymeric nanoparticles for dental delivery. *European Journal of Pharmaceutical Sciences* **2017,** *104*, 326-334.
156. Furtado, G. T. F. d. S.; Fideles, T. B.; Cruz, R. d. C. A. L.; Souza, J. W. d. L.; Rodriguez Barbero, M. A.; Fook, M. V. L. Chitosan/NaF Particles Prepared Via

Ionotropic Gelation: Evaluation of Particles Size and Morphology. *Materials Research* **2018,** *21* (4).

157. Fan, J.; Wang, S.; Sun, W.; Guo, S.; Kang, Y.; Du, J.; Peng, X. Anticancer drug delivery systems based on inorganic nanocarriers with fluorescent tracers. *AIChE Journal* **2018,** *64* (3), 835-859.
158. Ilhan-Ayisigi, E.; Yesil-Celiktas, O. Silica-based organic-inorganic hybrid nanoparticles and nanoconjugates for improved anticancer drug delivery. *Engineering in Life Sciences* **2018,** *18* (12), 882-892.
159. Pramanik, S. K.; Seneca, S.; Peters, M.; D'Olieslaeger, L.; Reekmans, G.; Vanderzande, D.; Adriaensens, P.; Ethirajan, A. Morphology-dependent pH-responsive release of hydrophilic payloads using biodegradable nanocarriers. *RSC Advances* **2018,** *8* (64), 36869-36878.
160. Wen, Y.; Oh, J. K. Recent strategies to develop polysaccharide-based nanomaterials for biomedical applications. *Macromolecular Rapid Communications* **2014,** *35* (21), 1819-1832.
161. De Koker, S.; Hoogenboom, R.; De Geest, B. G. Polymeric multilayer capsules for drug delivery. *Chemical Society Reviews* **2012,** *41* (7), 2867-2884.
162. Gaitzsch, J.; Huang, X.; Voit, B. Engineering functional polymer capsules toward smart nanoreactors. *Chemical Reviews* **2016,** *116* (3), 1053-1093.
163. Peres, L. B.; dos Anjos, R. S.; Tappertzhofen, L. C.; Feuser, P. E.; de Araújo, P. H.; Landfester, K.; Sayer, C.; Muñoz-Espí, R. pH-responsive physically and chemically cross-linked glutamic-acid-based hydrogels and nanogels. *European Polymer Journal* **2018,** *101*, 341-349.
164. Park, J.; Ye, M.; Park, K. Biodegradable Polymers for Microencapsulation of Drugs. *Molecules* **2005,** *10* (1).
165. Tsung, J.; Burgess, D. J. Biodegradable Polymers in Drug Delivery Systems. In *Fundamentals and Applications of Controlled Release Drug Delivery*, Siepmann, J.; Siegel, R. A.; Rathbone, M. J., Eds. Springer US: Boston, MA, 2012; pp 107-123.
166. Elzayat, A.; Tolba, E.; Pérez-Pla, F. F.; Oraby, A.; Muñoz-Espí, R. Increased Stability of Polysaccharide/Silica Hybrid Sub-Millicarriers for Retarded Release of Hydrophilic Substances. *Macromolecular Chemistry and Physics* **2021**, 2100027.

167. Kumar, S.; Shen, J.; Zolnik, B.; Sadrieh, N.; Burgess, D. J. Optimization and dissolution performance of spray-dried naproxen nano-crystals. *International Journal of Pharmaceutics* **2015,** *486* (1), 159-166.
168. Lee, S. H.; Heng, D.; Ng, W. K.; Chan, H.-K.; Tan, R. B. H. Nano spray drying: A novel method for preparing protein nanoparticles for protein therapy. *International Journal of Pharmaceutics* **2011,** *403* (1), 192-200.
169. Aranaz, I.; Paños, I.; Peniche, C.; Heras, Á.; Acosta, N. Chitosan Spray-Dried Microparticles for Controlled Delivery of Venlafaxine Hydrochloride. *Molecules* **2017,** *22* (11).
170. Schmid, K.; Arpagaus, C.; Friess, W. Evaluation of the Nano Spray Dryer B-90 for pharmaceutical applications. *Pharmaceutical Development and Technology* **2011,** *16* (4), 287-294.
171. Li, X.; Anton, N.; Arpagaus, C.; Belleteix, F.; Vandamme, T. F. Nanoparticles by spray drying using innovative new technology: The Büchi Nano Spray Dryer B-90. *Journal of Controlled Release* **2010,** *147* (2), 304-310.
172. Kašpar, O.; Jakubec, M.; Štěpánek, F. Characterization of spray dried chitosan–TPP microparticles formed by two- and three-fluid nozzles. *Powder Technology* **2013,** *240*, 31-40.
173. Liu, W.; Chen, X. D.; Selomulya, C. On the spray drying of uniform functional microparticles. *Particuology* **2015,** *22*, 1-12.
174. Wan, F.; Yang, M. Design of PLGA-based depot delivery systems for biopharmaceuticals prepared by spray drying. *International Journal of Pharmaceutics* **2016,** *498* (1), 82-95.
175. Kulkarni, A. D.; Bari, D. B.; Surana, S. J.; Pardeshi, C. V. In vitro, ex vivo and in vivo performance of chitosan-based spray-dried nasal mucoadhesive microspheres of diltiazem hydrochloride. *Journal of Drug Delivery Science and Technology* **2016,** *31*, 108-117.
176. Kumar, S.; Shen, J.; Burgess, D. J. Nano-amorphous spray dried powder to improve oral bioavailability of itraconazole. *Journal of Controlled Release* **2014,** *192*, 95-102.
177. Panos, I.; Acosta, N.; Heras, A. New Drug Delivery Systems Based on Chitosan. *Current Drug Discovery Technologies* **2008,** *5* (4), 333-341.

178. Sreekumar, S.; Lemke, P.; Moerschbacher, B. M.; Torres-Giner, S.; Lagaron, J. M. Preparation and optimization of submicron chitosan capsules by water-based electrospraying for food and bioactive packaging applications. *Food Additives & Contaminants: Part A* **2017,** *34* (10), 1795-1806.
179. Sinha, V. R.; Singla, A. K.; Wadhawan, S.; Kaushik, R.; Kumria, R.; Bansal, K.; Dhawan, S. Chitosan microspheres as a potential carrier for drugs. *International Journal of Pharmaceutics* **2004,** *274* (1), 1-33.
180. Klein, M. P.; Hackenhaar, C. R.; Lorenzoni, A. S. G.; Rodrigues, R. C.; Costa, T. M. H.; Ninow, J. L.; Hertz, P. F. Chitosan crosslinked with genipin as support matrix for application in food process: Support characterization and β-d-galactosidase immobilization. *Carbohydrate Polymers* **2016,** *137*, 184-190.
181. Sung, H.-W.; Huang, R.-N.; Huang, L. L. H.; Tsai, C.-C. In vitro evaluation of cytotoxicity of a naturally occurring cross-linking reagent for biological tissue fixation. *Journal of Biomaterials Science, Polymer Edition* **1999,** *10* (1), 63-78.
182. Food, U.; Administration, D. Database of select committee on GRAS substances (SCOGS) Reviews. *US Food and Drug Administration: Silver Spring, MD, USA* **2006**.
183. Desai, K. G. H.; Park, H. J. Preparation and characterization of drug-loaded chitosan–tripolyphosphate microspheres by spray drying. *Drug Development Research* **2005,** *64* (2), 114-128.
184. Shen, C.; Wang, Y. J.; Xu, J. H.; Wang, K.; Luo, G. S. Size Control and Catalytic Activity of Highly Dispersed Pd Nanoparticles Supported on Porous Glass Beads. *Langmuir* **2012,** *28* (19), 7519-7527.
185. Montsch, T.; Heuchel, M.; Traa, Y.; Klemm, E.; Stubenrauch, C. Selective hydrogenation of 3-Hexyn-1-ol with Pd nanoparticles synthesized via microemulsions. *Applied Catalysis A: General* **2017,** *539*, 19-28.
186. Thompson, S. T.; Lamb, H. H. Catalysts for selective hydrogenation of furfural derived from the double complex salt [Pd(NH3)4](ReO4)2 on γ-Al2O3. *Journal of Catalysis* **2017,** *350*, 111-121.
187. Liao, X.; Zhang, Y.; Hill, M.; Xia, X.; Zhao, Y.; Jiang, Z. Highly efficient Ni/CeO2 catalyst for the liquid phase hydrogenation of maleic anhydride. *Applied Catalysis A: General* **2014,** *488*, 256-264.

188. Regenhardt, S. A.; Meyer, C. I.; Garetto, T. F.; Marchi, A. J. Selective gas phase hydrogenation of maleic anhydride over Ni-supported catalysts: Effect of support on the catalytic performance. *Applied Catalysis A: General* **2012,** *449*, 81-87.
189. Berguerand, C.; Yuranov, I.; Cárdenas-Lizana, F.; Yuranova, T.; Kiwi-Minsker, L. Size-Controlled Pd Nanoparticles in 2-Butyne-1,4-diol Hydrogenation: Support Effect and Kinetics Study. *Journal of Physical Chemistry C* **2014,** *118* (23), 12250-12259.
190. Luo, C.; Zhang, Y.; Wang, Y. Palladium nanoparticles in poly(ethyleneglycol): the efficient and recyclable catalyst for Heck reaction. *Journal of Molecular Catalysis A: Chemical* **2005,** *229* (1), 7-12.
191. Liu, G.; Hou, M.; Song, J.; Jiang, T.; Fan, H.; Zhang, Z.; Han, B. Immobilization of Pd nanoparticles with functional ionic liquid grafted onto cross-linked polymer for solvent-free Heck reaction. *Green Chemistry* **2010,** *12* (1), 65-69.
192. Lan, W.; Li, S.; Xu, J.; Luo, G. One-step synthesis of chitosan-silica hybrid microspheres in a microfluidic device. *Biomedical Microdevices* **2010,** *12* (6), 1087-1095.
193. Varma, A. J.; Deshpande, S. V.; Kennedy, J. F. Metal complexation by chitosan and its derivatives: a review. *Carbohydrate Polymers* **2004,** *55* (1), 77-93.
194. Peniche-Covas, C.; Alvarez, L. W.; Argüelles-Monal, W. The adsorption of mercuric ions by chitosan. *Journal of Applied Polymer Science* **1992,** *46* (7), 1147-1150.
195. Randall, J. M.; Randall, V. G.; McDonald, G. M.; Young, R. N.; Masri, M. S. Removal of trace quantities of nickel from solution. *Journal of Applied Polymer Science* **1979,** *23* (3), 727-732.
196. Qian, S.; Huang, G.; Jiang, J.; He, F.; Wang, Y. Studies of adsorption behavior of crosslinked chitosan for Cr(VI), Se(VI). *Journal of Applied Polymer Science* **2000,** *77* (14), 3216-3219.
197. Wang, Q. Z.; Chen, X. G.; Liu, N.; Wang, S. X.; Liu, C. S.; Meng, X. H.; Liu, C. G. Protonation constants of chitosan with different molecular weight and degree of deacetylation. *Carbohydrate Polymers* **2006,** *65* (2), 194-201.
198. Haber, F. Gradual electrolytic reduction of nitrobenzene with limited cathode potential. *Elektrochem. Angew. Phys. Chem* **1898,** *22*, 506-514.

199. Corma, A.; Concepción, P.; Serna, P. A Different Reaction Pathway for the Reduction of Aromatic Nitro Compounds on Gold Catalysts. *Angewandte Chemie International Edition* **2007,** *46* (38), 7266-7269.
200. Ye, W.; Yu, J.; Zhou, Y.; Gao, D.; Wang, D.; Wang, C.; Xue, D. Green synthesis of Pt–Au dendrimer-like nanoparticles supported on polydopamine-functionalized graphene and their high performance toward 4- nitrophenol reduction. *Applied Catalysis B: Environmental* **2016,** *181*, 371-378.
201. Movahed, S. K.; Lehi, N. F.; Dabiri, M. Palladium nanoparticles supported on core-shell and yolk-shell Fe3O4@nitrogen doped carbon cubes as a highly efficient, magnetically separable catalyst for the reduction of nitroarenes and the oxidation of alcohols. *Journal of Catalysis* **2018,** *364*, 69-79.
202. Zhao, P.; Feng, X.; Huang, D.; Yang, G.; Astruc, D. Basic concepts and recent advances in nitrophenol reduction by gold- and other transition metal nanoparticles. *Coordination Chemistry Reviews* **2015,** *287*, 114-136.
203. Gu, S.; Wunder, S.; Lu, Y.; Ballauff, M.; Fenger, R.; Rademann, K.; Jaquet, B.; Zaccone, A. Kinetic Analysis of the Catalytic Reduction of 4-Nitrophenol by Metallic Nanoparticles. *The Journal of Physical Chemistry C* **2014,** *118* (32), 18618-18625.
204. Lara, L. R. S.; Zottis, A. D.; Elias, W. C.; Faggion, D.; Maduro de Campos, C. E.; Acuña, J. J. S.; Domingos, J. B. The catalytic evaluation of in situ grown Pd nanoparticles on the surface of Fe3O4@dextran particles in the p-nitrophenol reduction reaction. *RSC Advances* **2015,** *5* (11), 8289-8296.
205. Aditya, T.; Pal, A.; Pal, T. Nitroarene reduction: a trusted model reaction to test nanoparticle catalysts. *Chemical Communications* **2015,** *51* (46), 9410-9431.
206. Ródenas, M.; El Haskouri, J.; Ros-Lis, J. V.; Marcos, M. D.; Amorós, P.; Úbeda, M. Á.; Pérez-Pla, F. Highly Active Hydrogenation Catalysts Based on Pd Nanoparticles Dispersed along Hierarchical Porous Silica Covered with Polydopamine as Interfacial Glue. *Catalysts* **2020,** *10* (4).
207. Cerqueira, B. B. S.; Lasham, A.; Shelling, A. N.; Al-Kassas, R. Nanoparticle therapeutics: Technologies and methods for overcoming cancer. *European Journal of Pharmaceutics and Biopharmaceutics* **2015,** *97*, 140-151.
208. Becker Peres, L.; Becker Peres, L.; de Araújo, P. H. H.; Sayer, C. Solid lipid nanoparticles for encapsulation of hydrophilic drugs by an organic solvent free

double emulsion technique. *Colloids and Surfaces B: Biointerfaces* **2016,** *140*, 317-323.

209. Brunel, F.; Véron, L.; David, L.; Domard, A.; Delair, T. A Novel Synthesis of Chitosan Nanoparticles in Reverse Emulsion. *Langmuir* **2008,** *24* (20), 11370-11377.
210. Jiang, S.; Lv, L.-P.; Landfester, K.; Crespy, D. Nanocontainers in and onto Nanofibers. *Accounts of Chemical Research* **2016,** *49* (5), 816-823.
211. Thongchaivetcharat, K.; Jenjob, R.; Crespy, D. Encapsulation and Release of Functional Nanodroplets Entrapped in Nanofibers. *Small* **2018,** *14* (20), 1704527.
212. Generalova, A.; Asharchuk, I.; Zubov, V. Multifunctional polymer dispersions for biomedical assays obtained by heterophase radical polymerization. *Russian Chemical Bulletin* **2018,** *67* (10), 1759-1780.
213. Lerch, S.; Dass, M.; Musyanovych, A.; Landfester, K.; Mailänder, V. Polymeric nanoparticles of different sizes overcome the cell membrane barrier. *European Journal of Pharmaceutics and Biopharmaceutics* **2013,** *84* (2), 265-274.
214. Solomko, N.; Budishevska, O.; Voronov, S.; Landfester, K.; Musyanovych, A. pH-Sensitive Chitosan-based Hydrogel Nanoparticles through Miniemulsion Polymerization Mediated by Peroxide Containing Macromonomer. *Macromolecular Bioscience* **2014,** *14* (8), 1076-1083.
215. Stuart, M. A. C.; Huck, W. T.; Genzer, J.; Müller, M.; Ober, C.; Stamm, M.; Sukhorukov, G. B.; Szleifer, I.; Tsukruk, V. V.; Urban, M. Emerging applications of stimuli-responsive polymer materials. *Nature Materials* **2010,** *9* (2), 101-113.
216. Yang, S.; Chen, D.; Li, N.; Mei, X.; Qi, X.; Li, H.; Xu, Q.; Lu, J. A facile preparation of targetable pH-sensitive polymeric nanocarriers with encapsulated magnetic nanoparticles for controlled drug release. *Journal of Materials Chemistry* **2012,** *22* (48), 25354-25361.
217. Berger, J.; Reist, M.; Mayer, J. M.; Felt, O.; Peppas, N. A.; Gurny, R. Structure and interactions in covalently and ionically crosslinked chitosan hydrogels for biomedical applications. *European Journal of Pharmaceutics and Biopharmaceutics* **2004,** *57* (1), 19-34.
218. Mauri, E.; Negri, A.; Rebellato, E.; Masi, M.; Perale, G.; Rossi, F. Hydrogel-Nanoparticles Composite System for Controlled Drug Delivery. *Gels* **2018,** *4* (3).

219. Paiphansiri, U.; Tangboriboonrat, P.; Landfester, K. Polymeric Nanocapsules Containing an Antiseptic Agent Obtained by Controlled Nanoprecipitation onto Water-in-Oil Miniemulsion Droplets. *Macromolecular Bioscience* **2006,** *6* (1), 33-40.
220. Crespy, D.; Stark, M.; Hoffmann-Richter, C.; Ziener, U.; Landfester, K. Polymeric Nanoreactors for Hydrophilic Reagents Synthesized by Interfacial Polycondensation on Miniemulsion Droplets. *Macromolecules* **2007,** *40* (9), 3122-3135.
221. Landfester, K. Synthesis of Colloidal Particles in Miniemulsions. *Annual Review of Materials Research* **2006,** *36* (1), 231-279.
222. Xu, Z. Z.; Wang, C. C.; Yang, W. L.; Deng, Y. H.; Fu, S. K. Encapsulation of nanosized magnetic iron oxide by polyacrylamide via inverse miniemulsion polymerization. *Journal of Magnetism and Magnetic Materials* **2004,** *277* (1), 136-143.
223. Baier, G.; Musyanovych, A.; Dass, M.; Theisinger, S.; Landfester, K. Cross-linked starch capsules containing dsDNA prepared in inverse miniemulsion as "nanoreactors" for polymerase chain reaction. *Biomacromolecules* **2010,** *11* (4), 960-968.
224. Teo, G. H.; Kuchel, R. P.; Zetterlund, P. B.; Thickett, S. C. Polymer-inorganic hybrid nanoparticles of various morphologies via polymerization-induced self assembly and sol–gel chemistry. *Polymer Chemistry* **2016,** *7* (43), 6575-6585.
225. Toskas, G.; Cherif, C.; Hund, R.-D.; Laourine, E.; Mahltig, B.; Fahmi, A.; Heinemann, C.; Hanke, T. Chitosan(PEO)/silica hybrid nanofibers as a potential biomaterial for bone regeneration. *Carbohydrate Polymers* **2013,** *94* (2), 713-722.
226. Günter, E. A.; Markov, P. A.; Melekhin, A. K.; Belozerov, V. S.; Martinson, E. A.; Litvinets, S. G.; Popov, S. V. Preparation and release characteristics of mesalazine loaded calcium pectin-silica gel beads based on callus cultures pectins for colon-targeted drug delivery. *International Journal of Biological Macromolecules* **2018,** *120*, 2225-2233.
227. He, W.; Graf, R.; Vieth, S.; Ziener, U.; Landfester, K.; Crespy, D. The Cushion Method: A New Technique for the Recovery of Hydrophilic Nanocarriers. *Langmuir* **2016,** *32* (51), 13669-13674.

228. Martínez-Martínez, M.; Rodríguez-Berna, G.; Gonzalez-Alvarez, I.; Hernández, M. J.; Corma, A.; Bermejo, M.; Merino, V.; Gonzalez-Alvarez, M. Ionic Hydrogel Based on Chitosan Cross-Linked with 6-Phosphogluconic Trisodium Salt as a Drug Delivery System. *Biomacromolecules* **2018,** *19* (4), 1294-1304.
229. Hejjaji, E. M. A.; Smith, A. M.; Morris, G. A. Evaluation of the mucoadhesive properties of chitosan nanoparticles prepared using different chitosan to tripolyphosphate (CS:TPP) ratios. *International Journal of Biological Macromolecules* **2018,** *120*, 1610-1617.
230. Martins, A. F.; de Oliveira, D. M.; Pereira, A. G.; Rubira, A. F.; Muniz, E. C. Chitosan/TPP microparticles obtained by microemulsion method applied in controlled release of heparin. *International Journal of Biological Macromolecules* **2012,** *51* (5), 1127-1133.
231. Luo, Y.; Zhang, B.; Cheng, W.-H.; Wang, Q. Preparation, characterization and evaluation of selenite-loaded chitosan/TPP nanoparticles with or without zein coating. *Carbohydrate Polymers* **2010,** *82* (3), 942-951.
232. Vasconcellos, F. C.; Goulart, G. A.; Beppu, M. M. Production and characterization of chitosan microparticles containing papain for controlled release applications. *Powder Technology* **2011,** *205* (1-3), 65-70.